### POLITECNICO DI TORINO

Corso di Laurea Magistrale in Ingegneria Aerospaziale



Tesi di Laurea Magistrale

# Optimization of trajectories to Near-Earth asteroids

Relatore: Prof. Lorenzo Casalino Candidato: Edoardo Mastrazzo

A mio zio Renzo

# Acknowledgements

Desidero ringraziare, innanzitutto, il Prof. Lorenzo Casalino, che mi ha dato l'opportunità di approfondire un argomento molto stimolante e interessante, accompagnandomi sempre con disponibilità e professionalità durante lo svolgimento del lavoro.

Un grazie enorme alla mia famiglia: mia mamma, mio papà, i miei zii, i miei nonni e i miei cugini, che mi hanno sempre sostenuto in questi anni di Università, credendo in me e nelle mie capacità.

Ringrazio di cuore i miei coinquilini dell'alloggio "Montevideo", amici di sempre con cui ho condiviso esperienze, risate e momenti di spensieratezza, e le amiche di via Peyron, con cui abbiamo trascorso splendide serate e che hanno contribuito a rendere questa esperienza universitaria ancora più ricca e piacevole.

Un pensiero speciale va anche agli amici di Nizza, dal solito gruppo di uscite a quelli di infanzia, per la loro presenza costante e per le occasioni di divertimento che hanno reso questo mio "viaggio" più sereno e gioioso.

Ringrazio, infine, i compagni che ho conosciuto all'Università, con cui ho condiviso non solo il percorso di studi, ma anche momenti preziosi ed esperienze indimenticabili che porterò sempre con me.

Grazie di cuore a tutti.

# Abstract

The study of Near-Earth asteroids (NEAs) and potential interplanetary transfers to them is crucial for exploration, the extraction of resources useful to humanity and planetary defence. Indeed, their proximity to Earth, in addition to making them accessible via relatively simple trajectories, turning them into a potential resource for humanity, can also pose a threat due to potential collisions with the planet. Regarding this latter aspect, asteroid 2024 YR4, discovered in December 2024, has attracted particular interest in recent months due to its orbit and initial probability of collision with Earth. To date, the possibility of an impact between the planet and the asteroid has been ruled out, although a minimal possibility of collision with the Moon remains.

The purpose of this thesis is to research and analyse trajectories toward asteroid 2024 YR4 using indirect methods, with the goal of identifying solutions that allow for a transfer with minimal propellant consumption. The spacecraft under consideration has an initial mass of 1000 kg and is equipped with a low-thrust electric propulsion system. Specifically, the thesis focuses on the study of both direct trajectories and those involving Earth flyby. As the results show, flyby solutions are those that allow for the greatest fuel savings, since they effectively exploit the Earth's gravitational field. Among the solutions analysed, which envisage a mission duration of between 3 and 4.5 years, those with an arrival date prior to the possible impact with the Moon on December 22, 2032, are of particular interest. The optimization was performed using a Fortran code provided by the Polytechnic of Turin.

After introducing the basic concepts related to asteroids, orbital mechanics and space propulsion, the thesis presents the optimal control theory and the mathematical model adopted. In the final part, the solutions obtained are illustrated, analysed and compared in detail.

# Contents

Lis	st of	Figures	viii
Lis	st of	Tables	x
1	Intr 1.1 1.2	Thesis objective	2 2 2
2	Aste 2.1 2.2	eroids Classification Near-Earth asteroids 2.2.1 Asteroid impact prediction and avoidance 2.2.2 2024 YR4	4 5 6 8 10
3	3.1 3.2 3.3 3.4 3.5 3.6 3.7	Kepler's laws Newton's laws of motion and gravitational law N-body problem Two body problem Trajectory equation Characteristic speeds Coordinate systems 3.7.1 Heliocentric ecliptic coordinate system 3.7.2 Geocentric equatorial coordinate system 3.7.3 Topocentric coordinate system 3.7.4 Perifocal coordinate system Classical orbital elements Orbital manoeuvres 3.9.1 Impulsive manoeuvres 3.9.2 Low-thrust manoeuvres Interplanetary mission 3.10.1 Patched conics method 3.10.2 Phasing and launch windows 3.10.3 Planetary flyby	13 13 14 15 16 17 19 20 21 21 22 22 23 23 26 27 28 29
4	<b>Spa</b> 4.1 4.2	Ce propulsion Generalities of space propulsion Electric propulsion 4.2.1 Electrothermal propulsion 4.2.2 Electrostatic propulsion 4.2.3 Electromagnetic propulsion	31 34 34 35 38
5	Indi 5.1 5.2	irect optimization of space trajectories  Optimal control theory	<b>41</b> 41 45

6	Ma	thematical model	48
	6.1	Equations of motion	48
	6.2	Optimal controls	49
	6.3	Equations in spherical coordinates	50
	6.4	Initial conditions	52
	6.5	Boundary and optimal conditions	52
7	Mis	ssion analysis and numerical implementation	55
	7.1	Simplifying assumptions	55
	7.2	Initial data	55
	7.3	Synodic period	56
	7.4	Non-dimensional variables	56
	7.5	Code implementation and inputs	57
8	Res	sults	<b>58</b>
	8.1	Direct transfer trajectories	58
	8.2	Earth flyby transfer trajectories	63
	8.3	Later direct transfer solutions	68
	8.4	Later Earth flyby transfer solutions	70
	8.5	Trajectory options before the expected impact date	73
9	Cor	nclusions	<b>7</b> 8
Bi	bliog	graphy	80

# List of Figures

2.1	Main asteroid belt and Trojan asteroids [27]
2.2	Aten asteroids [23]
2.3	Apollo asteroids [23]
2.4	Amor asteroids [23]
2.5	Atira asteroids [23]
2.6	Torino scale [15]
2.7	Asteroid impact probability [12]
2.8	2024 YR4 orbit. Credit: ESA/PDO [2]
2.9	Graphic of the possible locations - represented by yellow points - of asteroid 2024
	YR4 on Dec. 22, 2032, as of Apr. 2, 2025 [18]
3.1	Visualization of Kepler's first law [26]
3.2	Visualization of Kepler's second law [26]
3.3	Visualization of Kepler's third law [5]
3.4	N-body problem [5]
3.5	Two body problem [5]
3.6	Conic sections [30]
3.7	Ellipse [24]
3.8	Heliocentric ecliptic coordinate system [4]
3.9	Geocentric equatorial coordinate system [5]
3.10	
3.11	Perifocal coordinate system [4]
3.12	Classical orbital elements [3]
3.13	Adjustment of apogee and perigee height [5]
3.14	Simple rotation of the line of apses [5]
3.15	Simple plane change [5]
	Hohmann transfer [28]
3.17	Patched conics method [29]
3.18	Phasing [29]
4.1	Momentum balance - thrust equation
4.2	Resistojet schematic [22]
4.3	Constricted arcjet schematic [8]
4.4	Ion thruster schematic [1]
4.5	FEEP schematic [8]
4.6	Hall thruster schematic [25]
4.7	MPD schematic [21]
4.8	PPT schematic [17]
4.9	VASIMR schematic [16]
6.1	Topocentric and inertial coordinate system [20]
8.1	Direct transfers - final mass vs $t_0$ (duration = 27)
8.2	Direct transfers - final mass vs duration $(t_0 = 181.4) \dots \dots$
8.3	Direct transfers - final mass vs $t_0$ (duration = 22.1)
8 4	Direct transfers - final mass vs $t_0$ (max duration = 27)

8.5	Solution 1 - Trajectory	)
8.6	Solution 2 - Trajectory	L
8.7	Solution 1 - Thrust	2
8.8	Solution 2 - Thrust	2
8.9	Solution 1 - Aphelion and perihelion	2
8.10	Solution 2 - Aphelion and perihelion	2
8.11	Solution 1 - Eccentricity	3
8.12	Solution 2 - Eccentricity	3
	Earth flyby transfers - final mass vs $t_0$ (duration = 21) 64	1
8.14	Earth flyby transfers - final mass vs $t_0$ (duration = 22) 64	1
8.15	Earth flyby transfers - final mass vs $t_0$ (duration = 23) 65	ó
8.16	Earth flyby transfers - final mass vs $t_0$ (duration = 24) 65	ó
8.17	Solution 3 - Trajectory	ó
	Solution 4 - Trajectory	3
	Solution 3 - Thrust	3
	Solution 4 - Thrust	3
	Solution 3 - Aphelion and perihelion	7
	Solution 4 - Aphelion and perihelion	7
	Solution 3 - Eccentricity	7
	Solution 4 - Eccentricity	7
	Solution 5 - Trajectory	3
	Solution 6 - Trajectory	)
	Solution 5 - Thrust	)
	Solution 6 - Thrust	)
8.29	Solution 5 - Aphelion and perihelion	)
8.30	Solution 6 - Aphelion and perihelion	)
8.31	Solution 5 - Eccentricity	)
8.32	Solution 6 - Eccentricity	)
8.33	Solution 7 - Trajectory	L
8.34	Solution 8 - Trajectory	2
8.35	Solution 7 - Thrust	2
8.36	Solution 8 - Thrust	2
8.37	Solution 7 - Aphelion and perihelion	3
8.38	Solution 8 - Aphelion and perihelion	3
8.39	Solution 7 - Eccentricity	3
8.40	Solution 8 - Eccentricity	3
	Earth flyby transfer - final mass vs duration ( $t_0$ =171.6)	1
8.42	Solution 9 - Trajectory	ó
8.43	Solution 10 - Trajectory	ó
8.44	Solution 9 - Thrust	3
8.45	Solution 10 - Thrust	3
8.46	Solution 9 - Aphelion and perihelion	3
8.47	Solution 10 - Aphelion and perihelion	;
8.48	Solution 9 - Eccentricity	7
8 49	Solution 10 - Eccentricity 77	7

# List of Tables

2.1	Approximate number of asteroids (N) larger than a certain diameter (D)	4
2.2	Orbital elements of 2024 YR4	10
3.1	Gravitational parameters of the main solar system bodies	17
3.2	Conic sections with eccentricity, energy and semi-major axis	18
7.1	Initial parameters for electric propulsion system	56
8.1	Direct transfers - duration and timeline comparison	58
8.2	Direct transfers - mass and $\Delta V$ comparison	58
8.3	Earth flyby transfers - duration and timeline comparison	64
8.4	Earth flyby transfers - mass and $\Delta V$ comparison	64
8.5	Later direct transfers - duration and timeline comparison	68
8.6	Later direct transfers - mass and $\Delta V$ comparison	68
8.7	Later Earth flyby transfers - duration and timeline comparison	71
8.8	Later Earth flyby transfers - mass and $\Delta V$ comparison	71
8.9	Earth flyby transfers before December 22, 2032 - duration and timeline comparison	74
8.10	Earth flyby transfers before December 22, 2032 - mass and $\Delta V$ comparison	74
9.1	Transfer solutions	78

# Chapter 1

## Introduction

Studying space trajectories toward Near-Earth Asteroids is essential for both exploration and planetary defence. NEAs are a potential resource, both for the materials they yield and because they can be used as intermediate body for long-duration missions into deep space. Beyond being a resource, however, due to their close proximity to Earth, these asteroids can be a threat to planetary security. It is therefore useful to study these objects to assess and mitigate potential impacts with both Earth and its natural satellite, the Moon.

In the past decades, interest in NEAs has grown considerably among the scientific community, driven by technological development and the need to discover adequate prevention and defence strategies. To date, numerous missions to near-Earth objects have been conducted. Among these are **OSIRIS-REx**, which was commissioned to obtain a sample from 101955 Bennu, and its successor, **OSIRIS-APEX**, which will study the physical changes of the asteroid Apophis after its close pass by Earth in 2029. Other missions of particular interest are **DART**, which was designed to test a method of planetary defence against near-Earth objects, and **DAWN**, a retired probe that was launched to explore the protoplanets Vesta and Ceres. Together with other missions and studies, these expeditions represent the growing interest in asteroid exploration.

In recent months, the asteroid 2024 YR4 has attracted particular attention. It was discovered on December 27, 2024, following a close approach to Earth. Initially, due to the limited precision with which its orbital parameters were known, a minimal probability of impact with the planet was predicted. Today, following numerous observations, it has been concluded that the risk of collision with Earth has been ruled out, while a minimal probability of impact with the Moon remains.

## 1.1 Thesis objective

The objective of this thesis was to investigate possible space trajectories toward asteroid 2024 YR4 with a satellite of initial mass 1000 kg using electric propulsion. The solutions were found using an indirect optimization method implemented in a Fortran code. Initially, the focus was on studying direct trajectories without considering constraints on the arrival date. Following the analysis and observation of the direct solutions, trajectories exploiting an Earth flyby were studied to conserve propellant, thereby reducing costs in terms of  $\Delta V$ . Finally, solutions with earlier departure dates were sought so that, for a similar duration, the arrival date at asteroid 2024 YR4 would be prior to the potential impact date, namely December 22, 2032. For both direct and flyby cases, mission durations were constrained to between 3 and 4.5 years.

### 1.2 Thesis overview

This first chapter provides a brief introduction explaining why NEAs are studied and outlining the objective of this thesis. Chapter 2 provides a description of asteroids, focusing specifically on near-

Chapter 1 Introduction

Earth asteroids and the characteristics of 2024 YR4. Chapters 3 and 4 then outline the theoretical foundations of orbital mechanics and space propulsion, focusing in particular on electric propulsion. Chapters 5 and 6 discuss optimal control theory and the mathematical model underlying space trajectories optimization. Chapter 7 introduces the assumptions and data used to find the solutions reported in Chapter 8. Finally, Chapter 9 presents the conclusions.

# Chapter 2

# Asteroids

Asteroids are rocky, metallic, or icy minor planets that orbit within the inner Solar System or share the same orbit as Jupiter. Most asteroids are concentrated in the region between Mars and Jupiter, or at a distance of 2 to 4 AU from the Sun. Instead, those that share the same orbit as Jupiter are called Trojan asteroids, which are celestial bodies that remain in stable positions near the planet's Lagrangian points L4 and L5. For the three-body problem, the Lagrangian point is defined as the point in space where the less massive body is in equilibrium with the two main bodies, that is, where the gravitational forces acting on the smaller body are balanced.

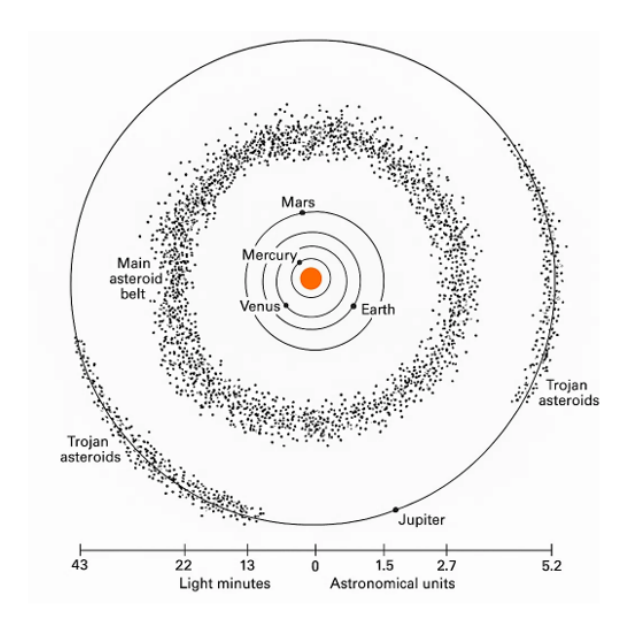


Figure 2.1: Main asteroid belt and Trojan asteroids [27]

The sizes of these celestial bodies vary greatly: from the largest asteroid, Ceres, which is also identified as a dwarf planet, with a diameter of almost 1000 km, to smaller bodies measuring less than a kilometre, many times in the order of tens of meters.

D (km)	0.1	0.3	0.5	1	3	5	10	30	50	100	200	300	500	900
N	25, 000,000	4,000,000	2,000,000	$750,\!000$	200,000	90,000	10,000	1,100	600	200	30	5	3	1

Table 2.1: Approximate number of asteroids (N) larger than a certain diameter (D)

To date, asteroids, as soon as they are discovered, are identified with a provisional designation

consisting of the year of discovery and an alphanumeric code indicating the half-month of discovery and the sequence within that half-month. Once the orbit is confirmed, a number is associated with them and in the future maybe even a name.

#### 2.1 Classification

There are several classifications into which asteroids can be divided. In particular asteroids are mainly classified based on their orbital characteristics (**orbital classification**) and based on their colour, albedo and spectral shape (**spectral classification**).

The **orbital classification** refers to the asteroid group (or family) to which the celestial body belongs. An asteroid group (or minor-planet group) refers to a population of minor planets that share similar orbits. An asteroid family, on the other hand, refers to a population of asteroids that share certain orbital parameters, such as semi-major axis, eccentricity and inclination. This latter classification is much more specific than an asteroid group. Indeed, despite sharing some orbital characteristics, the various members of an asteroid group may not be related to each other.

For spectral classification, a taxonomic system is used to divide asteroids by assigning them an asteroid spectral type based on their reflectance spectrum, colour and sometimes albedo. It is believed that these parameters are useful to understand the composition of a celestial body. For smaller bodies, the surface and internal compositions coincide in most cases. For larger bodies, however, it is known that an internal composition exists that is different from the external one. The most widely used classification is the **Tholen classification**, according to which asteroids are divided into 14 types:

#### • C-group

- C-type (e.g., 10 Hygiea): they represent 75% of the asteroids discovered to date. Since they are composed of a large amount of carbon (in addition to rocks and minerals), these objects have a low albedo. Furthermore they are volatile-rich and have an average density of about 1.7 g/cm<sup>3</sup>.
- **B-type** (e.g., 2 Pallas): spectrally blue objects whit an ultraviolet absorption below 0.5  $\mu$ m small or absent. They can be found in the outer asteroid belt and dominate the high-inclination Pallas family.
- **F-type** (e.g., 704 Interamnia): uncommon type of carbonaceous asteroids which have spectral characteristics similar to B-type asteroids but differ in the short wavelength portion of the ultraviolet spectrum below 0.4  $\mu$ m and lack the "water" absorption feature around 3  $\mu$ m indicative of hydrated minerals.
- **G-type** (e.g., 1 Ceres): uncommon type of carbonaceous asteroids which are similar to C-type objects but contain a strong ultraviolet absorption feature below 0.5  $\mu$ m and that can present an absorption feature around 0.7  $\mu$ m which is indicative of phyllosilicate minerals such as clays or mica.
- D-type (e.g., 624 Hektor): objects with very low albedo and featureless reddish spectrum. They have a composition of organic-rich silicates, carbon and anhydrous silicates, possibly with water ice in their interiors and they are found in the outer asteroid belt and beyond.
- **T-type** (e.g., 96 Aegle): inner-belt asteroids of unknown composition with dark, featureless and moderately red spectra, and a moderate absorption feature at wavelengths shorter than 0.85  $\mu$ m.

#### • S-group

- **S-type** (e.g., 15 Eunomia, 3 Juno): objects with a high density and a siliceous (i.e., stony) mineralogical composition. They represent 17% of all asteroids known to date.

- V-type (e.g., 4 Vesta): asteroids also known as Vestoids which have a spectral type that is the one of 4 Vesta. Approximately 6% of main-belt asteroids are Vestoids. They are bright and, compared to the S-types, they contain more pyroxene.

- **A-type** (e.g., 246 Asporina): relatively uncommon inner-belt asteroids that have a strong, broad 1  $\mu$ m olivine feature and a very reddish spectrum shortwards of 0.7  $\mu$ m.
- **Q-type** (e.g., 1862 Apollo): relatively uncommon inner-belt asteroids with a strong, broad 1  $\mu$ m olivine and pyroxene feature, and a spectral slope that indicates the presence of metal.
- **R-type** (e.g., 349 Dembowska): moderately bright, relatively uncommon inner-belt asteroids with a spectrum that shows distinct olivine and pyroxene features at 1 and 2  $\mu$ m, with a possibility of plagioclase.

#### • X-group

- M-type (e.g., 16 Psyche): objects that contain metal phases within them and are the main source from which iron meteorites arise. This type is the third most numerous.
- **E-type** (e.g., 44 Nysa): asteroids thought to have enstatite (MgSiO3) achondrite surfaces and with a high albedo. Their spectrum is featureless flat to reddish and they are small (only three have diameters above 50 kilometres and no others above 25 kilometres).
- P-type (e.g., 259 Aletheia, 190 Ismene): asteroids with low albedo, a featureless reddish spectrum and a composition of organic-rich silicates, carbon and anhydrous silicates, possibly with water ice in their interior. These asteroids are found in the outer asteroid belt and beyond.

Another classification based on spectral characteristics is the SMASS (Small Main-Belt Asteroid Spectroscopic Survey) classification, which divides asteroids into 24 different types. The Tholen classification, however, remains the most widely used.

Among these asteroids, a subcategory known as **Near-Earth asteroids** (**NEAs**) can be identified. These celestial bodies are asteroids with orbits close to Earth's and they will be discussed in the next section.

#### 2.2 Near-Earth asteroids

**Near-Earth Asteroids (NEAs)** are asteroids with an orbit close to Earth's. To date, several tens of thousands have been identified, and some of them may pose a risk, albeit low, of impacting our planet. To assess the possibility of a collision, asteroid impact prediction is used, a set of methods and systems that allow the estimation of the probability of an impact and the prediction, with some advance notice, of where and when such an event might occur.

Based on their orbital elements, NEAs can be divided into four types (q = perihelion distance, Q = aphelion distance, a = semi-major axis):

• Atens: asteroids with a semi-major axis less than 1 AU;



 $\begin{array}{c} a < 1.0 \text{ AU} \\ Q > 0.983 \text{ AU} \end{array}$ 

Figure 2.2: Aten asteroids [23]

• Apollos: asteroids with a semi-major axis greater than 1 AU and a perihelion radius less than 1.017 AU;

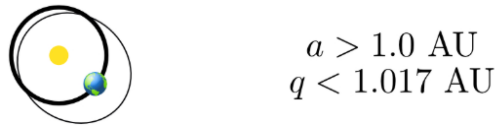


Figure 2.3: Apollo asteroids [23]

• Amors: asteroids with a mean orbital radius between that of Earth and Mars and a perihelion slightly outside Earth's orbit (about 1.017–1.3 AU).

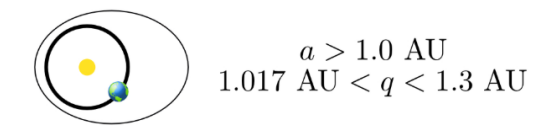


Figure 2.4: Amor asteroids [23]

• Atiras: asteroids with orbits contained entirely within that of the Earth.



$$\begin{array}{c} a < 1.0 \text{ AU} \\ Q < 0.983 \text{ AU} \end{array}$$

Figure 2.5: Atira asteroids [23]

NEAs represent both a potential resource for future space exploration and a threat to the planet. Their proximity to Earth makes them relatively easy to reach.

Rather than NEAs, a more general term Near-Earth Objects (NEOs) is used. This term also includes comets, which, however, represent only 1% of the total population (most NEOs are asteroids).

There are various classification methods that can be used to assess the impact risk of a near-Earth object, including two main ones:

- Torino scale;
- Palermo scale.

The **Torino scale** is an indicator of the danger posed by a NEO impact with Earth. This classification allows an object to be assigned an integer (no fractions or decimals are used) ranging from 0 to 10 based on the statistical probability of collision with Earth and the kinetic energy released by the impact itself in megatons. A number of 0 identifies asteroids with a zero probability of collision or whose impact with Earth would have effects comparable to those of normal space dust. A number of 10 indicates a certain collision, with potentially disastrous consequences.

The following figure shows a graph that, based on the kinetic energy released upon impact and the probability of impact, enables the determination of a specific level of danger for the NEO. Specifically:

- in white  $\Rightarrow$  zero risk;
- in green  $\Rightarrow$  extremely low probability of collision;

- in yellow  $\Rightarrow$  worthy of astronomers' attention;
- in orange ⇒ events of concern;
- in red  $\Rightarrow$  certain collision.

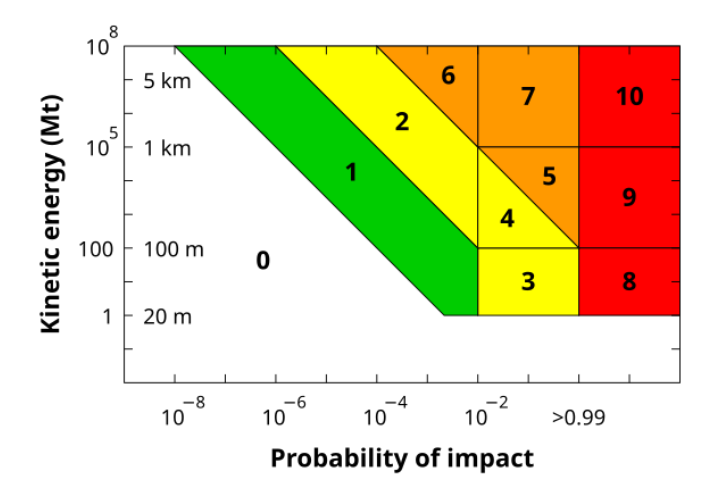


Figure 2.6: Torino scale [15]

The **Palermo scale** is similar but more technical and complex. Here too, both the probability of impact and the kinetic energy released by such a collision are combined into a single value. A risk value of 0 indicates a risk equal to the background risk, which is the average risk that another object of the same or greater size might impact Earth within the same time frame, i.e., up to the possible impact date. A reading of +2 implies a risk that is 100 times greater than the background risk. Scores under -2 on the Palermo scale indicate situations for which no severe consequences are expected, and scores ranging from -2 to 0 indicate situations to be watched with caution.

The P-value of the Palermo scale is defined as follows:

$$P = \log_{10} \frac{p_i}{f_B T} \tag{2.1}$$

where  $p_i$  is the probability of impact and the denominator represents the background risk over time (in T years) that elapses before the possible impact. The annual background risk, i.e., the annual frequency of an impact, is calculated as follows:

$$f_B = 0.03E^{-0.8} (2.2)$$

where E represents the energy released by the impact in megatons.

Obviously, the more observations of an asteroid are made, the more precise the trajectory prediction will be, and consequently the risk value may vary.

#### 2.2.1 Asteroid impact prediction and avoidance

Predicting the impact of a near-Earth object with the Earth consists of 3 main phases:

- 1. Discovery of the asteroid and preliminary definition of its orbit through an observation typically lasting less than two weeks.
- 2. Further observations to improve orbit determination.
- 3. Calculate if, where, and when the asteroid's orbit may intersect Earth's in the future.

In most cases, a new asteroid is discovered using a telescope with a large Field of View (FoV), taking images and using software to compare them with other observations of the same portion of the sky obtained in previous days. Calculations relating to the intersection of the various orbits are then carried out by two independent systems: one managed by NASA (Sentry) and one by ESA (NEODyS).

To predict a future impact, it is important to define the **minimum orbital intersection distance** (MOID). This parameter corresponds to the minimum distance between the two closest points of the two orbits. If this value is less than 0.05 AU and the asteroid has an absolute magnitude brighter than 22, which implies that the object is large enough and may be dangerous, then it can be considered a potentially hazardous asteroid.

It is obviously useful to run simulations after determining the initial orbit to assess the likelihood of an impact. If the distance between the asteroid and the centre of the Earth is calculated to be less than the planet's radius, then a potential future impact is predicted.

The following figure shows an elliptical view of the possible predicted positions of an asteroid relative to Earth as observations are made.

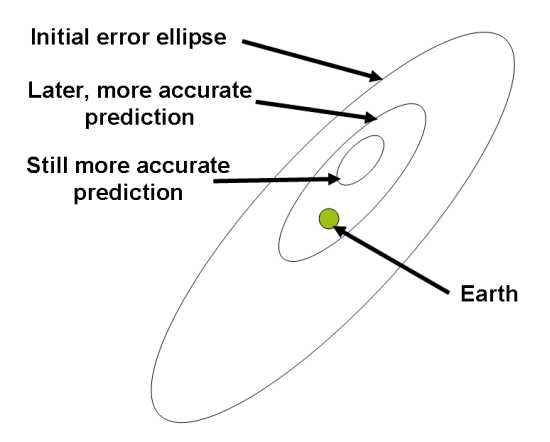


Figure 2.7: Asteroid impact probability [12]

Over time, and hence with an increasing number of observations, the orbit and future positions are increasingly more precise, and consequently the ellipse shrinks. If, as the ellipse shrinks, the Earth or body in question remains within the ellipse, the probability of collision increases. On the other hand, if, as observations are made, the ellipse becomes narrower until it excludes the Earth, the danger of impact drops sharply until it is negligible. This is why the probability of collision will initially rise with increasing observations and then, in certain situations, plummet.

Countermeasures can be implemented to prevent a possible asteroid impact with Earth in the future. The two major asteroid impact avoidance methods are fragmentation and delay. The goal of the first method is to render the asteroid harmless by breaking it in such a manner that either its fragments miss Earth or burn up in the atmosphere. The other strategy seeks to delay (or advance) the arrival of the asteroid at the impact location in order to avoid the collision between the two bodies.

In general, methods differ based on the type of mitigation (deflection or fragmentation), the source of energy and the approach strategy to the NEO.

One of the test missions in planetary defence was the **Double Asteroid Redirection Test** (**DART**). The target of the mission was Dimorphos, a minor-planet moon of the asteroid Didymos. The mission was successful, and by momentum transfer from the probe to the asteroid, the

Dimorphos orbit was shortened by 32 minutes, well beyond the pre-defined success metric of 73 seconds.

#### $2.2.2 \quad 2024 \text{ YR4}$

Asteroid 2024 YR4 is a Near-Earth asteroid with dimensions ranging from 40 to 100 meters in diameter. NASA's estimated average diameter is 58.42 meters. Specifically, it is classified as an Apollo asteroid, meaning, as previously mentioned, an asteroid with a semi-major axis greater than 1 AU and a perihelion radius less than 1.017 AU. 2024 YR4 was discovered on December 27, 2024, by the Asteroid Terrestrial-impact Last Alert System (ATLAS) program.

From preliminary observations carried out using the Gran Telescopio Canarias and the Lowell Discovery Telescope, it has been concluded that 2024 YR4 is a rocky asteroid of the S or L type of the SMASS classification, types of asteroids that correspond to the S group of the Tholen classification.

Using the Very Large Telescope (VLT) and the 1.54-meter Danish telescope at the La Silla Observatory, the rotation period of this asteroid was observed to be 19.5 minutes. The revolution period can be calculated using the semi-major axis of the orbit of 2024 YR4 as follows:

$$T = 2\pi \sqrt{\frac{a^3}{\mu_{\odot}}} \tag{2.3}$$

where:

- semimajor axis:  $a = 2.5158704 \,\mathrm{AU} = 3.7637 \cdot 10^8 \,\mathrm{km}$
- solar standard gravitational parameter:  $\mu_{\odot} = 1.32712440018 \cdot 10^{11} \frac{\mathrm{km}^3}{\mathrm{s}^2}$

It is thus obtained a revolution period equal to  $T = 1457.574 \,\mathrm{days} = 3.9934 \,\mathrm{years}$ .

Below are orbital parameters and other characteristics related to 2024 YR4.

Parameter	Value
Semimajor axis $a$	2.5158704 AU
Eccentricity e	0.66154859
Inclination $i$	3.40818°
Argument of perihelion $\omega$	134.36136°
Longitude of ascending node $\Omega$	271.36562°
Mean anomaly $M$	40.4025104°
Absolute magnitude $H$	23.96
Slope parameter $G$	0.15

Table 2.2: Orbital elements of 2024 YR4

As can be immediately noted from the orbital parameters, the type of orbit is slightly inclined but very eccentric, with a semi-major axis such that the value of the apogee radius almost reaches that of Jupiter, as can be seen from the figure 2.8. In particular, the apogee and perigee radii are:

$$\begin{cases} r_a = a(1+e) = 4.17 \,\text{AU} \\ r_p = a(1-e) = 0.85 \,\text{AU} \end{cases}$$
 (2.4)

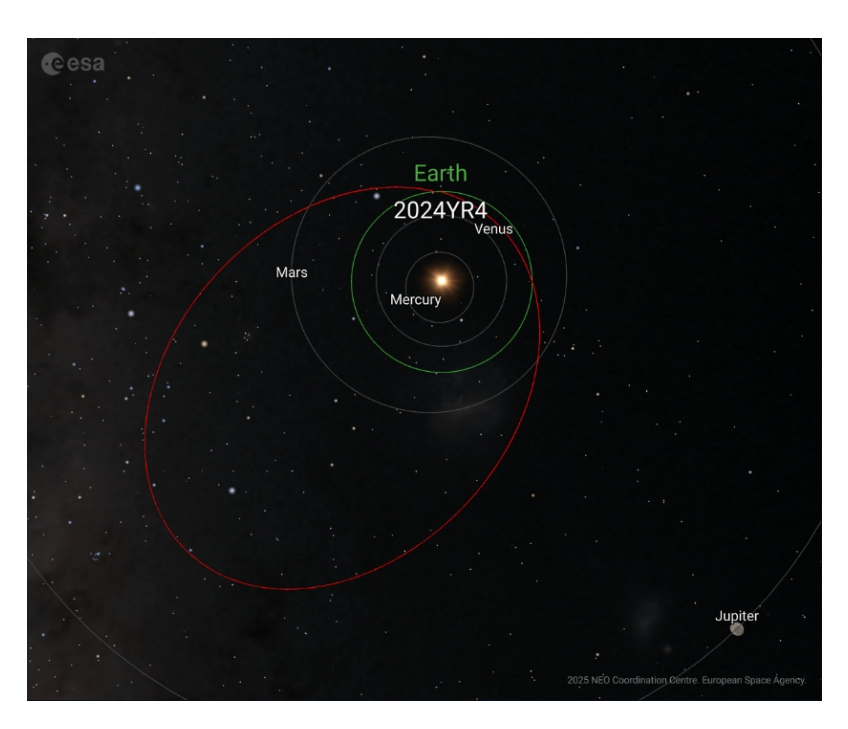


Figure 2.8: 2024 YR4 orbit. Credit: ESA/PDO [2]

Regarding its mass, considering a density of  $2.6\,\mathrm{g/cm^3}$ , NASA estimates it to be  $2.2\cdot10^8\,\mathrm{kg}$ . Considering the approximate values of mass, density and size together with an impact velocity of  $17.32\,\mathrm{km/s}$ , a collision between this asteroid and the Earth would release energy equal to 8 megatons of TNT equivalent, enough energy to generate an explosion that would cause localized destruction up to 50 km from the impact site.

To date, however, after having reached a hazard index of 3 on the Torino scale on January 25, 2025, and a value of -0.32 on the Palermo scale on February 6, 2025, the risk of collision with the Earth has almost disappeared on February 25, 2025, reaching an impact probability of 0.001%, which corresponds to a value of 0 on the Torino scale.

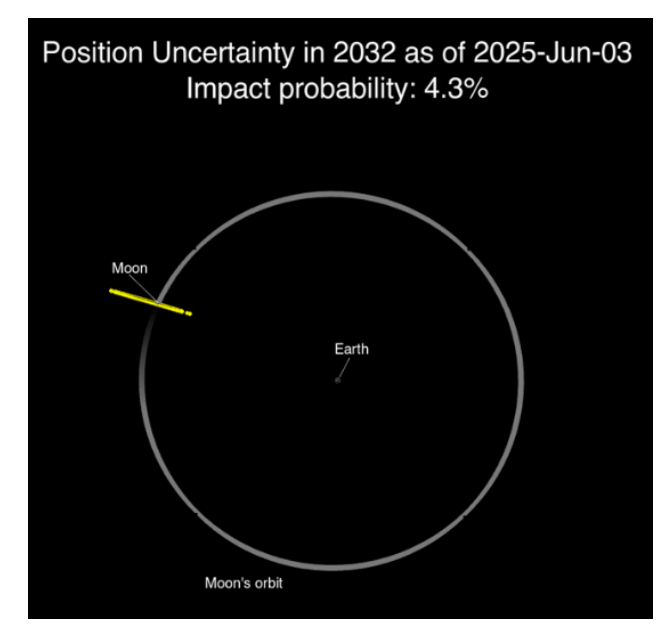


Figure 2.9: Graphic of the possible locations - represented by yellow points - of asteroid 2024 YR4 on Dec. 22, 2032, as of Apr. 2, 2025 [18]

Although the possibility of the asteroid impacting Earth has practically dropped to zero, there remains a minimal probability that it could impact the Moon. The latest update available on the NASA website (data provided by the Jet Propulsion Laboratory) is dated June 3, 2025. Compared to the previous update, dated April 2, 2025, the probability of impact with the natural satellite has increased from 3.8% to 4.3%. Figure 2.9 shows the predicted position of 2024 YR4 as of December 22, 2032.

An impact of this asteroid with the Moon would create a crater between 500 and 2,000 meters in diameter, releasing an energy equivalent to 5.2 megatons. However, the collision would not cause any change in the Moon's orbit.

In Chapter 8, the orbital trajectories optimized to reach the asteroid will be analysed, considering both direct transfers and Earth flybys.

# Chapter 3

## Fundamentals of orbital mechanics

This chapter introduces the fundamental principles of orbital mechanics, from Kepler's laws to interplanetary missions. In short, astrodynamics, another name for orbital mechanics, involves the application of the laws of ballistics and celestial mechanics to rockets, satellites and spacecrafts. It is therefore useful to understand these concepts in order to design trajectories toward NEAs.

### 3.1 Kepler's laws

Around the early 1600s, Kepler formulated three laws concerning the motion of the planets. Before him, several theories of celestial mechanics already existed, including those of Aristotle and Ptolemaeus, who believed in geocentrism, and that of Kopernik, the first astronomer to formulate a scientific-based heliocentric cosmology.

Kepler, on the other hand, believed in a sort of "celestial harmony" and, like Copernicus, thought that the planets were bright spots on a concentric sphere with the Sun at the centre. He was the first to introduce the idea that planetary orbits could be elliptical. The first two laws he formulated were presented in his *Astronomia Nova* in 1609, while the third law was announced in the *Harmonices Mundi* in 1619:

#### • First Law

The orbit of each planet is an ellipse with the Sun at one focus.

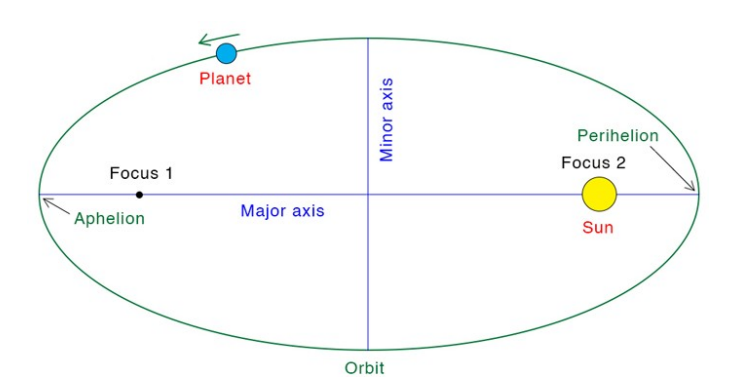


Figure 3.1: Visualization of Kepler's first law [26]

#### • Second Law

The line from the Sun to a planet sweeps out equal areas in equal time.

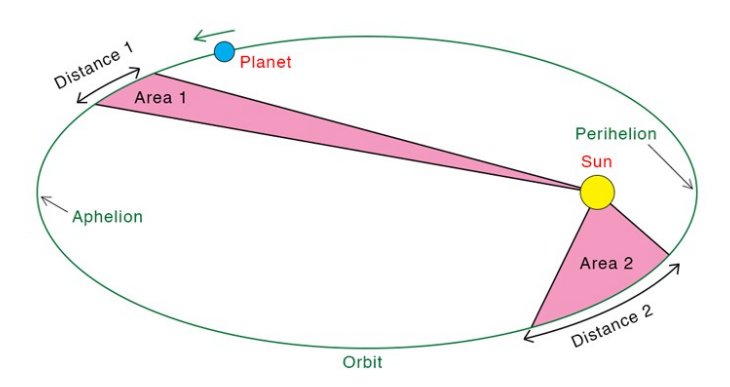


Figure 3.2: Visualization of Kepler's second law [26]

#### • Third Law

The squares of the orbital periods of the planets are proportional to the cubes of their mean distances from the Sun.

This law can be written by symbol as follows:

$$T^2 \propto a^3 \tag{3.1}$$

where T is the orbital period and a is the semimajor axis. Figure 3.3 shows a log-log graph with the orbit's semi-major axis on the x-axis and the orbital period of some celestial bodies in the solar system on the y-axis. Note how the value  $a^3/T^2$ , represented by the green line, remains constant.

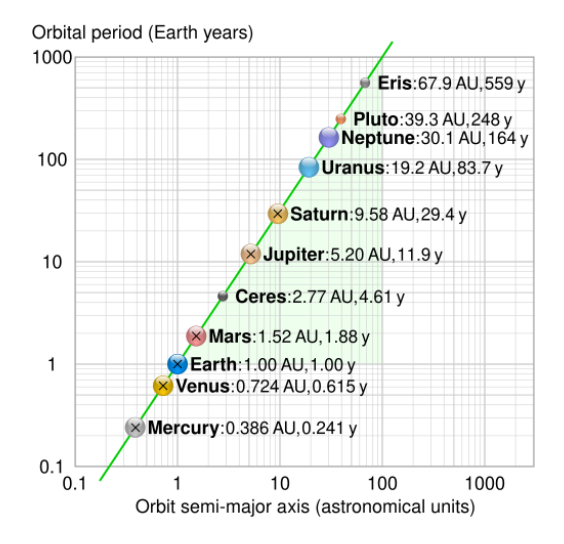


Figure 3.3: Visualization of Kepler's third law [5]

## 3.2 Newton's laws of motion and gravitational law

In 1687, in his work *Philosophiae Naturalis Principia Mathematica*, Isaac Newton formulated the three laws of motion and the law of universal gravitation. While Kepler's laws are useful only for describing orbits, Newton's laws are used to explain planetary motion.

The three laws of motion are as follows:

#### • Newton's First Law

Every body maintains its state of rest or uniform rectilinear motion if the sum of the forces acting on it is zero.

#### • Newton's Second Law

The resultant force acting on a body is directly proportional to the product of its mass and its acceleration, with which it shares direction and orientation.

$$\vec{F} = m\vec{a} \tag{3.2}$$

#### • Newton's Third Law

If a body A exerts a force on a body B, then body B exerts an equal and opposite force on A.

The law of universal gravitation states that two bodies, whose masses are denoted by M and m, respectively, attract each other along the line joining them with a force proportional to the product of their masses and inversely proportional to the square of the distance between them.

$$F = -G\frac{Mm}{r^3}\vec{r} \tag{3.3}$$

where r is the distance between the two bodies and G is the universal gravitational constant, which is equal to  $G = 6.673 \cdot 10^{-11} \frac{m^3}{kq \, s^2}$ .

### 3.3 N-body problem

It is possible to extend Newton's gravitational law to a system of n-bodies, each of which is subject to the gravitational attraction of the others.

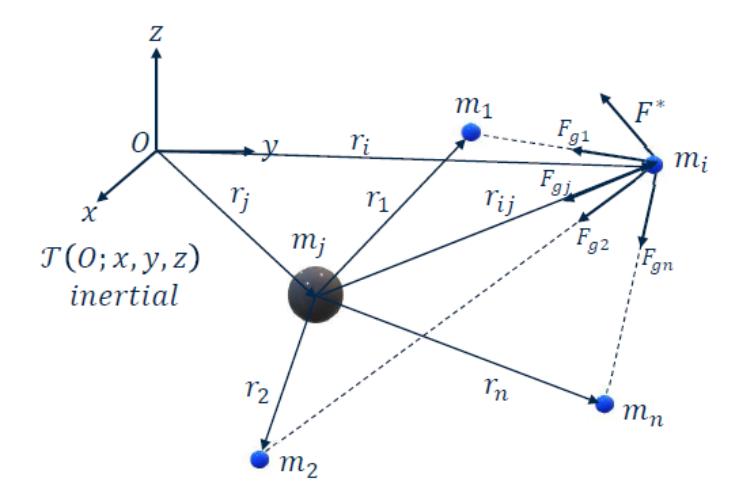


Figure 3.4: N-body problem [5]

Considering an inertial system of n-masses, the force acting on the i-th body can be written as follows:

$$\vec{F} = \vec{F}^* + \sum_{j=1, j \neq i}^{n} \vec{F}_{gj}$$
(3.4)

where  $\vec{F}$  indicates the non-gravitational resultant force (such as forces due to imperfect symmetry of a body, the thrust generated by a spacecraft or atmospheric drag), while  $\vec{F}_{gj}$  is the force that

the j-th body exerts on the i-th mass.

Substituting the formula 3.3 for this last term, it is obtained:

$$\vec{F} = \vec{F}^* - Gm_i \sum_{j=1, j \neq i}^{n} \frac{m_j}{r_{ij}^3} \vec{r}_{ij}$$
(3.5)

Now introducing Newton's second law:

$$\vec{F} = \frac{d}{dt} \left( m_i \vec{v}_i \right) \tag{3.6}$$

and neglecting the term related to non-gravitational forces, it is possible to derive the formula of the n-body problem:

$$\ddot{\vec{r}}_i = -G \sum_{j=1, j \neq i}^n \frac{m_j}{r_{ij}^3} \vec{r}_{ij}$$
 (3.7)

### 3.4 Two body problem

The two-body problem is a simplification of the n-body case. Before deriving the corresponding formulas, some assumptions must be made:

- the system is composed of two masses  $m_1$  and  $m_2$  with  $m_1 > m_2$ ;
- other than gravitational forces, no other forces act on the system;
- the bodies are spherically symmetric.

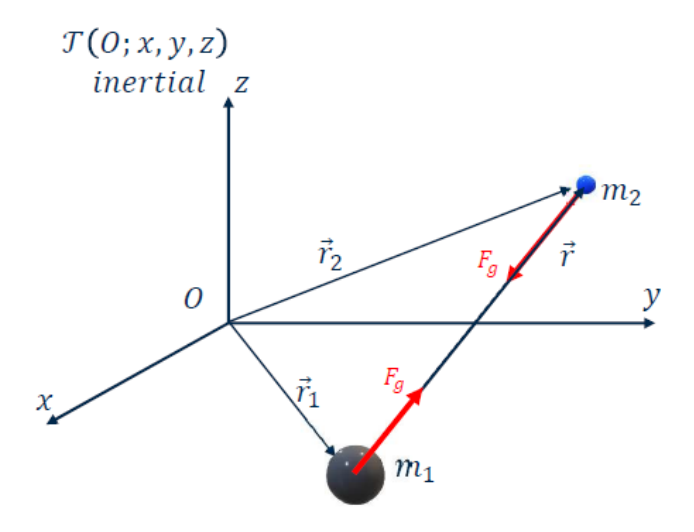


Figure 3.5: Two body problem [5]

By writing the law of universal gravitation for each mass and also using Newton's second law, the following formulation can be derived:

$$\ddot{\vec{r}} = -G \frac{m_1 + m_2}{r^3} \vec{r} \tag{3.8}$$

Considering that the cases of interest mainly concern a satellite of mass m orbiting a celestial body of mass M, with M >> m, the formula becomes:

$$\ddot{\vec{r}} + \frac{\mu}{r^3} \vec{r} = 0 \tag{3.9}$$

where  $\mu$  is the gravitational parameter and is defined as:

$$\mu \triangleq GM \tag{3.10}$$

The value of  $\mu$  varies from one celestial body to another:

Body	Symbol	$\mu \left(m^3  s^{-2}\right)$
Sun	$\mu_{\odot}$	$1.32712440018 \times 10^{20}$
Mercury	$\mu_{\coloredge}$	$2.2032 \times 10^{13}$
Venus	$\mu_{\mathbb{Q}}^{T}$	$3.24859 \times 10^{14}$
Earth	$\mu_{\oplus}$	$3.986004418 \times 10^{14}$
Moon	$\mu_{\mathbb{Q}}$	$4.9048695 \times 10^{12}$
Mars	$\mu_{\sigma}$	$4.282837 \times 10^{13}$
Jupiter	$\mu_{2}$	$1.26686534 \times 10^{17}$
Saturn	$\mu_{\begin{subarray}{c} \mu_{\begin{subarray}{c} h \end{subarray}}$	$3.7931187 \times 10^{16}$
Uranus	$\mu_{\delta}$	$5.793939 \times 10^{15}$
Neptune	$\mu_{\Xi}$	$6.836529 \times 10^{15}$
Pluto	$\mu_{P}^{O}$	$8.71 \times 10^{11}$

Table 3.1: Gravitational parameters of the main solar system bodies

Before integrating the equation of motion to obtain the trajectory equation, it's possible to consider some constants of motion. In particular, the gravitational field is conservative, so an object moving under the influence of gravity neither gains nor loses mechanical energy. This is therefore a constant of motion and is obtained from the sum of kinetic and potential energy. In orbital mechanics, it is common to refer to the specific energy  $\epsilon$ :

$$\epsilon = \frac{v^2}{2} - \frac{\mu}{r} = -\frac{\mu}{2a} = \text{constant} \tag{3.11}$$

This means that at points in the orbit where potential energy is low, kinetic energy will be high, and vice versa. For example, at perigee, where the velocities involved are highest, there will be a greater contribution of kinetic energy and a smaller contribution of potential energy than at apogee, where the opposite occurs.

From the equation 3.11, it's possible to derive the vis-viva equation:

$$v^2 = \mu \left(\frac{2}{r} - \frac{1}{a}\right) \tag{3.12}$$

In addition to mechanical energy, another quantity that remains constant throughout the orbit is the specific angular momentum:

$$\vec{h} = \vec{r} \times \vec{v} = \text{constant} \tag{3.13}$$

From the above equation, it can be observed that the angular momentum vector is perpendicular to the plane containing  $\vec{r}$  and  $\vec{v}$ . The conservation of this quantity therefore implies that the trajectory of the satellite remains confined in a plane called the orbital plane.

### 3.5 Trajectory equation

Rewriting the equation of motion as follows:

$$\ddot{\vec{r}} = -\frac{\mu}{r^3}\vec{r} \tag{3.14}$$

and multiplying both terms by  $\vec{h}$  and then integrating, the following equation is obtained:

$$r = \frac{\frac{h^2}{\mu}}{1 + \frac{B}{\mu}\cos\nu} \tag{3.15}$$

where  $\vec{B}$  is a constant of integration and  $\nu$ , the true anomaly, is the angle between  $\vec{B}$  and  $\vec{r}$ . Considering that the radius assumes its minimum value when the denominator is maximum, i.e. for  $\cos \nu = 1$  or  $\nu = 0$ , it follows that that  $\vec{B}$  is a vector pointing to the periastron.

The equation 3.15, which is expressed in polar coordinates, can be compared to that of a conic section:

$$r = \frac{p}{1 + e\cos\nu} = \frac{a(1 - e^2)}{1 + e\cos\nu}$$
 (3.16)

where e is the eccentricity, which is useful to identify the type of curve followed by the spacecraft, and p is the semilatus rectum, defined as the ratio between the square of the specific angular momentum and the gravitational parameter:

$$p = \frac{h^2}{\mu} \tag{3.17}$$

More precisely, the trajectory travelled by the spacecraft can be of four types: circular, elliptical, parabolic or hyperbolic.

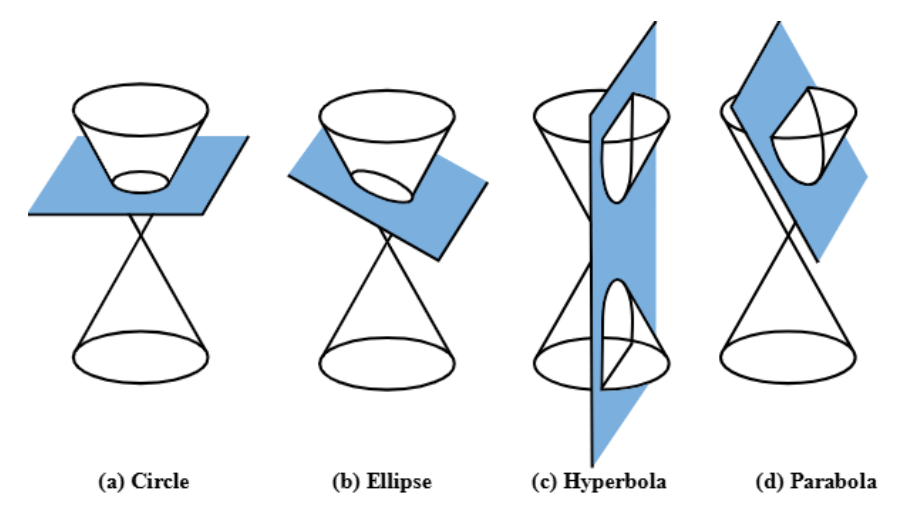


Figure 3.6: Conic sections [30]

The value of the eccentricity allows an immediate identification of the corresponding case.

Conic Type	Eccentricity $e$	Specific Energy $\varepsilon$	Semi-major Axis $a$
Circle	0	$\varepsilon < 0$	a = r
Ellipse	0 < e < 1	$\varepsilon < 0$	a > 0
Parabola	e = 1	$\varepsilon = 0$	$a \to \infty$
Hyperbola	e > 1	$\varepsilon > 0$	a < 0

Table 3.2: Conic sections with eccentricity, energy and semi-major axis

In particular, the conic section of greatest interest is the ellipse, since, as already seen from Kepler's laws, the planets (and more generally the celestial bodies) are characterized by an elliptical orbit with the Sun positioned at one focus.

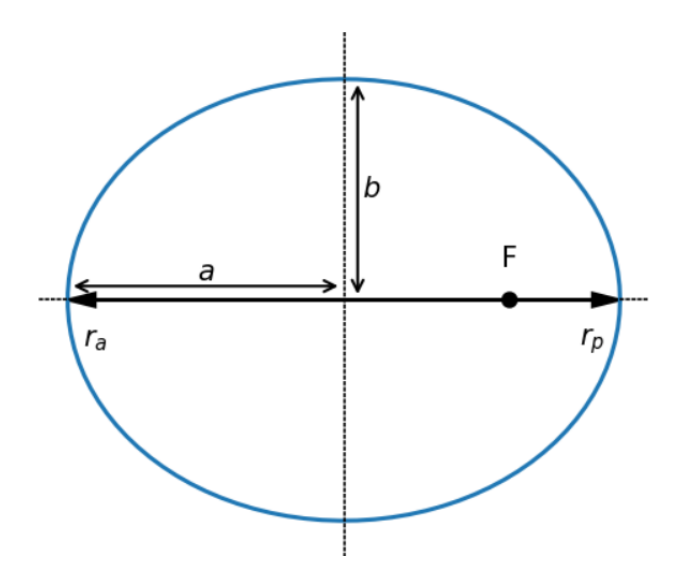


Figure 3.7: Ellipse [24]

The main parameters characterizing a conic section are derived below.

• Eccentricity

$$e = \frac{r_a - r_p}{r_a + r_p} \tag{3.18}$$

• Semimajor axis

$$a = \frac{r_a + r_p}{2} \tag{3.19}$$

• Periapsis

$$r_p = a(1 - e) (3.20)$$

• Apoapsis

$$r_p = a(1+e)$$
 (3.21)

• Semilatus rectum

$$p = a(1 - e^2) (3.22)$$

### 3.6 Characteristic speeds

From the conservation of mechanical energy, it is possible to derive some characteristic velocities.

#### Circular speed

Circular speed is the velocity required to maintain a satellite in a circular orbit of radius r = a.

$$v_c = \sqrt{\frac{\mu}{r}} \tag{3.23}$$

From the formula 3.23, it can be observed that larger values of the radius correspond to lower circular velocities and vice versa. This means that the further away one is from the main body, the lower the velocity required to maintain a satellite in a circular orbit.

#### Escape speed

Escape speed is the minimum velocity a satellite must have to be able to move indefinitely away from a force field to which it is subjected. It is therefore the speed at which it is possible to "escape" from a body's gravitational field.

$$v_e = \sqrt{\frac{2\mu}{r}} = \sqrt{2}v_c \tag{3.24}$$

Starting from this velocity, at a distance  $r \to \infty$  the velocity will be  $v_{\infty} \to 0$ 

#### Hyperbolic excess velocity

Hyperbolic excess velocity is the residual velocity of a spacecraft upon exiting the sphere of influence of the main body, i.e., the velocity at  $r_{\infty}$ .

$$v_e = \sqrt{-\frac{\mu}{a}} \tag{3.25}$$

It is interesting to note that the minus sign appears under the root since, if there is a residual velocity upon exiting the sphere of influence, the satellite will move along a hyperbolic trajectory characterized by a < 0.

### 3.7 Coordinate systems

This section describes the main coordinate systems used in orbital mechanics. Depending on the type of mission considered, it may be more convenient to refer to one system rather than another.

#### 3.7.1 Heliocentric ecliptic coordinate system

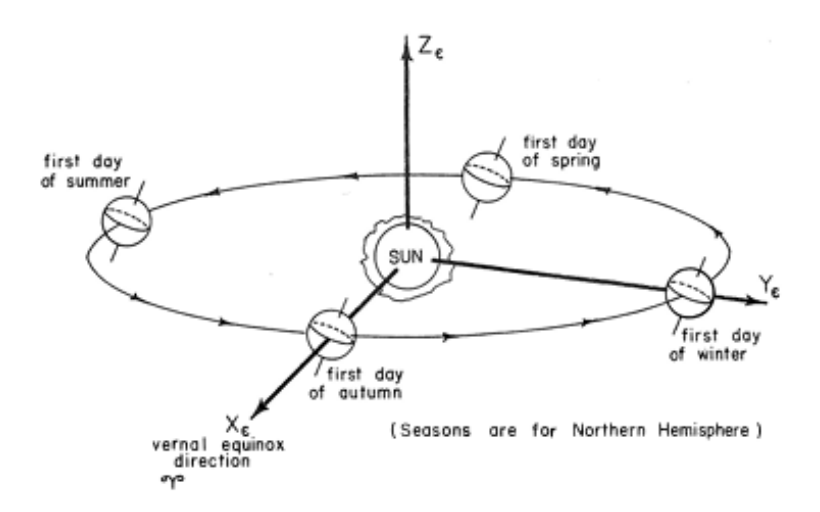


Figure 3.8: Heliocentric ecliptic coordinate system [4]

The heliocentric ecliptic coordinate system is used primarily to describe the motion of bodies within the solar system and is therefore a useful reference system for studying and analysing interplanetary transfers. The origin of the coordinate system is the Sun and the fundamental plane is the ecliptic plane (the plane defined by the Earth's orbit around the Sun), spanned by  $\hat{X}$  and  $\hat{Y}$ . The  $\hat{X}$  axis is identified by the intersection of the ecliptic plane with the equatorial plane during the autumnal equinox (or vernal equinox). This direction is the one in which the Earth, during the vernal equinox, views the Sun in the Aries constellation. The  $\hat{Z}$  axis is perpendicular to the ecliptic plane and directed toward the hemisphere containing Polaris. Finally, the  $\hat{Y}$  axis completes the right-hand triad.

#### 3.7.2 Geocentric equatorial coordinate system

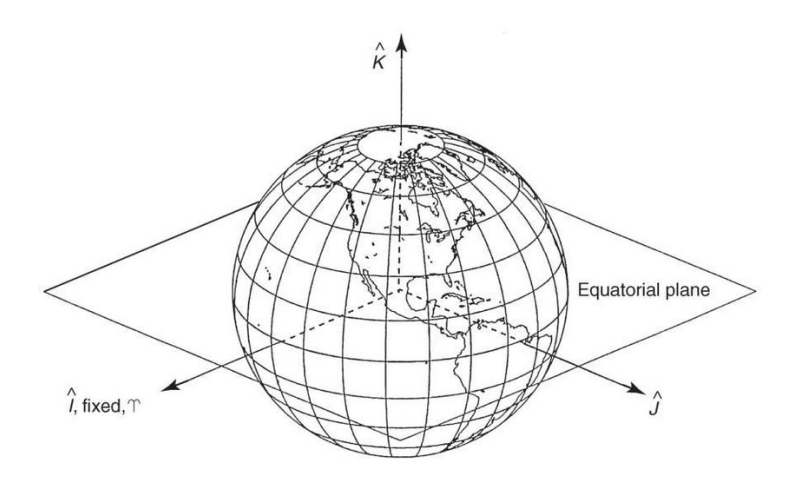


Figure 3.9: Geocentric equatorial coordinate system [5]

The equatorial geocentric reference system, also called Earth-Centred Inertial (ECI) system, is used primarily to describe the motion of objects around the Earth (for example, the position of Earth's satellites) or to determine the position of celestial bodies relative to the Earth (in this case, it refers mainly to astronomical studies). The origin of this coordinate system is the centre of the Earth and the fundamental plane is the equatorial plane, defined by  $\hat{I}$  and  $\hat{J}$ . The  $\hat{I}$  axis is always parallel to the  $\hat{X}$  axis of the heliocentric elliptic coordinate system, the  $\hat{K}$  axis is perpendicular to the equatorial plane, pointing toward the hemisphere containing Polaris, and the  $\hat{J}$  axis completes the right-hand triad.

#### 3.7.3 Topocentric coordinate system

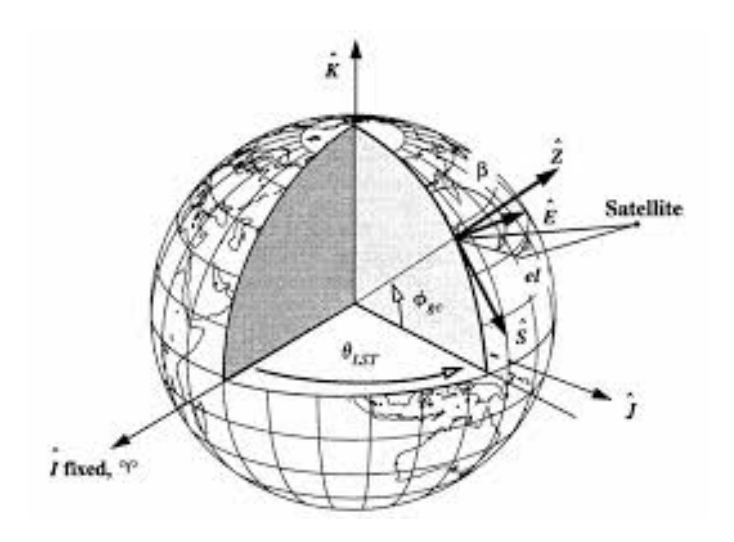


Figure 3.10: Topocentric coordinate system [5]

The topocentric coordinate system is used mainly for the Earth satellite observation. The origin of this reference system is the observation point (topos) on the Earth's surface and the fundamental plane is that of the local horizon, identified by  $\hat{S}$  and  $\hat{E}$ . The  $\hat{Z}$  axis is directed toward the zenith (radially) outward from the site, the  $\hat{S}$  axis is identified by the intersection of the local horizon with the local meridian and is directed South, and the  $\hat{E}$  axis is defined by the intersection of the local horizon with the plane passing through the local parallel and is directed East.

#### 3.7.4 Perifocal coordinate system

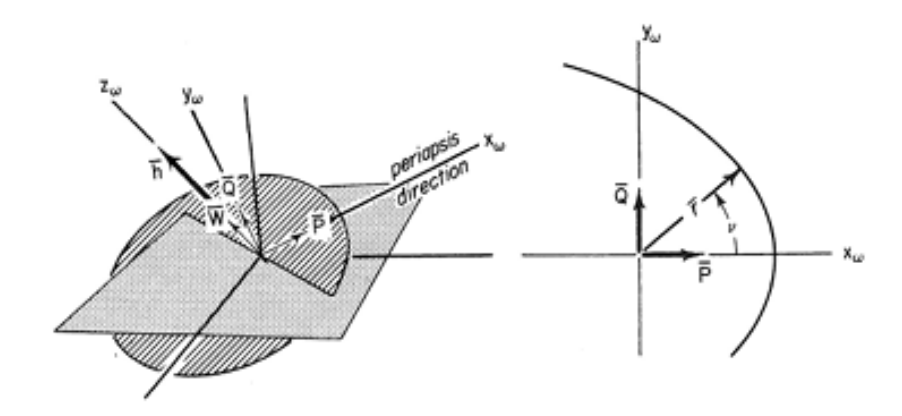


Figure 3.11: Perifocal coordinate system [4]

The perifocal coordinate system is used to describe the motion of a body along its orbit. The origin of this system is the centre of the Earth and the fundamental plane is the orbital plane, defined by  $\hat{p}$  and  $\hat{q}$ . The  $\hat{p}$  axis is directed toward the perigee, the  $\hat{q}$  axis is offset 90° from the  $\hat{p}$  axis in the direction of the satellite's motion (identifying the semilatus rectum) and the  $\hat{w}$  axis is normal to the orbit.

#### 3.8 Classical orbital elements

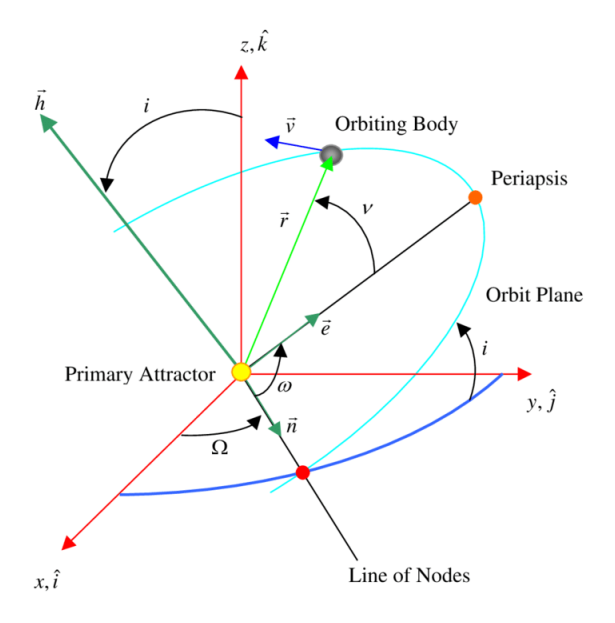


Figure 3.12: Classical orbital elements [3]

Classical orbital elements are used in a two-body system to describe a Keplerian orbit. There are six parameters in total to describe an orbit:

- eccentricity (e): defines the shape of the orbit, describing how much it deviates from a perfect circle. The values this parameter can assume are listed in Table 3.2;
- semi-major axis (a): defines the size of the orbit and is positive for elliptical orbits, infinite for parabolic trajectories and negative for hyperbolic ones;

- inclination (i): defines the inclination of the orbital plane and is the angle measured between the unit vector  $\hat{K}$  and the angular momentum vector  $\hat{h}$ ;
- right ascension of the ascending node  $(\Omega)$ : is the angle measured eastward between the  $\hat{I}$  axis of the non-rotating reference frame and the ascending node, i.e., the point where the spacecraft crosses the fundamental plane while moving in the northerly direction;
- argument of periapsis ( $\omega$ ): is the angle measured in the direction of the satellite in the orbital plane between the ascending node and the periapsis;
- true anomaly ( $\nu$ ): is the angle measured in the orbital plane between the periapsis and the position of the satellite at "epoch", or at  $t_0$ .

The eccentricity and the semi-major axis determine the conic section. The inclination and the right ascension of the ascending node determine the orbital plane. The argument of periapsis defines the orientation of the orbit within that plane, and the true anomaly is used to identify the position of the satellite.

#### 3.9 Orbital manoeuvres

To study interplanetary missions, it is useful to analyse the main space manoeuvres, distinguishing between impulsive ones, typical of chemical propulsion, and low-thrust ones, typical of electric propulsion.

#### 3.9.1 Impulsive manoeuvres

Impulsive manoeuvres are those in which finite variations in velocity occur in a very short time interval. For calculation purposes, in fact, an infinitesimal  $\Delta t$  is typically considered necessary for the manoeuvre, and consequently the position of the spacecraft is fixed ( $\vec{r} = \text{constant}$ ).

#### Adjustment of apogee and perigee height

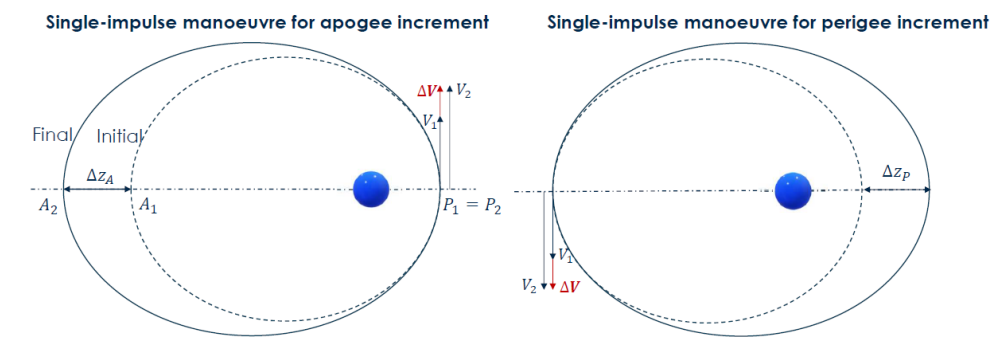


Figure 3.13: Adjustment of apogee and perigee height [5]

Figure 3.13 shows the manoeuvres useful for raising apogee and perigee. In general,  $\Delta V$  is applied when the spacecraft is on the line of apses: near perigee to raise apogee and vice versa. The cost in terms of  $\Delta V$  for this manoeuvre is as follows:

$$\Delta V = V_2 - V_1 = \sqrt{2\left(\frac{\mu}{r_P} - \frac{\mu}{r_P + r_{A2}}\right)} - \sqrt{2\left(\frac{\mu}{r_P} - \frac{\mu}{r_P + r_{A1}}\right)}$$
(3.26)

The same reasoning and formula apply to lowering perigee and apogee, which require  $\Delta V$  in the opposite direction to the motion, i.e., braking.

#### Simple rotation of the line of apses

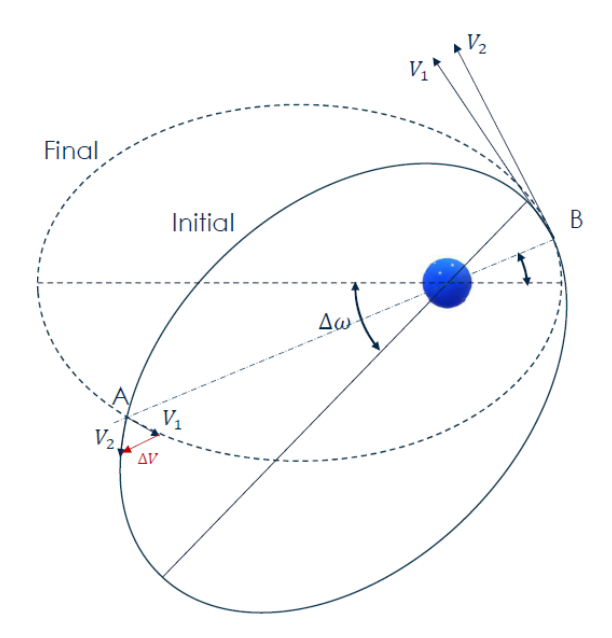


Figure 3.14: Simple rotation of the line of apses [5]

In order to rotate the line of apses by a certain angle  $\Delta\omega$  without altering the shape and size of the orbit, it is necessary to perform the manoeuvre at the point where the initial and final ellipses intersect on the bisector of the angle  $\Delta\omega$ , that is:

$$\nu = \frac{\Delta\omega}{2} \quad \text{or} \quad \nu = \frac{\Delta\omega}{2} + \frac{\pi}{2}$$
 (3.27)

The cost in terms of  $\Delta V$  to perform this manoeuvre is as follows:

$$\Delta V = 2\frac{\mu}{h}e\left|\sin\left(\frac{\Delta\omega}{2}\right)\right| \tag{3.28}$$

#### Simple plane change

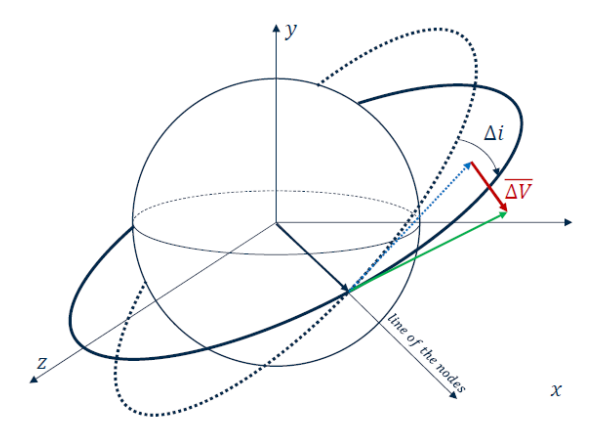


Figure 3.15: Simple plane change [5]

The plane-change manoeuvre is typically performed on the line of nodes and consists of changing the inclination of the orbital plane without changing velocity and flight-path angle. The cost in

terms of  $\Delta V$  is equal to:

$$\Delta V = 2V_t \sin \frac{\Delta i}{2} \tag{3.29}$$

where  $V_t$  indicates the tangential velocity. The minimum  $\Delta V$  is therefore obtained at the point where this quantity is minimum, that is, along the line of nodes. If the manoeuvre is performed at any point in the orbit other than this, the formula 3.29 is no longer valid: the cost required to achieve the same  $\Delta i$  will be greater, since the cost is also in terms of  $\Delta \psi$  and the line of nodes  $\Delta \Omega$  will also rotate.

#### Transfer between coplanar circular orbits

The manoeuvres seen so far are single-impulse, while the transfer between coplanar circular orbits requires two impulsive manoeuvres. The transfer trajectory must be a conic section that intersects both circular orbits. In particular, considering a transfer from an internal orbit of radius  $r_1$  to an external one of radius  $r_2$ , the following conditions must be satisfied:

$$\begin{cases} r_P = \frac{p}{1+e} \le r_1 \\ r_A = \frac{p}{1-e} \ge r_2 \text{ or } e \ge 1 \end{cases} \Rightarrow \begin{cases} e \ge \frac{p}{r_1} - 1 \\ e \ge 1 - \frac{p}{r_2} \end{cases}$$
 (3.30)

#### Hohmann transfer

Among transfers between coplanar circular orbits, the least expensive is the Hohmann, where:

$$\begin{cases}
r_P = r_1 \\
r_A = r_2
\end{cases}$$
(3.31)

The departure and arrival velocities are parallel and there are no losses due to misalignment. The only losses are those due to gravity, which are minimized since there is no waste in terms of  $\Delta V$ . The trajectory followed by the spacecraft is an ellipse with a semi-major axis equal to:

$$a_H = \frac{r_1 + r_2}{2} \tag{3.32}$$

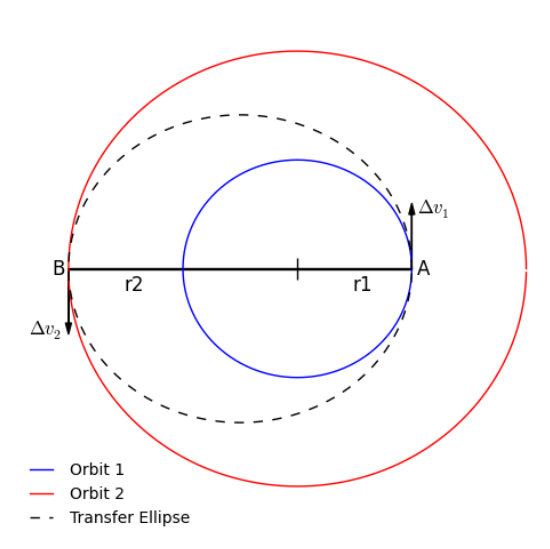


Figure 3.16: Hohmann transfer [28]

Starting from the conservation of mechanical energy, it is possible to derive the formulas for the velocities on the transfer orbit at the departure and arrival:

$$\begin{cases} V_1 = \sqrt{2\mu \left(\frac{1}{r_1} - \frac{1}{r_1 + r_2}\right)} \\ V_2 = \sqrt{2\mu \left(\frac{1}{r_2} - \frac{1}{r_1 + r_2}\right)} \end{cases}$$
(3.33)

from which it is possible to obtain the costs in terms of  $\Delta V$ :

$$\begin{cases}
\Delta V_1 = |V_1 - V_{c1}| = \left| V_{c1} \left( \sqrt{\frac{2r_2}{r_1 + r_2}} - 1 \right) \right| \\
\Delta V_2 = |V_2 - V_{c2}| = \left| V_{c2} \left( \sqrt{\frac{2r_1}{r_1 + r_2}} - 1 \right) \right|
\end{cases}$$
(3.34)

where  $V_c$  indicates the circular velocities of the initial and final orbits.

The total cost of the mission in terms of  $\Delta V$  is:

$$\Delta V_H = \Delta V_1 + \Delta V_2 \tag{3.35}$$

The first impulse  $\Delta V_1$  is used to place the spacecraft into the elliptical transfer orbit, while the second impulse  $\Delta V_2$  is used to circularize the orbit once the destination is reached.

#### 3.9.2Low-thrust manoeuvres

Low-thrust manoeuvres are typical of electric propulsion. Unlike chemical propulsion, which is used to perform impulsive manoeuvres, with electric propulsion the thrust applied to the spacecraft is continuous and can last for longer periods of time.

If the mission's orbits are nearly circular and with a low-inclination, and the thrust is relatively low, the Edelbaum's approximation can be applied. However, for transfers to asteroid 2024 YR4, this approximation is not valid, given the asteroid's highly eccentric orbit.

#### Edelbaum's approximation

As previously mentioned, the Edelbaum's approximation is valid only if the following assumptions are satisfied:

- almost-circular orbit  $\to r \approx a \approx p$ ,  $V^2 \approx \frac{\mu}{r}$ ,  $e \approx 0$ ,  $E \approx \nu \approx M$ ,  $\theta = \Omega + \omega + \nu$ ;
- low-inclination orbit  $\rightarrow \sin i \approx i$ ,  $\cos i \approx 1$ ;
- very-low thrust  $\rightarrow a_V = a_T << \frac{\mu}{r^2}, \ a_R << \frac{\mu}{r^2}, \ a_W << \frac{\mu}{r^2}$

where the subscripts T, R and W indicate the tangential (along V), radial and perpendicular directions, respectively.

By defining  $\alpha$  as the angle between the tangential direction and the acceleration vector in the plane, and  $\beta$  as the angle between the plane and the acceleration vector out of the plane, the three components can be written as follows:

$$a_{T} = \frac{T}{m}\cos\alpha\cos\beta \qquad (3.36)$$

$$a_{R} = \frac{T}{m}\sin\alpha\cos\beta \qquad (3.37)$$

$$a_R = \frac{T}{m}\sin\alpha\cos\beta\tag{3.37}$$

$$a_W = \frac{T}{m}\sin\beta\tag{3.38}$$

From Gauss's planetary equations, based on the approximations made, it is possible to derive the Edelbaum equations:

$$V\frac{\dot{a}}{a} = 2a_T \tag{3.39}$$

$$V\dot{e} = 2\cos\nu a_T + \sin\nu a_R \tag{3.40}$$

$$V\dot{i} = \cos(\omega + \nu)a_W \tag{3.41}$$

$$iV\dot{\Omega} = \sin(\omega + \nu)a_W \tag{3.42}$$

$$V\dot{\omega} = -V\dot{\Omega} + \frac{2\sin\nu a_T - \cos\nu a_R}{e} \tag{3.43}$$

$$\dot{\vartheta} = n = \sqrt{\mu/a^3} \tag{3.44}$$

The most interesting changes in orbital parameters over a revolution are those involving the semimajor axis, eccentricity and inclination. For each change, there is an optimal direction of thrust for which a given parameter is maximized:

- to maximize  $\Delta a$ , thrust must be applied at  $\alpha = 0^{\circ}$  and  $\beta = 0^{\circ}$ , that is, in the plane and in a tangential direction;
- to maximize  $\Delta e$ , the optimal thrust law is as follows:

$$\tan \alpha = \frac{1}{2} \tan \nu \tag{3.45}$$

which, as a first approximation, means that thrust must be applied at  $\alpha \approx \nu$ ;

• to maximize  $\Delta i$ , thrust must be applied out of the plane at an angle  $\beta = \pm 90^{\circ}$ .

When considering variations over multiple spins, the focus is on the variations of  $\Delta a$  and  $\Delta i$  (not so much on  $\Delta e$ , since for orbits that are too eccentric, the Edelbaum's approximation doesn't hold). The idea is to maximize a linear combination of  $\Delta a$  and  $\Delta i$ :

$$\dot{a} + ki \tag{3.46}$$

Following simple mathematical steps, it is obtained that the linear combination is maximized for:

$$\tan \beta = k \cos(\omega + \nu) \tag{3.47}$$

The optimal  $\beta$  value would therefore vary continuously as  $\omega + \nu$  varies. Since it is practically impossible to guarantee this continuous variation, the Edelbaum's approximation consists in using a constant  $\bar{\beta}$  value over half a turn, which effectively represents the ideal behaviour of  $\beta$ .

#### Limits of the Edelbaum's approximation and adopted approach

The Edelbaum solution is a classic reference for the study of low-thrust transfers, as it provides a compact estimate of the propulsive cost required for transitions between almost-circular and low-inclined orbits, assuming continuous and constant thrust. However, this formulation is no longer valid when the orbit has a high eccentricity.

In the case of asteroid 2024 YR4, characterized by a highly elliptical orbit, the Edelbaum approach is therefore not applicable. For trajectories to this asteroid, therefore, it is necessary to resort to an indirect optimization method, based on the formulation of the optimal control problem and the resolution of the optimality conditions derived from the Pontryagin Maximum Principle. This approach allows to simultaneously determine the optimal trajectory and control law, ensuring a realistic description of rendezvous manoeuvres with a body in an elliptical orbit.

## 3.10 Interplanetary mission

An interplanetary mission consists of a spacecraft travelling from a celestial body to another for exploration or demonstration purposes. This section presents the fundamental concepts related to interplanetary missions.

## 3.10.1 Patched conics method

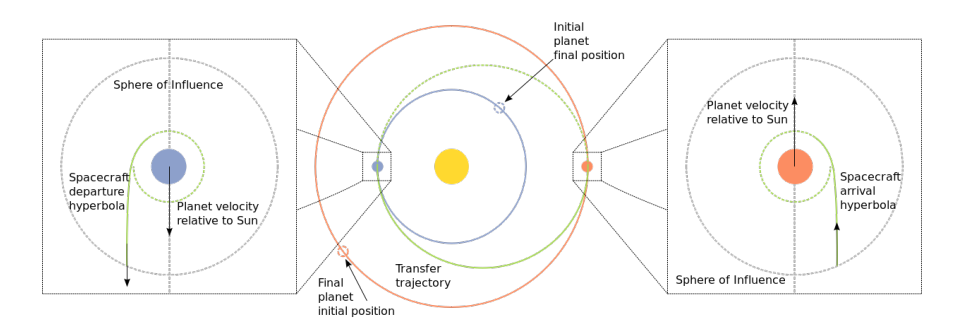


Figure 3.17: Patched conics method [29]

The **patched conics method** is an approximation used to simplify calculations for interplanetary transfers that divides the mission into three phases:

- 1. a hyperbolic trajectory within the sphere of influence of the departure planet in order to escape from it;
- 2. an elliptical trajectory with the Sun as the main body, starting from the exit of the departure planet's sphere of influence and ending at the entrance of the arrival planet's sphere of influence;
- 3. a hyperbolic trajectory within the sphere of influence of the arrival planet in order to be captured in orbit around it.

The **sphere of influence** is defined as the portion of space in which the planet's gravitational pull dominates over that of other bodies in the system, thus making the main contribution in determining the motion of a body in that region. The radius of the sphere of influence is calculated as follows:

$$r_{SOI} = R \left(\frac{m_p}{m_s}\right)^{\frac{2}{5}} \tag{3.48}$$

where R is the radius of the planet's orbit around the Sun,  $m_p$  is the mass of the celestial body, and  $m_s$  is the mass of the Sun.

## 3.10.2 Phasing and launch windows

A launch window is the time interval within which a launch can be conducted in order to allow the spacecraft to be in the best conditions to intercept the target planet, minimizing the amount of propellant required for the mission and consequently maximizing the payload. The launch window depends on the position along the orbit and the relative motion of the departure and arrival planets at the time of launch.

The outer planets, moving in orbits with higher radii, will move more slowly and take longer to sweep a given angle than a inner planet. Consequently, in an interplanetary mission, the outer planet must be further ahead the inner planet, since the spacecraft's speed during the transfer will be greater than the speed of the target planet. A similar but inverse reasoning can be made regarding transfers to inner planets.

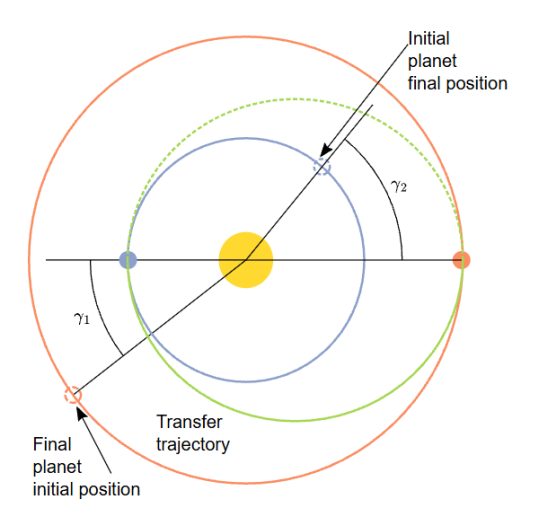


Figure 3.18: Phasing [29]

As can be seen from the image 3.18, the target planet will have to be ahead of the starting planet by an angle equal to  $\gamma_1$ . To find this angle, it is necessary to first define the mean motion of the target planet:

$$n_2 = \frac{2\pi}{T} = \sqrt{\frac{\mu_{\odot}}{a^3}} \tag{3.49}$$

Considering that the spacecraft moves along a Hohmann transfer, during which it travels an angle equal to 180°, it is possible to calculate the angle  $\gamma_1$  as follows:

$$\gamma_1 + n_2 t_H = \pi \Rightarrow \gamma_1 = \pi - n_2 t_H \tag{3.50}$$

where  $t_H$  indicates the time required to complete the Hohmann transfer, which is equal to half the period required to complete the entire orbit, since the spacecraft only travels half:

$$t_H = \frac{1}{2} 2\pi \sqrt{\frac{a_H^3}{\mu_{\odot}}} = \pi \sqrt{\frac{a_H^3}{\mu_{\odot}}}$$
 (3.51)

If a launch opportunity is missed, it will be possible to perform the same transfer after a **synodic period**, i.e., the minimum period of time required for the planets to find themselves in the same relative position. The formula needed to calculate this value is the following:

$$\tau_s = \frac{2\pi}{|w_1 - w_2|} = \frac{T_1 T_2}{|T_1 - T_2|} \tag{3.52}$$

where  $w_1$  and  $w_2$  are the angular velocities of the planets and  $T_1$  and  $T_2$  are their periods of revolution.

## 3.10.3 Planetary flyby

A planetary flyby, also known as a gravity assist, is a manoeuvre used to redirect or accelerate a spacecraft without using propellant. By entering the celestial body's sphere of influence at an angle different from its current direction, a change in velocity vector, both in magnitude and direction, can be achieved solely through the effect of the planet's gravitational field. Therefore, if used optimally, a flyby allows for fuel savings and, consequently, increases the payload mass that can be transported during the mission.

Flybys can be divided into two different types:

• a leading-side flyby: a gravity assist which results in a decreasing in the spacecraft heliocentric speed;

• a trailing-side flyby: a gravity assist which results in an increasing of the spacecraft heliocentric speed.

During a flyby, an exchange of momentum occurs between the spacecraft and the planet. From a physical point of view, the planet provides orbital energy to the spacecraft (or subtracts it) through its gravitational pull. However, due to the enormous difference in masses involved, the variations in the planet's trajectory are practically zero and negligible, while those of the spacecraft are significant and exploitable for the mission.

However, there are limitations associated with this type of manoeuvre:

- a flyby is only possible in correspondence with very specific orbital configurations. The planets must be in favourable positions to be exploited during space missions to other celestial bodies. For example, the alignment of Jupiter, Saturn, Uranus and Neptune exploited by the Voyager probes will not be repeated until the mid-22nd century.
- for bodies without an atmosphere, the lower the flyby, the greater the effect the spacecraft will experience in terms of velocity vector. The problem arises when the gravity assist of a planet with an atmosphere is exploited, inside which the spacecraft would be slowed down by the atmospheric drag. This effect must be avoided, as the energy lost could exceed the gain obtained from the flyby.
- a further limit is given by the mass and orbital velocity of the celestial body: the larger they are, the greater the effect of gravity assist. For this reason, flybys are particularly effective when using massive planets with high orbital velocities, such as Jupiter.

As will be seen in Chapter 8, interplanetary transfers to a steroid 2024 YR4 can be made exploiting an Earth flyby. This manoeuvre will save nearly 100 kg of propellant, thanks to a reduction of approximately 4 km/s in  $\Delta V$  compared to a direct transfer.

# Chapter 4

# Space propulsion

This chapter introduces the fundamental concepts of propulsion, starting with general aspects and then moving on to analyse the various types. Electric propulsion will receive particular attention, since the trajectories to NEAs considered are based on low-thrust systems.

## 4.1 Generalities of space propulsion

Propulsion is defined as the ability to generate a force, called thrust, that is used to change the momentum of a spacecraft. Thrust is generally denoted by the letter T and is achieved through the principle of action and reaction, more specifically through the exhaust propellant in the opposite direction of motion.

Space propulsion can be of two types based on the manoeuvres performed and the required  $\Delta V$ :

- **primary propulsion:** propulsion used for manoeuvres generally with higher  $\Delta V$  where a change in velocity is required, such as orbit changes;
- auxiliary propulsion: propulsion used for manoeuvres with lower  $\Delta V$ , such as maintaining a satellite in a given orbit subject to perturbations or changing its attitude.

Based on how thrust is generated, propulsion can be divided into two main types:

- **chemical propulsion (CP):** gases are heated by a chemical reaction and expanded in a nozzle that converts thermal energy into kinetic energy;
- **electric propulsion (EP):** the propellant is accelerated by converting electrical energy into kinetic energy.

## Thrust equation

A fundamental relation in propulsion analysis is the **thrust equation**, which can be derived by considering an object of mass m that simulates the spacecraft from which, after a certain time interval dt, a mass of propellant  $dm_p$  is expelled.

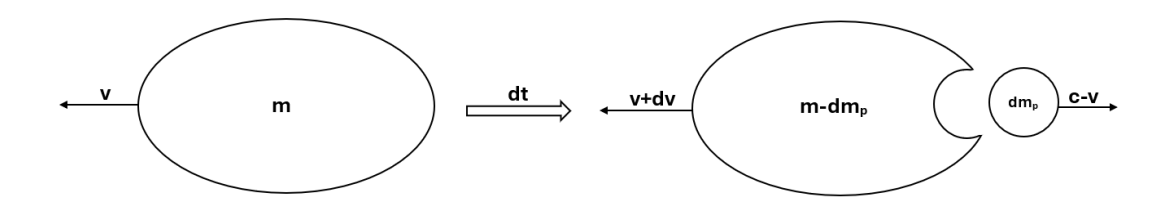


Figure 4.1: Momentum balance - thrust equation

The velocity c, called the **effective exhaust velocity**, is the speed of the propellant relative to the system.

To derive the thrust equation, two assumptions need to be introduced:

- all velocities are aligned with each other;
- the system is isolated, therefore, other than thrust, there are no other forces acting on the mass m.

Knowing that in an isolated system the momentum remains constant, the thrust T can be derived by equating the values before and after the change in velocity:

$$mv = (m - dm_p)(v + dv) - dm_p(c - v)$$
 (4.1)

Simplifying the equal terms on the right and left of the equals sign, the following formulation is obtained:

$$mdv = dm_p c (4.2)$$

To move from the discrete to the continuous formulation, a propellant mass flow rate must be defined and dv should be expressed as acceleration over time:

$$\dot{m}_p = \frac{dm_p}{dt} \tag{4.3}$$

$$dv = \frac{dv}{dt}dt \tag{4.4}$$

Now the thrust equation can be derived:

$$T = m\frac{dv}{dt} = \dot{m}_p c \tag{4.5}$$

From this equation, the effective exhaust velocity can be calculated as follows:

$$c = \frac{T}{\dot{m}_p} \tag{4.6}$$

Since the goal is to save propellant mass, the thrust equation shows that achieving high thrust values with low propellant mass flow rates requires high effective exhaust velocities. The problem is that this quantity cannot be raised too much, since a higher c requires more power to accelerate the gases, which is a cost to consider.

$$P_T = \frac{\dot{m}_p c^2}{2} = \frac{Tc}{2} \tag{4.7}$$

It is therefore necessary to have small propellant flow rates without excessively increasing the power required by the propulsion system to accelerate the gases.

## Propulsion system performance

Starting from the thrust, it is possible to derive the total impulse, obtained by integrating T between the initial and final instants:

$$I_{tot} = \int_{t_0}^{t_f} Tdt \tag{4.8}$$

from which it is possible to derive the specific impulse, defined as follows:

$$I_{sp} = \frac{I_{tot}}{m_p g_0} \tag{4.9}$$

where  $g_0$  corresponds to the value of the gravitational acceleration on Earth (equal to 9.80665 m/s<sup>2</sup>) and  $m_p$  is the propellant mass, defined as the integral of the propellant mass flow rate over time:

$$m_p = \int_{t_0}^{t_f} \dot{m}_p dt \tag{4.10}$$

It can be observed that, for a given total impulse, the specific impulse increases as the propellant mass  $m_p$  decreases, which must therefore be as low as possible.

If the effective exhaust velocity is constant throughout the mission, the specific impulse can be rewritten as follows:

 $I_{sp} = \frac{c}{g_0} = \frac{T}{\dot{m}_p} \tag{4.11}$ 

Specific impulse is one of the most important performance parameters, since it measures how efficiently the propellant mass is used.

For chemical propulsion, the value of the specific impulse is limited by the energy of the internal reaction:

$$\dot{m}_p \frac{c^2}{2} = \dot{m}_p E_{ch} \Rightarrow c = \sqrt{2E_{ch}} \tag{4.12}$$

The maximum achievable specific impulse values are around 450 s.

With electric propulsion, however, the value of  $I_{sp}$  increases by decreasing  $\dot{m}$  and T if the value of  $P_E$  is fixed, or by increasing the electric power (for example, using larger solar panels), which cannot be increased infinitely as it is a cost:

$$\eta P_E = \dot{m}_p \frac{c^2}{2} = \frac{Tc}{2} \Rightarrow c = \sqrt{\frac{2\eta P_E}{\dot{m}_p}} = \frac{2\eta P_E}{T}$$
(4.13)

where:

$$P_E = \frac{P_T}{\eta} = \frac{\dot{m}_p c^2}{2\eta} = \frac{Tc}{2\eta} \tag{4.14}$$

Therefore, for electric propulsion, in order to have high c values, it will be necessary to have small thrust values and therefore use low-thrust propulsion. In this case,  $I_{sp}$  can even reach values around 10000 s.

## Tsiolkowski's equation

To relate the propellant mass and the propulsive  $\Delta V$ , or the  $\Delta V$  that would be obtained if only the thrust T were considered and the thrust were parallel to the velocity (therefore without considering losses), it is useful to derive **Tsiolkowski's equation** (or rocket equation). The propulsive  $\Delta V$  is defined as follows:

$$\Delta V = \int_{t_0}^{t_f} \frac{T}{m} dt \tag{4.15}$$

Returning to the thrust equation and rewriting  $\dot{m}_p$  as the variation of the propellant mass over time, it is obtained:

$$\Delta V = \int_{m_0}^{m_f} -\frac{c}{m} dm \tag{4.16}$$

Considering c = constant, Tsiolkowski's equation is obtained:

$$\Delta V = -c \ln \left( \frac{m_f}{m_0} \right) = c \ln \left( \frac{m_0}{m_f} \right) \tag{4.17}$$

from which the propellant mass required for that  $\Delta V$  can be derived as follows:

$$\frac{m_f}{m_0} = e^{-\frac{\Delta V}{c}} \Rightarrow m_p = m_0 - m_f = m_0 \left(1 - e^{-\frac{\Delta V}{c}}\right)$$
 (4.18)

In order to obtain high values of  $\frac{m_f}{m_0}$ , and therefore reduce costs in terms of propellant mass and increase the transportable payload mass, it is necessary to have values of c comparable with  $\Delta V$ . In particular, as c increases, the term  $\frac{\Delta V}{c}$  decreases and, consequently, fuel consumption will also be lower.

## 4.2 Electric propulsion

Based on the physical principle by which particles are accelerated, three types of electric propulsion can be distinguished:

- electrothermal propulsion: gases are heated by electrical energy and then expanded in a nozzle;
- electrostatic propulsion: the propellant is accelerated using electrostatic forces;
- electromagnetic propulsion: the propellant is accelerated using electromagnetic forces.

The following paragraphs describe the various types of propulsion and explain the physical principles through which the main propulsion systems work.

## 4.2.1 Electrothermal propulsion

Electrothermal propulsion is based on the conversion of electrical energy into thermal energy and the subsequent conversion of the latter into kinetic energy. The propellants used are hydrogen, ammonia, hydrazine and water, and the two main propulsion systems are resistojets and arcjets.

### Resistojet

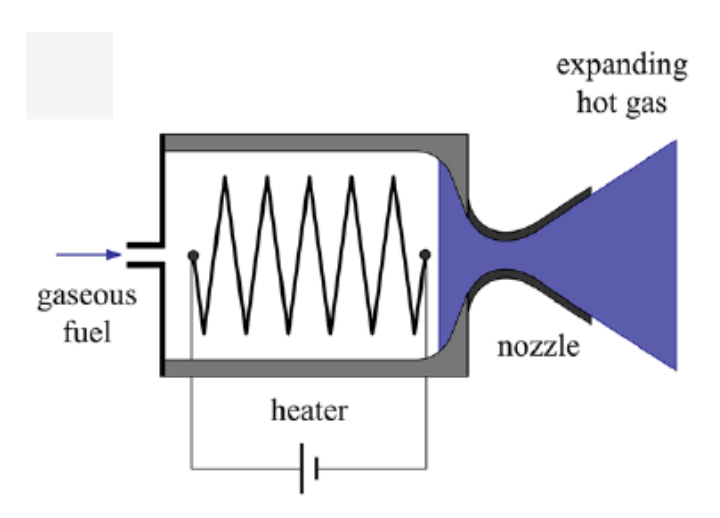


Figure 4.2: Resistojet schematic [22]

The propellant is heated by the Joule effect by an electric resistance that can be in direct contact with it or separated from it by a heat exchanger inside a sealed cavity. In the first case, heat transfer occurs by convection, while in the second case, it occurs through radiation. Performance is very similar for both solutions. Regarding specific impulse, high values cannot be achieved, but values comparable to chemical propulsion can be obtained ( $I_{sp}$  around 350 s maximum). This occurs because the temperature the resistor can reach is limited by the materials it is constructed from. Consequently, beyond a certain temperature the propellant can no longer be heated and a maximum specific impulse will be achieved.

## Arcjet

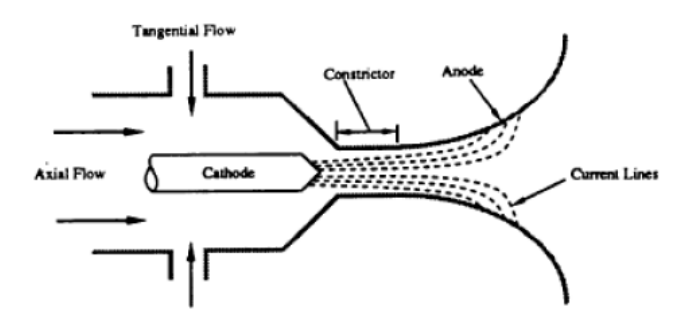


Figure 4.3: Constricted arcjet schematic [8]

Arcjets are thrusters consisting of a cylindrical cathode with a conical tip and a coaxial anode that forms the walls of the nozzle. With these engines, the problem of heating the resistor is no longer present, since the Joule effect causes the electric current to pass directly into the propellant. Direct heating of the fuel occurs by creating an electric arc, which, however, must be kept away from the walls. To this end, a phenomenon called the **pinch effect** is exploited, forcing the arc to collapse on itself. This effect is caused by the forces generated through the interaction of the current with the magnetic field it induces.

In arcjets, temperatures reach up to  $10000~\mathrm{K}$  and specific impulses are achieved in the order of  $800~\mathrm{s}\text{-}1000~\mathrm{s}$ .

## 4.2.2 Electrostatic propulsion

Electrostatic propulsion uses an electric field to accelerate particles, more specifically ions. The mechanism on which these thrusters are based can be divided into three phases:

- ionization: to extract the ions, the propellant, which is initially neutral, must be ionized;
- acceleration: following ionization, the ions must be extracted and accelerated;
- **neutralization:** to avoid drawing the ions back, the charge at the exit must be neutral; therefore, for every ion emitted, an electron must also be emitted.

The main thrusters are ion thrusters, FEEPs, colloidal thrusters and Hall thrusters.

### Ion thruster

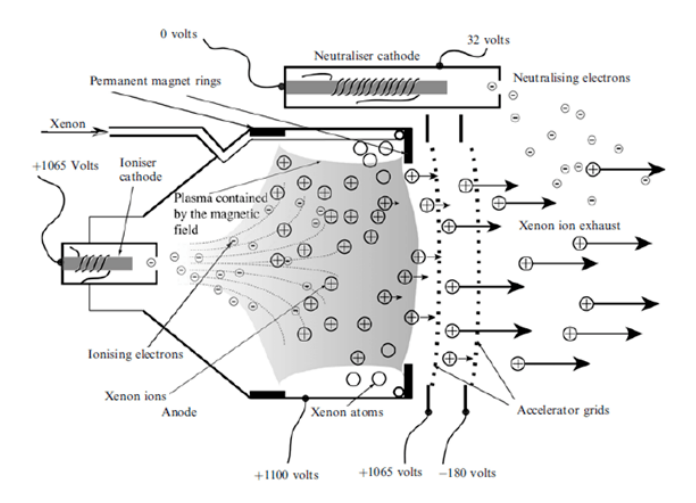


Figure 4.4: Ion thruster schematic [1]

An ion thruster consists of a chamber containing xenon atoms, the typical propellant used for this engine, which are ionized through collisions with electrons emerging from the cathode. Following ionization, the ions pass through two grids: a screen grid, designed to allow only ions to pass through and repel electrons, and an accelerator grid, through which the ions are accelerated and thrust is generated. Finally, at a precise distance from the grids, there is a hollow cathode that is used to neutralize the ion beam by creating a plasma bridge.

The problem with these thrusters is that there is a limit to the number of ions, and therefore the amount of current, that can pass between the grids. The limiting situation arises when an ion, attracted by the electric field, encounters enough other charged particles in front of it to create a repelling field of equal magnitude. In this situation, no further particle can enter between the grids until one exits. This results in a maximum current that can be calculated using Child's law as follows:

$$j_{max} = \frac{4\epsilon_0}{9} \left(\frac{2q}{m_+}\right)^{\frac{1}{2}} \frac{V_G^{\frac{3}{2}}}{x_a^2} \tag{4.19}$$

where:

- $\epsilon_0$  is the vacuum permittivity;
- q is the charge of the ion;
- $m_+$  is the mass of the ion;
- $V_G$  is the intragrid potential, or the potential difference between the screen grid and the accelerator grid;
- $x_a$  is the distance between the screen grid and the accelerator grid.

The current limit also translates into a limit on the thrust density:

$$\frac{T}{A} = \frac{\dot{m}c}{A} = \frac{jm_+}{q}c\tag{4.20}$$

According Child's law, it is possible to increase the maximum current that can flow between the grids, and therefore also the thrust density, by increasing the intragrid potential, reducing the distance between the grids, or by combining both strategies.

Regarding performance, typical specific impulse values range from 2000 s to 5000 s. Typically, values do not fall below 2000 s, as efficiency drops dramatically. For specific impulses around 1000 s - 2000 s Hall thrusters are used.

#### FEEP and colloidal thruster

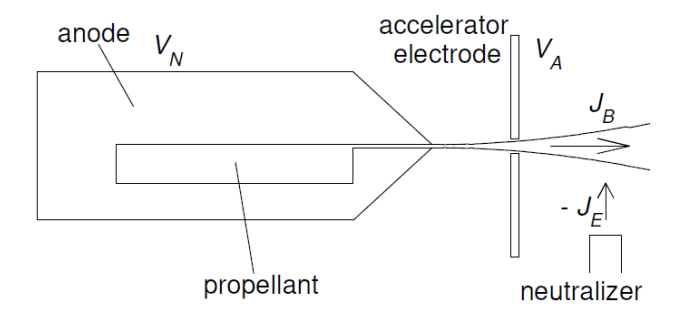


Figure 4.5: FEEP schematic [8]

Field effect electric propulsion (FEEP) involves extracting ions from a liquid propellant using a sufficiently large electric field generated by a high potential difference. This type of thruster consists of two plates separated by a gap and a cavity containing the propellant, which, due to capillary action, will fill the space between them. The high potential difference generated is around 10000 V and is achieved by charging the anode to +6000 V and the accelerator electrode to -4000 V. This generates a strong electric field that attracts all the nuclei of the atoms and repels the electrons in the opposite direction, forming **Taylor cones** at the exit of the thruster.

Typically metals such as caesium or iridium are used as propellants. The thrust values are very low (in the order of  $\mu N$ ) and the specific impulse is around 6000 s.

Colloidal thrusters are based on the same operating principle as FEEPs but have some differences: the geometry is not linear but axisymmetric and they use either colloidal liquids (such as formamide) to which a salt is added to make it ionizable or ionic liquids, which are salts that are liquid at room temperature.

### Hall thruster

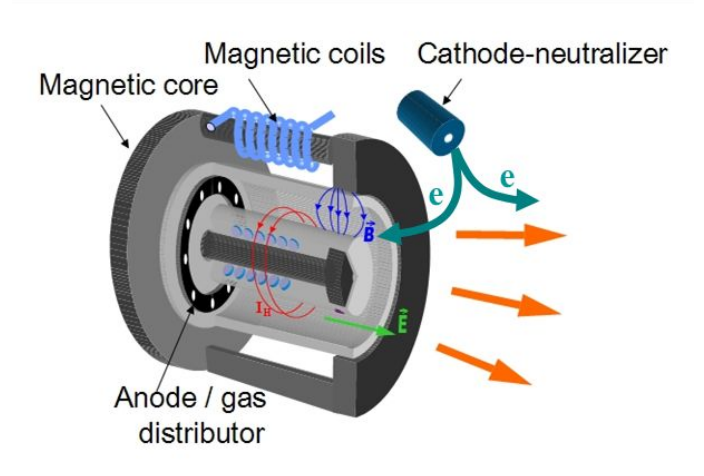


Figure 4.6: Hall thruster schematic [25]

Unlike ion thrusters, Hall thrusters are not subject to the thrust density limitation imposed by Child's law. To circumvent the limitation imposed by Child's law, the basic idea behind these thrusters is to have both ions and electrons within the chamber. To maintain the useful effect, since if only the electric field were present the electrostatic force would disappear and consequently no thrust would be generated, a magnetic field is present, ensuring that the electrons are subjected to zero force and the ions are accelerated. It is interesting to note that, by balancing the forces, from the thruster's perspective, they are electromagnetic thrusters, while from the propellant's

perspective, they are electrostatic thrusters. It can therefore be said that they are a hybrid between electrostatic and electromagnetic propulsion.

As can be seen from the image 4.6, the geometry is axial-symmetric. Specifically, they feature a solid internal cylinder and a hollow external one.

The problem with these thrusters is that the potential difference, and consequently the specific impulse, cannot be increased too much, since the more energetic the plasma, the more likely it is to experience instability phenomena that cause channel erosion.  $I_{sp}$  values are achieved in the range of 1000 s - 2000 s, complementary to ion thrusters, which have higher specific impulses. These two thrusters cover a wide range of specific impulses, thus avoiding the need to resort to suboptimal propulsion systems for missions requiring particular  $I_{sp}$  values.

## 4.2.3 Electromagnetic propulsion

Electromagnetic propulsion is based on three fundamental principles:

- the electron stream gains energy and is accelerated by the electric field;
- the electrons' velocity is curved by the magnetic field, which can be self or applied;
- the electrons collide with atoms and collectively transfer momentum to the propellant. The entire propellant is accelerated by the magnetic field as if it were a single block, thus generating thrust.

This type of propulsion therefore exploits collisions, without which thrust could not be generated.

Two types of electromagnetic thrusters can be distinguished:

- **steady**, whose geometry is typically axial-symmetric;
- unsteady, whose geometry can be either one-dimensional or axial-symmetric.

The operation of three propulsion systems is described below: MPD, PPT and VASIMR, a hybrid electromagnetic–electrothermal thruster.

## Self-field and applied-field MPD thruster

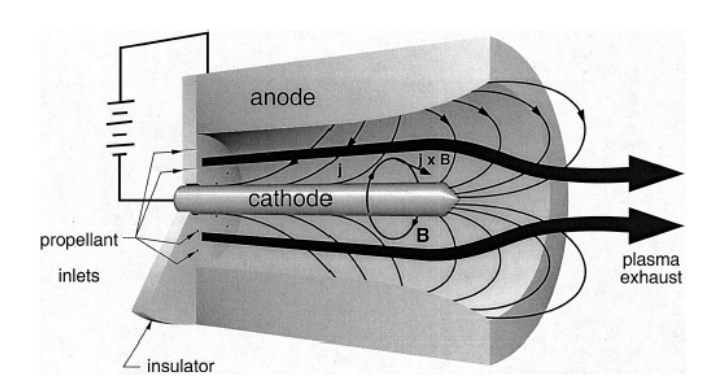


Figure 4.7: MPD schematic [21]

MPD thrusters are steady devices and are essentially arcjets, but differ in their operating principle. While arcjets rely on low currents and high flow rates, resulting in a low magnetic interaction parameter, the opposite occurs in MPDs. In these thrusters, the high magnetic interaction parameter values allow the effects of the magnetic field to prevail over the electrothermal ones, and

acceleration occurs through electromagnetic forces.

They are divided into self-field and applied field thrusters:

• in self-field thrusters the current generates an induced magnetic field that has a predominantly tangential direction;

• in applied field thrusters, in addition to the magnetic field induced by the currents, there is an axial magnetic field (with a small component also in the radial direction) generated by coils surrounding the thruster.

Thrust is generated by exploiting two contributions:

- blowing: thrust contribution in the axial direction arising from the interaction between the radial current and the tangential magnetic field. This effect generates a direct thrust;
- pumping: thrust contribution in the radial direction arising from the interaction between the axial current and the tangential magnetic field. In this case, the thrust derives from the increased pressure on the cathode surface.

In applied field thrusters, since other magnetic field components are present in addition to the tangential one, a swirling thrust contribution arises from the interaction between the currents and the magnetic field in the axial and radial directions.

The specific impulses achievable with these thrusters range from 2000 s to 5000 s, values similar to those of ion thrusters. They are mainly used for large masses and high  $\Delta V$  missions, such as human missions where durations must be reasonable. The problem with these thrusters, however, is the high power required and the challenges associated with its management.

#### PPT

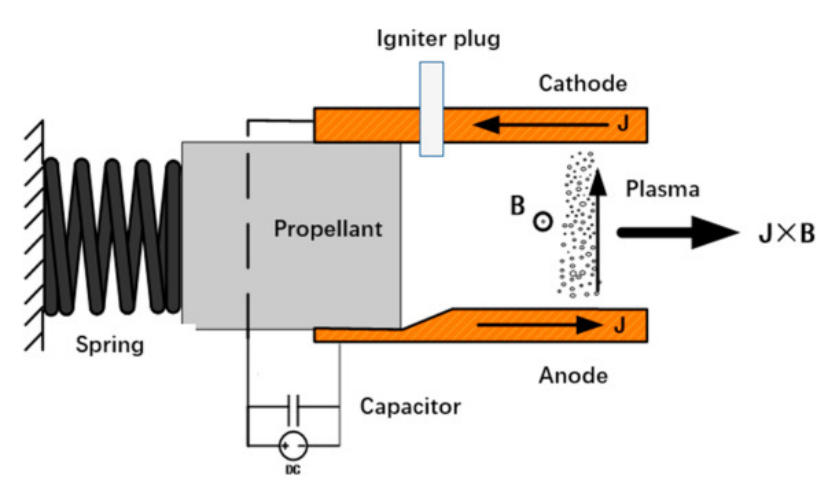


Figure 4.8: PPT schematic [17]

Pulsed plasma thrusters are based on an unsteady operating principle and consist of a block of solid propellant, typically Teflon, held in place by a spring at the entrance to a conduit where a discharge is generated. Within the channel, a potential difference is generated between the walls by an energy-storing capacitor, and the discharge is set in motion by magnetic body force. The succession of pulses, alternating at a certain frequency called the discharge frequency, produces thrust.

For the thruster to function properly, in addition to storing energy within capacitors, it is also necessary to synchronize the propellant with the discharge and its ionization at the right time. For this purpose, two measures are adopted: the solid propellant, which thanks to the spring always exposes its surface to the conduit, and an igniter plug placed at the entrance, which supplies the

electrons needed to ionize the Teflon.

The performances of these thrusters are similar to that of MPDs. Compared to the latter, however, they have lower efficiency and not very high output velocities, in addition to being very heavy thrusters. Values of  $I_{sp}$  are reached in the order of 500 s - 1000 s. These thrusters, although not having such promising performance, are very useful for performing precision manoeuvres (such as pointing manoeuvres) since it is possible to adjust the average thrust through the discharge frequency.

#### VASIMR

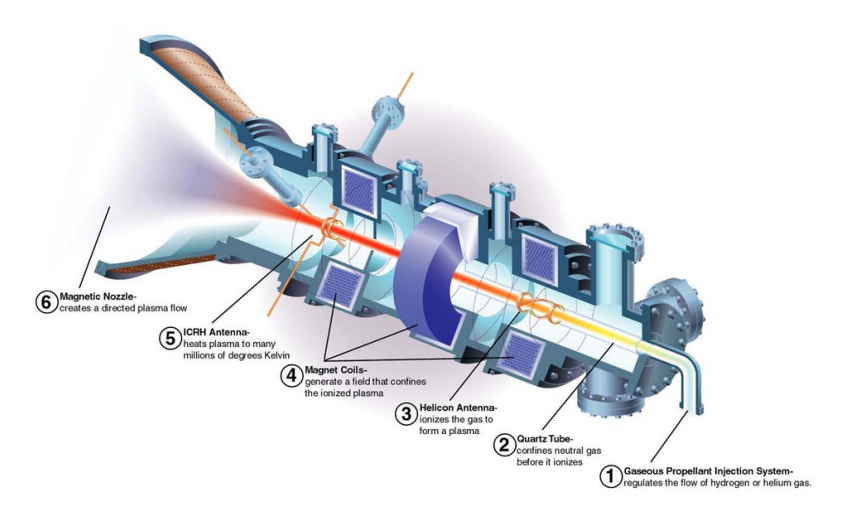


Figure 4.9: VASIMR schematic [16]

The VAriable Specific Impulse Magnetoplasma Rocket is a hybrid between an electromagnetic and an electrothermal thruster. This engine operates on three key points:

- 1. propellant ionization;
- 2. ion cyclotron-resonance heating, which heats the propellant;
- 3. expansion in a magnetic nozzle.

At the initial stage of the thruster, there is a quartz tube surrounded by a helicon antenna, which ionizes the propellant through collisions.

The propellant then passes into the heating chamber, where a constant axial magnetic field generated by solenoids induces rotation in the ions at a certain angular velocity. The chamber contains an ICRF antenna that produces an electromagnetic wave with a frequency corresponding to the cyclotron frequency of the ions' Larmor motion. The resulting electric field continuously accelerates the ions, while the electrons are unaffected by the resonance effect.

Finally, the propellant passes through the magnetic nozzle, where the magnetic field decreases. Due to conservation of energy and angular momentum, the Larmor radius increases, the tangential velocity decreases and the axial velocity increases, thus accelerating the ions and generating thrust.

A challenge with this thruster is that the solenoids require superconductors, which must be cooled to very low temperatures to function.

The VASIMR allows for efficient power distribution between ionization and heating, achieving specific impulses ranging from 2000 s to 5000 s. Thanks to these characteristics, it is an ideal thruster for manned Martian missions, where short travel times are required.

# Chapter 5

# Indirect optimization of space trajectories

Optimization means finding the control law that maximizes or minimizes a given performance index. For space trajectories, it is crucial to maximize the final mass at the end of the mission or, equivalently, minimize the propellant mass required for the transfer. In general, therefore, the optimization problem consists of maximizing the final mass of the spacecraft at the end of the mission, but one can also choose to maximize other parameters. For example, if the weight of the propulsion system is known, it may be useful to find the control law that maximizes the payload.

Among the various numerical methods, a distinction can be made between direct and indirect methods:

- direct methods require a large number of parameters and are based on the "discretization" of the trajectory;
- indirect methods exploit the principles of variational calculus, converge even with a small number of parameters and have limited computation times, generating solutions with high numerical precision.

The latter, however, present poor robustness and greater difficulty in convergence, since the solution search depends heavily on the initial guesses.

# 5.1 Optimal control theory

Optimal control theory is based on the principles of variational calculus. Specifically, the goal is to find a curve such that a certain quantity J is maximized (or minimized) while simultaneously satisfying the differential equations and algebraic conditions at the endpoints. Having defined a vector of state variables  $\vec{x}$ , it is possible to describe its evolution over time using differential equations written as follows:

$$\frac{d\vec{x}}{dt} = \vec{f}(\vec{x}, \vec{u}, t) \tag{5.1}$$

where  $\vec{u}$  is the control vector and t is the independent variable time.

It is useful to divide the trajectory into n subintervals. By doing so, it is possible to identify the start and end of the j-th subinterval using the times  $t_{(j-1)_+}$  and  $t_{j-}$ , which correspond to the values of the variables  $\vec{x}_{(j-1)_+}$  and  $\vec{x}_{j-}$ , respectively. This is useful in order to account for any discontinuities such as impulsive manoeuvres, flybys and stage separations.

After having divided the trajectory in this way, it is necessary to introduce boundary conditions of the form:

$$\vec{\chi}\left(\vec{x}_{(j-1)_{+}}, \vec{x}_{j_{-}}, t_{(j-1)_{+}}, t_{j_{-}}\right) = 0 \qquad j = 1, \dots, n$$
 (5.2)

As can be seen, the boundary conditions concern both the state variables and the independent time variable at both the external and internal boundaries. Constraints may also be imposed regarding controls  $\vec{u}$ .

In order to solve the optimization problem, it is necessary to maximize a functional J, which in its general form is expressed as follows:

$$J = \varphi(\vec{x}_{(j-1)_{+}}, \vec{x}_{j_{-}}, t_{(j-1)_{+}}, t_{j_{-}}) + \sum_{j} \int_{t_{(j-1)_{+}}}^{t_{j_{-}}} \Phi(\vec{x}(t), \vec{u}(t), t) dt \qquad j = 1, \dots, n$$
 (5.3)

The J functional is therefore composed of two terms:

- the  $\varphi$  function, which depends on the values assumed by the state variable and the independent variable time at the internal and external boundaries;
- the integral extended over the entire interval of the  $\Phi$  function, which depends on time and the values assumed at each point of the state variable and the controls.

In particular, it is interesting to note that there can be two formulations such that one of the two functions is nullified:

- Lagrange formulation  $\Rightarrow \varphi = 0$
- Mayer formulation  $\Rightarrow \Phi = 0$

For the indirect optimization of space trajectories, Mayer's formulation is preferred.

It is useful to rewrite the functional J by introducing the Lagrange multipliers  $\vec{\mu}$  and the adjoint variables  $\vec{\lambda}$ :

$$J^* = \varphi + \vec{\mu}^T \vec{\chi} + \sum_{j} \int_{t_{(j-1)_+}}^{t_{j_-}} \left( \Phi + \vec{\lambda}^T (\vec{f} - \dot{\vec{x}}) \right) dt \qquad j = 1, \dots, n$$
 (5.4)

The two functionals depend on time t, on the state variables  $\vec{x}$  and their derivatives  $\vec{x}$ , and on the controls  $\vec{u}$ . If boundary conditions and state equations are satisfied, then the functionals J and  $J^*$  coincide, and consequently the extremal values are also the same. In order to eliminate the dependence on  $\dot{\vec{x}}$ , it is useful to integrate by parts, thus obtaining:

$$J^* = \varphi + \vec{\mu}^T \vec{\chi} + \sum_{j} \left( \vec{\lambda}_{(j-1)_{+}}^T \vec{x}_{(j-1)_{+}} - \vec{\lambda}_{j_{-}}^T \vec{x}_{j_{-}} \right) +$$

$$+ \sum_{j} \int_{t_{(j-1)_{+}}}^{t_{j_{-}}} \left( \Phi + \vec{\lambda}^T \vec{f} - \dot{\vec{\lambda}}^T \vec{x} \right) dt \qquad j = 1, \dots, n$$
(5.5)

Introducing the Hamiltonian H as follows:

$$H = \Phi + \vec{\lambda}^T \vec{f} \tag{5.6}$$

and differentiating, it is obtained (square brackets indicate a matrix):

$$\delta J^* = \left( -H_{(j-1)_+} + \frac{\partial \varphi}{\partial t_{(j-1)_+}} + \vec{\mu}^T \frac{\partial \vec{\chi}}{\partial t_{(j-1)_+}} \right) \delta t_{(j-1)_+} + \left( H_{j_-} + \frac{\partial \varphi}{\partial t_{j_-}} + \vec{\mu}^T \frac{\partial \vec{\chi}}{\partial t_{j_-}} \right) \delta t_{j_-} +$$

$$+ \left(\vec{\lambda}_{(j-1)_{+}}^{T} + \frac{\partial \varphi}{\partial \vec{x}_{(j-1)_{+}}} + \vec{\mu}^{T} \left[ \frac{\partial \vec{\chi}}{\partial \vec{x}_{(j-1)_{+}}} \right] \right) \delta \vec{x}_{(j-1)_{+}} +$$

$$+ \left( -\vec{\lambda}_{j_{-}}^{T} + \frac{\partial \varphi}{\partial \vec{x}_{j_{-}}} + \vec{\mu}^{T} \left[ \frac{\partial \vec{\chi}}{\partial \vec{x}_{j_{-}}} \right] \right) \delta \vec{x}_{j_{-}} +$$

$$+ \sum_{j} \int_{t_{(j-1)_{+}}}^{t_{j_{-}}} \left( \left( \frac{\partial H}{\partial \vec{x}} + \dot{\vec{\lambda}}^{T} \right) \delta \vec{x} + \frac{\partial H}{\partial \vec{u}} \delta \vec{u} \right) dt \qquad j = 1, \dots, n$$

$$(5.7)$$

At a maximum or a minimum the functional  $\delta J^*$  must vanish for any variation of  $\delta \vec{x}$ ,  $\delta \vec{u}$ ,  $\delta \vec{x}_{(j-1)_+}$ ,  $\delta \vec{x}_{j_-}$ ,  $\delta t_{(j-1)_+}$  and  $\delta t_{j_-}$  compatible with the differential and boundary equations. An appropriate choice of constants and adjoint variables is useful to cancel the coefficient of each of the variations of the equation above, thus ensuring the stationarity of the functional expressed as  $\delta J^* = 0$ . By cancelling the coefficients  $\delta \vec{x}$  and  $\delta \vec{u}$  inside the integral for each point of the trajectory, it is obtained:

• Euler-Lagrange differential equations for the adjoint variables

$$\frac{d\vec{\lambda}}{dt} = -\left(\frac{\partial H}{\partial \vec{x}}\right)^T \tag{5.8}$$

• the algebraic equations for the controls

$$\left(\frac{\partial H}{\partial \vec{u}}\right)^T = 0 \tag{5.9}$$

It is interesting to note how the control laws (and also the boundary conditions) are independent of the search for maxima and minima of J.

Care must be taken when applying a constraint to one of the controls. In this case, the latter must belong to a feasible domain. Only cases in which the constraint is explicit and constant are considered, not those in which it depends on time and state variables. By the **Pontryagin Maximum Principle**, when a constraint is present on the control, the optimal value at each point of the trajectory is the one that, belonging to the feasible domain, maximizes or minimizes (depending on whether maxima or minima of J are sought) the Hamiltonian at that point. Two cases can be distinguished:

- locally "unconstrained" control → the equation 5.9 provides the optimal value of the control if it falls within the feasible domain and therefore the constraint does not apply at that point;
- "constrained" control → if the equation 5.9 does not provide a value within the feasible domain, then the control assumes the maximum or minimum value. The optimal value is therefore at the extremes of the domain.

A special case is when the Hamiltonian is linear with respect to the control to which a constraint is applied. Since the control does not appear within the equation 5.9 and, consequently, cannot be determined, two further cases can be distinguished:

- bang-bang control  $\rightarrow$  if the control coefficient in the 5.6 equation is non-zero, according to the Pontryagin Maximum Principle, H is maximized for the maximum value of the control if the coefficient is positive and minimum if it is negative;
- singular arc → if the control coefficient in the 5.6 equation is identically zero for a certain time interval, then all successive derivatives of the coefficient with respect to time must be cancelled until one is encountered in which the control is explicitly present. Setting this derivative equal to zero yields the optimal value of the control.

The missing boundary conditions concern the j-th contour and are written by considering the final endpoint of the (j-1)-th interval or the initial endpoint of the j-th interval. By cancelling the coefficients  $\delta \vec{x}_{j-}$ ,  $\delta \vec{x}_{j+}$ ,  $\delta t_{j-}$  and  $\delta t_{j+}$  in the equation 5.7, it is obtained:

$$-\vec{\lambda}_{j_{-}}^{T} + \frac{\partial \varphi}{\partial \vec{x}_{j_{-}}} + \vec{\mu}^{T} \left[ \frac{\partial \vec{\chi}}{\partial \vec{x}_{j_{-}}} \right] = 0, \qquad j = 1, \dots, n$$
 (5.10)

$$\vec{\lambda}_{j_{+}}^{T} + \frac{\partial \varphi}{\partial \vec{x}_{j_{+}}} + \vec{\mu}^{T} \left[ \frac{\partial \vec{\chi}}{\partial \vec{x}_{j_{+}}} \right] = 0, \qquad j = 0, \dots, n - 1$$
 (5.11)

$$H_{j_{-}} + \frac{\partial \varphi}{\partial t_{j_{-}}} + \vec{\mu}^{T} \frac{\partial \vec{\chi}}{\partial t_{j_{-}}} = 0, \qquad j = 1, \dots, n$$
 (5.12)

$$-H_{j_{+}} + \frac{\partial \varphi}{\partial t_{j_{+}}} + \vec{\mu}^{T} \frac{\partial \vec{\chi}}{\partial t_{j_{+}}} = 0, \qquad j = 0, \dots, n-1$$
 (5.13)

As can be seen from the values assumed by j in the above expressions, the equations 5.10 and 5.12 have no meaning at the beginning of the trajectory, while the equations 5.11 and 5.13 have none at the end. The optimal boundary conditions are obtained by eliminating the adjoint constants  $\vec{\mu}$  from the equations 5.10, 5.11, 5.12 and 5.13:

$$\vec{\sigma}\left(\vec{x}_{(j-1)_{+}}, \vec{x}_{j_{-}}, \vec{\lambda}_{(j-1)_{+}}, \vec{\lambda}_{j_{-}}, t_{(j-1)_{+}}, t_{j_{-}}\right) = 0$$
(5.14)

Together with the given conditions 5.2, these equations complete the differential system given by the expressions 5.1 and 5.8.

Equations 5.10 and 5.11 provide particular optimality conditions for an adjoint variable  $\lambda_x$  corresponding to a generic state variable x subject to particular boundary conditions:

- if the state variable x is explicitly assigned at the initial time ( $\vec{\chi}$  contains the equation  $x_0 a = 0$  with an assigned value), there are no constraints on the corresponding adjoint variable  $\lambda_{x_0}$  and it is defined as "free" (the same argument can be made at the final time);
- if the initial value of the state variable  $x_0$  does not appear either in the function  $\varphi$  or in the boundary conditions, then the corresponding adjoint variable is zero at the initial time (the same argument can be made at the final time);
- if a state variable is continuous and not assigned to the interior point i ( $\vec{\chi}$  contains the equation  $x_{j_+} = x_{j_-}$ ), the corresponding adjoint variable is also continuous  $\lambda_{x_{j_+}} = \lambda_{x_{j_-}}$ ;
- if a state variable is continuous and is explicitly assigned to an interior boundary ( $\vec{\chi}$  contains the equation  $x_{j_+} = x_{j_-} = a$ ), the corresponding adjoint variable has a "free" discontinuity. The value of  $\lambda_{x_{j_+}}$  is independent of  $\lambda_{x_{j_-}}$  and is determined by the optimization process.

Similarly, equations 5.12 and 5.13 also provide special boundary conditions in some cases if the Hamiltonian does not explicitly depend on time:

- if the initial time  $t_0$  does not appear either in the function  $\varphi$  or in the boundary conditions, the Hamiltonian at the initial instant is zero (the same reasoning applies to the final time if it does not explicitly appear in  $\vec{\chi}$  and  $\varphi$ );
- if the intermediate time  $t_j$  does not appear in  $\varphi$  (the only condition in  $\vec{\chi}$  that involves it is the continuity of the time  $t_{j_+} = t_{j_-}$ ), the Hamiltonian is continuous at j ( $H_{j_+} = H_{j_-}$ );
- if the time  $t_j$  is explicitly assigned (in  $\vec{\chi}$  the equations  $t_{j+} = t_{j-} = a$  appear), the Hamiltonian presents a "free" discontinuity at that point.

# 5.2 Boundary Value Problem (BVP)

The indirect method for orbital transfer optimization applies optimal control theory to system 5.1, with boundary conditions set by the orbits involved. The problem is reformulated as a boundary value problem (BVP), where some initial values are unknown. Its solution consists in identifying the initial conditions that, through numerical integration, satisfy both imposed and optimal boundary constraints.

The optimal control problem is thus expressed as a set of differential equations 5.1 and 5.8, coupled with algebraic conditions 5.6, subject to boundary constraints 5.2 and optimal conditions 5.14. The problem also exhibits specific features discussed below:

- The integration interval is divided into subintervals, in each of which the differential equations can take on different expressions;
- The duration of a subinterval is generally unknown;
- Boundary conditions can be non-linear and can involve the values of the variables at both the external and internal boundaries;
- Variables can be discontinuous at the internal boundaries and their values after the discontinuity can be unknown.

The main challenge of indirect optimization methods lies in solving the boundary value problem (BVP) arising from their application. A suitable solution method is therefore essential and must be consistent with the specific characteristics of the problem. In this work, the BVP is solved by reducing it to a sequence of initial value problems, iteratively converged through Newton's method. For the sole purpose of integration, the independent variable t is replaced with a new variable t to resolve the uncertainty associated with the duration of each subinterval. This parameter is defined as follows:

$$\epsilon = j - 1 + \frac{t - t_{j-1}}{t_i - t_{j-1}} = j - 1 + \frac{t - t_{j-1}}{\tau_j} \tag{5.15}$$

where  $\tau_j$  is the duration of the subinterval, which is generally unknown. Therefore, thanks to the introduction of the unknown parameters  $\tau_j$ , the external and internal contours are fixed and correspond to consecutive integer values of the new independent variable  $\epsilon$ .

Referring to the generic system of equations 5.1 and 5.8 in which the controls have been replaced by 5.9, a differential problem in the variables, both state and adjoint, now no longer distinct,  $\vec{y} = (\vec{x}, \vec{\lambda})$ , is obtained:

$$\frac{d\vec{y}}{dt} = \vec{f}^*(\vec{y}, \epsilon) \tag{5.16}$$

However, it must also be taken into account the presence of constant parameters such as  $\tau_j$  or the value of a variable following a discontinuity. For this purpose, a new vector z = (y, c) is introduced, containing the state variables, the additional variables and the new vector c of constant parameters. Applying the change of independent variable, the system of differential equations becomes:

$$\frac{d\vec{z}}{d\epsilon} = \vec{f}(\vec{z}, \epsilon) \tag{5.17}$$

Expressing explicitly the second member of this equation, for the state and adjoint variables it is obtained:

$$\frac{d\vec{y}}{d\epsilon} = \tau_j \frac{d\vec{y}}{dt} \tag{5.18}$$

while for constant parameters it obviously holds that:

$$\frac{d\vec{c}}{d\epsilon} = 0 \tag{5.19}$$

Boundary conditions are expressed without distinguishing between optimal and imposed conditions as follows:

$$\vec{\Psi}(\vec{s}) = 0 \tag{5.20}$$

where s is a vector containing the values that the variables assume on the internal and external contours and the unknown parameters:

$$\vec{s} = (\vec{y}_0, \vec{y}_1, \dots, \vec{y}_n, \vec{c})$$
 (5.21)

Some of the variables are unknown. Their values must be determined through an iterative process so that they satisfy the boundary conditions above. It is assumed initially that all variables are unknown and the r-th iteration begins by integrating the differential equations 5.17 with the  $\vec{p}^r$  values obtained from the previous iteration. Accordingly, the following is defined:

$$\vec{z}(0) = \vec{p}^r \tag{5.22}$$

Obviously, in order to begin the iterative procedure, it is necessary to choose initial trial values  $\vec{p}^{1}$ . When integrating the equations, any discontinuities present at the internal boundaries are also taken into account. At the end of the r-th integration, after calculating the values of the state variables at each of the boundaries, the error on the boundary conditions  $\vec{\Psi}^{r}$  is calculated.

If there is a variation  $\Delta \vec{p}$ , then, considering only the first-order terms, the error on the boundary conditions varies by an amount equal to:

$$\Delta \vec{\Psi} = \left[ \frac{\partial \vec{\Psi}}{\partial \vec{p}} \right] \Delta \vec{p} \tag{5.23}$$

Cancelling the error on the boundary conditions means obtaining a  $\Delta \vec{\Psi}$  equal to  $-\vec{\Psi}^r$ . Therefore, at each iteration, the initial values are corrected by an amount:

$$\Delta \vec{p} = \vec{p}^{r+1} - \vec{p}^r = -\left[\frac{\partial \vec{\Psi}}{\partial \vec{p}}\right]^{-1} \vec{\Psi}^r \tag{5.24}$$

until the boundary conditions are satisfied with the desired precision. The matrix appearing in the equation above is obtained by multiplying two matrices:

$$\left[\frac{\partial \vec{\Psi}}{\partial \vec{p}}\right] = \left[\frac{\partial \vec{\Psi}}{\partial \vec{s}}\right] \left[\frac{\partial \vec{s}}{\partial \vec{p}}\right]$$
(5.25)

The first matrix is obtained by deriving the boundary conditions with respect to the variables contained in the vector  $\vec{s}$ , while the second matrix, which contains the derivatives of the values assumed by the variables at the boundaries with respect to the initial values, or rather the values assumed at the boundaries by the matrix

$$\left[\frac{\partial \vec{z}}{\partial \vec{p}}\right] = [\vec{g}(\epsilon)] \tag{5.26}$$

is obtained by integrating the system of differential equations that results from differentiating the main system 5.17 with respect to each initial value:

$$\left[\dot{\vec{g}}\right] = \frac{d}{d\epsilon} \left[\frac{\partial \vec{z}}{\partial \vec{p}}\right] = \left[\frac{\partial}{\partial \vec{p}} \left(\frac{d\vec{z}}{d\epsilon}\right)\right] = \left[\frac{\partial \vec{f}}{\partial \vec{p}}\right]$$
(5.27)

where the dot above the letter now indicates the first derivative with respect to the independent variable  $\epsilon$ . By making explicit the Jacobian of the main system 5.17, the equation 5.27 takes the following form:

$$\left[ \dot{\vec{g}} \right] = \left[ \frac{\partial \vec{f}}{\partial \vec{z}} \right] \left[ \frac{\partial \vec{z}}{\partial \vec{p}} \right] = \left[ \frac{\partial \vec{f}}{\partial \vec{z}} \right] [\vec{g}]$$
 (5.28)

The initial values for the homogeneous system above are obtained by deriving the relation 5.22, thus obtaining the identical matrix:

$$[\vec{g}(0)] = \left[\frac{\partial \vec{z}(0)}{\partial \vec{p}}\right] = \left[\vec{I}\right] \tag{5.29}$$

This method also allows to take into account discontinuities in the variables since, for a discontinuity in the point i, it is sufficient to update both the vector of variables  $\vec{z}$  and the matrix  $\vec{g}$  using the relation  $\vec{h}$  which links the values of the variables before and after the variation:

$$\vec{z}_{i+} = \vec{h}(\vec{z}_{i-}) \tag{5.30}$$

$$\left[\vec{g}_{i_{+}}\right] = \left[\frac{\partial \vec{h}}{\partial \vec{z}}\right] \left[\vec{g}_{i_{-}}\right] \tag{5.31}$$

Obviously, if some initial values of the variables are known, the problem simplifies since the vector  $\vec{p}$  reduces to only the unknown components of  $\vec{z}(0)$  and the vector  $\vec{\Psi}$  to the non-explicit boundary conditions at the initial time.

The matrix of equation 5.24 can be calculated numerically: its *i*-th row is obtained by perturbing the *i*-th component of  $\vec{p}$  by a small amount  $\Delta p$  (keeping the others fixed) and integrating equations 5.17. In this way, the variation  $\Delta \vec{\Psi}(\Delta p)$  is evaluated and, by linearizing, the corresponding row is obtained as  $\Delta \vec{\Psi}^T/\Delta p$ . This procedure can lead to a simpler and faster solution of the BVP (with  $\Delta p \approx 10^{-6} \div 10^{-7}$ ), but it does not always guarantee convergence, since the matrix obtained in the equation 5.24 is less accurate than the calculation using system 5.27. Given the sensitivity of the problem, numerical approximations can compromise its stability.

A similar approach can be used to calculate the Jacobian and the matrix  $\left[\partial \vec{\Psi}/\partial \vec{s}\right]$ , but it is preferred to maintain their analytical evaluation, using the numerical values only for verification purposes.

The integration of the differential equations, both of the main system 5.17 and the homogeneous system 5.27, is performed with a variable-step and variable-order method based on the Adams formulas.

The linearization used to calculate the correction  $\Delta \vec{p}$  using equation 5.24, to be applied to the initial trial values, inevitably introduces errors that can compromise convergence, increasing rather than reducing the error on the boundary conditions. For this reason, some measures have been adopted:

• Reducing the correction: to avoid deviating too far from the solution, the applied correction is actually only a fraction of the calculated one:

$$\vec{p}^{r+1} = \vec{p}^r + K_1 \Delta \vec{p} \tag{5.32}$$

with  $K_1$  between 0.1 and 1. The value is chosen empirically based on the distance of the initial solution from the desired one.

• Error check: after updating  $\vec{p}^{r+1}$  using formula 5.32 and integrating the equations of motion, the maximum error on the boundary conditions  $E_{\max}^{r+1}$  is compared with that of the previous iteration  $E_{\max}^r$ . The next iteration is accepted only if:

$$E_{\text{max}}^{r+1} < K_2 E_{\text{max}}^r \tag{5.33}$$

with  $K_2 > 1$  (typically between 2 and 3), so as to tolerate a possible increase in the error in the first iterations without compromising convergence.

• **Bisection of the correction:** if, however, the error is too large compared to the previous one, the correction applied is halved:

$$\vec{p}^{r+1} = \vec{p}^r + \frac{K_1 \Delta \vec{p}}{2} \tag{5.34}$$

and the comparison is repeated. If necessary, the bisection can be repeated up to a maximum of 5 times. Beyond this limit, the process stops, indicating that the chosen tentative solution does not allow convergence.

# Chapter 6

# Mathematical model

This section describes the mathematical model used for the optimization problem. Specifically, for the optimization of space trajectories, an inertial and heliocentric reference frame is considered so as to avoid drag and Coriolis accelerations, which would complicate the evaluation of the Jacobian of the system required for the BVP solution.

The transfer from Earth to the asteroid is studied using the patched conics method, which assumes that, outside the sphere of influence of a planet, the spacecraft follows an unperturbed Keplerian orbit around the Sun. The forces acting on the spacecraft are therefore solely the solar gravitational attraction and the thrust generated by the propulsion system.

## 6.1 Equations of motion

The motion of the spacecraft along its orbit around the Sun is described by the equations of motion of the two-body problem:

$$\frac{d\vec{r}}{dt} = \vec{V} \tag{6.1}$$

$$\frac{d\vec{V}}{dt} = \vec{g} + \frac{\vec{T}}{m} \tag{6.2}$$

$$\frac{dm}{dt} = -\frac{T}{c} \tag{6.3}$$

where:

- $\vec{r}$  is the position vector;
- $\vec{V}$  is the velocity vector;
- $\vec{q}$  is the gravitational acceleration generated by the Sun which is equal to

$$\vec{g} = -\frac{\mu_{\odot}\vec{r}}{r^3} \tag{6.4}$$

where  $\mu_{\odot}$  is the standard gravitational parameter of the Sun;

- $\vec{T}$  is the thrust of the spacecraft;
- *m* is the mass of the spacecraft;
- ullet c is the effective exhaust velocity.

The adjoint variable vector is defined as

$$\vec{\lambda} = \begin{bmatrix} \vec{\lambda_r} \\ \vec{\lambda_V} \\ \lambda_m \end{bmatrix}$$

Using this definition, it is possible to write the Hamiltonian, parameter that appears in optimal control theory, in the following way:

$$H = \vec{\lambda}_r^T \vec{V} + \vec{\lambda}_V^T \vec{g} + S_F T \tag{6.5}$$

where  $S_F$  is the **switching function** and is calculated as follows:

$$S_F = \frac{\vec{\lambda}_V^T \vec{T}}{mT} - \frac{\lambda_m}{c} \tag{6.6}$$

The switching function therefore depends on the adjoint variables related to velocity and mass, while those related to position do not appear in the expression.

# 6.2 Optimal controls

Since the Pontryagin Maximum Principle requires the Hamiltonian to be maximized, the scalar product between  $\vec{\lambda}_V$  and the thrust must be as high as possible in the expression for  $S_F$ . Therefore,  $\vec{\lambda}_V \parallel \vec{T}$  is considered, resulting in the following formulation of the switching function:

$$S_F = \frac{\lambda_V}{m} - \frac{\lambda_m}{c} \tag{6.7}$$

The switching function therefore determines the optimal control law and, based on its value, regulates the operation of the propulsion system. In particular, considering the effective exhaust velocity constant, the switching function can assume positive, negative or zero values:

- if  $S_F > 0$ , the thrust is maximum;
- if  $S_F < 0$ , the thrust is minimum (typically zero);
- if  $S_F \equiv 0$  over an interval, a singular arc occurs.

Further observations can be made by considering c and T variable, given a power  $P = \frac{Tc}{2}$ . The optimal value of the effective exhaust velocity is obtained by differentiating the Hamiltonian with respect to c and setting it equal to zero. It is obtained:

$$c_{ott} = \frac{2m\lambda_m}{\lambda_V} \tag{6.8}$$

Based on the value obtained using the above expression, three cases can be distinguished:

- if  $c_{min} < c_{ott} < c_{max}$ , then  $c = c_{ott}$ ;
- if  $c_{ott} < c_{min}$ , then  $c = c_{min}$ ;
- if  $c_{ott} > c_{max}$ , then  $c = c_{max}$ .

Returning to reasoning about the value assumed by the switching function, maximum power will be obtained when  $S_F > 0$  and minimum when  $S_F < 0$ . Since  $S_F$  is minimum when the effective exhaust velocity assumes the minimum value, the switching function is always positive if  $c_{min} = 0$ , that is, if c is not bounded.

If  $c = c_{ott}$  then:

$$T = \frac{P\lambda_V}{m\lambda_m} \tag{6.9}$$

and therefore:

$$\frac{T}{m} = \frac{P\lambda_V}{m^2\lambda_m} \tag{6.10}$$

If there are no constraints on c, then  $m^2 \lambda_m$  is constant and, consequently,  $\frac{T}{m} \propto \lambda_V$ 

## 6.3 Equations in spherical coordinates

This section introduces the vector form of the equations underlying the optimization problem. These equations must be projected into a suitable reference system, which, as previously mentioned, is an inertial and heliocentric reference frame.

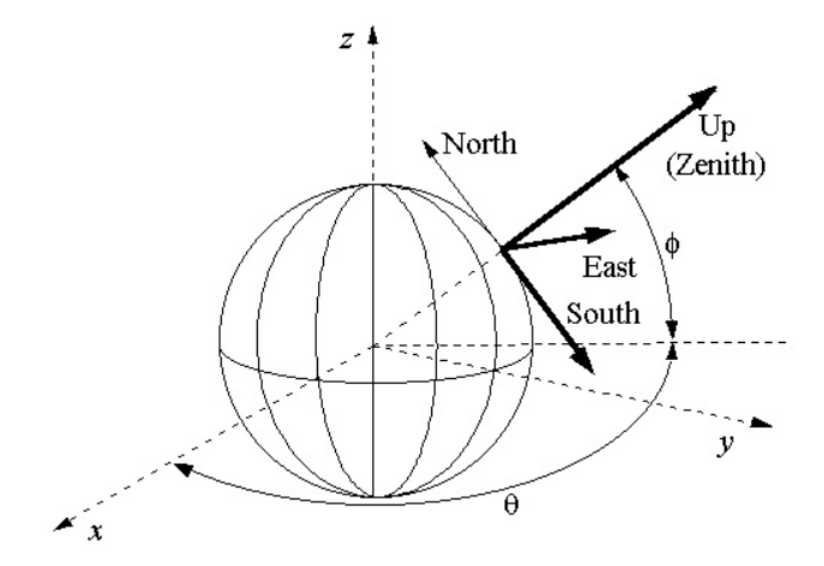


Figure 6.1: Topocentric and inertial coordinate system [20]

Therefore, spherical coordinates are used:

- r is the spacecraft's distance from the Sun;
- $\theta$  is the longitude;
- $\phi$  is the latitude;
- u is the radial component of the velocity (the component directed toward the Zenith);
- $\bullet$  v is the eastward component of the velocity;
- $\bullet$  w is the northward component of the velocity.

The velocity is projected into a local North-East-Zenith reference system so as to have a simpler relationship between relative and absolute velocity.

The state variables vector can therefore be written as follows:

$$\vec{x} = \begin{bmatrix} r \\ \theta \\ \phi \\ u \\ v \\ w \\ m \end{bmatrix}$$

Before listing the differential equations, it is necessary to introduce two more angles:

- flight path angle  $(\gamma)$ : measured from the horizontal plane with positive angles upward;
- heading angle ( $\psi$ ): measured counter-clockwise from the parallel with positive angles towards the north.

Projecting the state equations into the reference system, it is obtained:

$$\frac{dr}{dt} = u \tag{6.11}$$

$$\frac{d\theta}{dt} = \frac{v}{r\cos\phi}$$

$$\frac{d\phi}{dt} = \frac{w}{r}$$
(6.12)

$$\frac{d\phi}{dt} = \frac{w}{r} \tag{6.13}$$

$$\frac{du}{dt} = -\frac{1}{r^2} + \frac{v^2}{r} + \frac{w^2}{r} + \frac{T}{m}\sin\gamma_T$$
 (6.14)

$$\frac{dv}{dt} = -\frac{uv}{r} + \frac{vw}{r}\tan\phi + \frac{T}{m}\cos\gamma_T\cos\psi_T$$
(6.15)

$$\frac{dw}{dt} = -\frac{1}{r} + \frac{1}{r} \tan \phi + \frac{1}{m} \cos \gamma_T \cos \psi_T \qquad (6.15)$$

$$\frac{dw}{dt} = -\frac{uw}{r} - \frac{v^2}{r} \tan \phi + \frac{T}{m} \cos \gamma_T \sin \psi_T \qquad (6.16)$$

$$\frac{dm}{dt} = -\frac{T}{c} \qquad (6.17)$$

$$\frac{dm}{dt} = -\frac{T}{c} \tag{6.17}$$

The flight path angle and the heading angle depend only on the state variables:

$$\sin \gamma = \frac{u}{V_r} \tag{6.18}$$

$$\cos\gamma\cos\psi = \frac{v - \omega r\cos\phi}{V_r} \tag{6.19}$$

$$\cos\gamma\sin\psi = \frac{w}{V_r} \tag{6.20}$$

where the modulus of the relative velocity is equal to:

$$V_r = \sqrt{u^2 + (v - \omega r \cos \phi)^2 + w^2}$$
 (6.21)

The control vector is defined as follows:

$$\vec{u} = \begin{bmatrix} \gamma_T \\ \psi_T \end{bmatrix}$$

The thrust direction is determined by the  $\gamma_T$  and  $\psi_T$  controls. Optimal thrust angles can be obtained by explicitly writing the Hamiltonian and setting its partial derivatives with respect to  $\gamma_T$  and  $\psi_T$  to zero:

$$\sin \gamma_T = \frac{\lambda_u}{\lambda_V} \tag{6.22}$$

$$\cos \gamma_T \cos \psi_T = \frac{\lambda_v}{\lambda_V} \tag{6.23}$$

$$\cos \gamma_T \sin \psi_T = \frac{\lambda_w}{\lambda_V} \tag{6.24}$$

(6.25)

where  $\vec{\lambda}_V$  is the **primer vector** and, as previously mentioned, is parallel to the thrust. Its magnitude is defined as follows:

$$\lambda_V = \sqrt{\lambda_u^2 + \lambda_v^2 + \lambda_w^2} \tag{6.26}$$

After defining the vector of adjoint variables:

$$\vec{\lambda} = \begin{bmatrix} \lambda_r \\ \lambda_\theta \\ \lambda_\phi \\ \lambda_u \\ \lambda_v \\ \lambda_w \\ \lambda_m \end{bmatrix}$$

it is possible to write the differential equations through the Euler-Lagrange equations for the adjoint variables:

$$\dot{\lambda}_r = \frac{1}{r^2} \left( \lambda_\theta \frac{v}{\cos \phi} + \lambda_\phi w + \lambda_u \left( -\frac{2}{r} + v^2 + w^2 \right) + \lambda_v (-uw + vw \tan \phi) + \lambda_w (-uv - v^2 \tan \phi) \right) + \frac{2qS}{mV_r} \lambda_v \omega \cos \phi$$
(6.27)

$$\dot{\lambda}_{\theta} = 0 \tag{6.28}$$

$$\dot{\lambda}_{\phi} = \frac{1}{r \cos^2 \phi} \left( -\lambda_{\theta} w \sin \phi - \lambda_{\phi} v w + \lambda_u w^2 \right) + \frac{2qS}{mV_r} \lambda_v \omega r \sin \phi \tag{6.29}$$

$$\dot{\lambda}_u = \frac{1}{r} \left( -\lambda_r + \lambda_\theta v + \lambda_\phi w \right) - \frac{2qS}{mV_r} \lambda_v \tag{6.30}$$

$$\dot{\lambda}_v = \frac{1}{r} \left( -\lambda_\theta \frac{1}{\cos \phi} - 2\lambda_u v + \lambda_w (u - w \tan \phi) \right) +$$

$$+2\lambda_v w \tan \phi - \frac{2qS}{mV_r} \lambda_v \tag{6.31}$$

$$\dot{\lambda}_w = \frac{1}{r} \left( -\lambda_\phi v - 2\lambda_u w - \lambda_v u \tan \phi + \lambda_w u \right) - \frac{2qS}{mV_r} \lambda_v \tag{6.32}$$

$$\dot{\lambda}_m = \frac{T}{m^2} \lambda_v \tag{6.33}$$

## 6.4 Initial conditions

In order to solve the optimality problem, it is necessary to define the initial conditions of the problem that the code uses as input to start the iteration. More precisely, the initial values are contained in a vector  $\vec{p}$ :

$$\vec{p} = [t_0, t_f, r_0, \theta_0, \phi_0, u_0, v_0, w_0, \lambda_{r_0}, \lambda_{\theta_0}, \lambda_{\phi_0}, \lambda_{u_0}, \lambda_{v_0}, \lambda_{w_0}]^T$$
(6.34)

where:

- $t_0$  identifies the departure date;
- $t_f$  identifies the arrival date;
- $r_0$ ,  $\theta_0$  and  $\phi_0$  identify the initial position of the spacecraft;
- $u_0$ ,  $v_0$  and  $w_0$  are the components of the spacecraft's initial velocity;
- $\lambda_{r_0}$ ,  $\lambda_{\theta_0}$ ,  $\lambda_{\phi_0}$ ,  $\lambda_{u_0}$ ,  $\lambda_{v_0}$  and  $\lambda_{w_0}$  are the initial adjoint variables.

Starting from the initial values, the code begins the iterative process. Following the integration of the differential equations, the solutions are compared with the boundary conditions discussed in Section 6.5, by evaluating the resulting errors. If the values assumed by these errors fall within the required tolerance, then the code converges. Otherwise, the initial values must be adjusted in order to obtain the optimal solution.

# 6.5 Boundary and optimal conditions

The mission under consideration involves departure from Earth and a possible intermediate flyby before reaching the target asteroid. Specifically, the trajectory can be divided into N sub-intervals, where N corresponds to the number of celestial bodies visited, excluding the departure body. For each sub-interval, it is necessary to outline the boundary conditions of the problem, which are therefore defined not only at the endpoints of the trajectory, but also at the intermediate points where the flyby occurs. More precisely, it is required to impose continuity on the interface of each interval for both state and adjoint variables.

## Departure and arrival

The boundary conditions at departure are as follows:

$$\vec{V}(t_0) = \vec{r}_{Earth}(t_0)$$

$$\vec{V}(t_0) = \vec{V}_{Earth}(t_0)$$

$$m_0 = 1000 \text{ kg}$$

It is therefore assumed that the spacecraft's position and velocity are equal to those of Earth, although the initial phase within the sphere of influence is not considered in this case study. This assumption can be made since the size of the sphere of influence is small compared to the dimensions involved during the transfer.

Upon arrival, similar boundary conditions apply:

$$\vec{r}(t_f) = \vec{r}_{asteroid}(t_f)$$

$$\vec{V}(t_f) = \vec{V}_{asteroid}(t_f)$$

In this case, the spacecraft's radius and velocity must be the same as the target asteroid. The final mass, however, is determined at the end of the optimization process.

The values of  $t_0$  and  $t_f$  are set as initial values by providing the departure date and mission duration to the code, but they can also be optimized.

## Intermediate flyby

Among the various solutions found, some involve an intermediate flyby before reaching the asteroid. It is therefore necessary to impose boundary conditions also at the intermediate points corresponding to the j-th flyby. In particular, it is necessary to ensure the continuity of the state variables before and after the flyby, setting them equal to those of the intermediate body. In the case study, the celestial body encountered during the flyby is the Earth. Therefore, in the instant immediately before and after this manoeuvre, the following conditions apply:

$$\begin{split} \vec{r}\left(t_{j_{-}}\right) &= \vec{r}_{Earth}\left(t_{j_{-}}\right) \\ \vec{V}\left(t_{j_{-}}\right) &= \vec{V}_{Earth}\left(t_{j_{-}}\right) \\ \vec{r}\left(t_{j_{+}}\right) &= \vec{r}_{Earth}\left(t_{j_{+}}\right) \\ \vec{V}\left(t_{j_{+}}\right) &= \vec{V}_{Earth}\left(t_{j_{+}}\right) \end{split}$$

where the value of  $t_{j_{+}}$  is obtained by adding the residence time near the main body to  $t_{j_{-}}$ :

$$t_{i_{+}} = t_{i_{-}} + t_{stay}$$

For simplicity, as also reported further on in the assumptions made in Section 7.1, the residence time is assumed to be zero. It is therefore possible to rewrite the conditions as follows:

$$\vec{r}\left(t_{j_{-}}\right) = \vec{r}\left(t_{j_{+}}\right) = \vec{r}_{Earth}\left(t_{j}\right)$$

$$\vec{V}\left(t_{j_{-}}\right) = \vec{V}\left(t_{j_{+}}\right) = \vec{V}_{Earth}\left(t_{j}\right)$$

$$m\left(t_{j_{-}}\right) = m\left(t_{j_{+}}\right)$$

While searching for solutions, it was observed that in most cases, considering a free flyby of the planet led to trajectories that were too low. Therefore, in some analyses, a constrained flyby model was adopted, which requires introducing an additional condition related to the rotation angle  $\delta$ , which is:

$$\sin \delta_j = \frac{\left\| \vec{V}_{\infty}(t_{j_+}) \times \vec{V}_{\infty}(t_{j_-}) \right\|}{\left\| \vec{V}_{\infty}(t_{j_+}) \right\| \left\| \vec{V}_{\infty}(t_{j_-}) \right\|}$$

The optimal conditions are instead obtained by guaranteeing the continuity between the adjoint variables for the speed:

$$\lambda_{u}\left(t_{j_{-}}\right) = \lambda_{u}\left(t_{j_{+}}\right)$$
$$\lambda_{v}\left(t_{j_{-}}\right) = \lambda_{v}\left(t_{j_{+}}\right)$$
$$\lambda_{w}\left(t_{j_{-}}\right) = \lambda_{w}\left(t_{j_{+}}\right)$$

# Chapter 7

# Mission analysis and numerical implementation

Trajectories toward NEAs were studied using an optimization code written in Fortran provided by the Polytechnic of Turin. The code, through an iterative process, allows to derive the optimal thrust law that achieves the maximum final mass (and therefore the minimum  $\Delta V$ ) at the end of the mission. This chapter presents some aspects related to the mission analysis, before moving on to explain how the code works.

# 7.1 Simplifying assumptions

In order to simplify the calculations related to the analysis of space trajectories, the following assumptions are made:

- for the calculations, only the heliocentric phase of the patched conics method is considered, while the departure and arrival phases within the spheres of influence are not considered;
- the asteroid's orbital parameters are considered correct, even though they may change with further observations;
- even though this is not the case in reality, the time spent near a celestial body during a flyby is taken to be zero. This approximation is valid considering the extended mission times.

## 7.2 Initial data

In order to study the mission, it is necessary to define a set of variables and assign them specific values. These variables constitute the initial data of the problem and are incorporated into the optimization code for the subsequent analysis.

For the Earth–2024 YR4 interplanetary transfer, a spacecraft with an initial mass of 1000 kg and an available power of 4.2 kW was considered.

Assuming an efficiency of 0.625, the corresponding nominal thrust can be computed as follows:

$$T = \frac{2\eta P_E}{c} = 0.1622 \text{ N} = 162.2 \text{ mN}$$
 (7.1)

where:

$$c = I_{SP}g_0 = 32361.945 \,\mathrm{m/s} \tag{7.2}$$

Below are the values of the variables inserted into the code.

Initial mass $m_0$	1000 kg
Specific impulse $I_{sp}$	$3300 \mathrm{\ s}$
Power P	$4.2~\mathrm{kW}$
Nominal thrust T	$162.2 \mathrm{mN}$
Efficiency $\eta$	0.625

Table 7.1: Initial parameters for electric propulsion system

There are also coefficients that take into account the duty cycle, since there are moments during the flight when the engines turn off. To compensate for these shutdown periods, the available thrust is assumed to be 90% of its actual thrust. In the moments before arriving at the target body or before a flyby, since navigation is required and therefore the spacecraft's position relative to the main body must be monitored, the duty cycle is further reduced to 70%.

## 7.3 Synodic period

For the study of the trajectories towards the asteroid 2024 YR4, it is useful to calculate the value of the synodic period in order to know after how long the missions are repeated. As already seen in section 3.10.2, the formula used to calculate the synodic period is the following:

$$\tau_s = \frac{2\pi}{|w_1 - w_2|} = \frac{T_1 T_2}{|T_1 - T_2|} \tag{7.3}$$

where  $w_1$  and  $w_2$  are the angular velocities of the planets and  $T_1$  and  $T_2$  are their periods of revolution.

Knowing the period of revolution of the Earth and the asteroid 2024 YR4 around the Sun, a synodic period equal to 487.4 days (or 1.34 years) is obtained. This synodic period implies that, after approximately 4 years, orbital conditions will repeat themselves in a similar way. Specifically, since the asteroid has an orbital period of 1457.574 days (or 3.9934 years), after four years, the Earth will have completed approximately four revolutions, while the asteroid will have completed only one. Consequently, a mission departing at  $t_0$  and a second departing approximately after 4 years should present very similar characteristics in terms of orbital geometry and launch window. Solutions with later departure dates will be discussed later in Sections 8.3 and 8.4.

## 7.4 Non-dimensional variables

For calculation purposes, some variables are non-dimensionalised using appropriate constant parameters implemented within the code. Specifically, radius, velocity, mass, thrust and time are non-dimensionalised using the following conversion parameters:

• Reference mass: mass of the satellite

$$m_0 = 1000 \text{ kg}$$
 (7.4)

• Reference distance: Earth-Sun distance equal to 1 AU

$$r_{conv} = 1.49597870691 \times 10^8 \text{ km} = 1 \text{ AU}$$
 (7.5)

$$v_{conv} = \sqrt{\frac{\mu_{\odot}}{r_{conv}}} = 29.784692 \text{ km/s}$$
 (7.6)

• Reference acceleration: acceleration relative to the Earth's orbit around the Sun

$$a_{conv} = \frac{\mu_{\odot}}{r_{conv}^2} = 5.930084 \times 10^{-6} \text{ km/s}^2$$
 (7.7)

## • Reference time

$$t_{conv} = \frac{1}{86400} \frac{v_{conv}}{a_{conv}} = \frac{1}{86400} \sqrt{\frac{r_{conv}^3}{\mu_{\odot}}} = 58.132441 \,\text{days}$$
 (7.8)

It follows that a period equal to one year can be non-dimensionalised as follows:

$$\frac{365 \text{ days}}{t_{conv}} = 2\pi \tag{7.9}$$

That is, in non-dimensional units, one year corresponds to  $2\pi$ . In particular, the days are counted starting from J2000, i.e., from January 1, 2000, at 12:00 UTC.

#### • Reference thrust

$$T_{rif} = 1000 \cdot m_0 \cdot a_{conv} = 5.930084 \,\mathrm{N}$$
 (7.10)

## 7.5 Code implementation and inputs

The code is based on an iterative process that finds the best trajectory toward NEAs in terms of mass and  $\Delta V$ .

Specifically, the code requires input from both data that the user can enter manually and values saved in a file. The latter are the tentative values from which the program will start the iterative process and are:

- departure and arrival dates:  $t_0$  and  $t_f$ ;
- $v_{\infty}$  at departure;
- spacecraft position:  $r, \theta, \phi$ ;
- spacecraft velocity: u, v, w;
- values of adjoint variables:  $\lambda_r$ ,  $\lambda_\theta$ ,  $\lambda_\phi$ ,  $\lambda_u$ ,  $\lambda_v$ ,  $\lambda_w$ ;
- non-dimensional mass.

The values requested from the user are the following:

- integration control parameters: rmin, pbis, jmax;
- thrust multiplicative coefficient: thrcoeff;
- duration;
- departure, intermediate (in the case of a flyby) and arrival celestial bodies;
- non-dimensional mass: am0;
- arrival and residence times at the intermediate celestial body in the case of a flyby: *tmid* and *tstay*.

To facilitate convergence, it is helpful if the  $t_0$  in the file containing the tentative values is the same as the one entered by the user.

From this data, and using files containing the orbital parameters of the asteroids, the code performs the calculations through various subroutines. If the selected initial guesses are not adequate, the code will not converge. It is therefore essential to carefully choose the tentative values and, in particular, the integration parameters.

If convergence occurs, the code produces several output files containing the transfer parameters, such as the evolution of the thrust and the switching function over time, the position of the spacecraft in spherical coordinates, the energy, the inclination and the eccentricity of the transfer orbit.

# Chapter 8

# Results

This chapter analyses the trajectory solutions to 2024 YR4 obtained through the optimization code. Specifically, five categories of solutions were considered:

- Direct transfers;
- Earth flyby transfers;
- Later direct transfer solutions;
- Later Earth flyby transfer solutions:
- Trajectory options before the expected impact date.

## 8.1 Direct transfer trajectories

This section presents the results related to direct transfers. For this type of trajectory, mission durations between 22 and 28 were considered, which correspond to transfer times ranging from 3.5 to 4.4 years.

A large number of solutions were identified, and the most relevant ones are reported in the tables 8.1 and 8.2.

Solution	Duratio	Duration		1	$\mathbf{t_f}$	
Solution	Normalized	Days	Normalized	Date	Normalized	Date
1	27.6	1604.46	181.4	14/11/2028	209	06/04/2033
2	22.1	1284.73	186.14	16/08/2029	208.24	21/02/2033

Table 8.1: Direct transfers - duration and timeline comparison

Solution	$\mathbf{M_f} \; [\mathrm{kg}]$	$\Delta V \; [\mathrm{km/s}]$
1	697.100	11.677
2	673.212	12.805

Table 8.2: Direct transfers - mass and  $\Delta V$  comparison

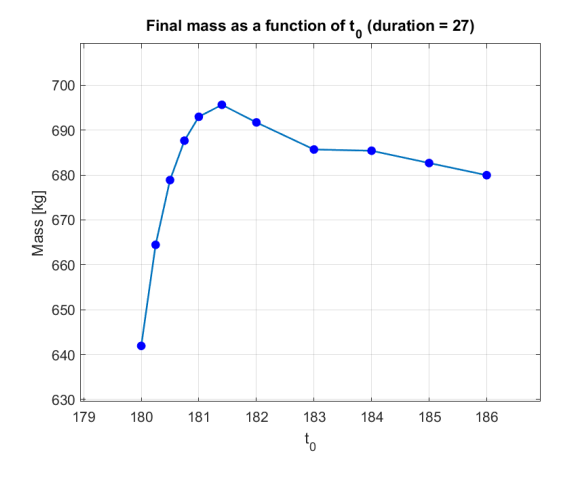
These two solutions represent, respectively, the one with the lowest propellant consumption among all those found, and the shortest one that still preserves a high final mass.

As can be observed, this type of mission requires a high total  $\Delta V$ . As a result, the propellant consumption is significant. For this reason, alternative solutions involving an Earth flyby were also identified, with the goal of reducing both the  $\Delta V$  cost and the associated propellant consumption

Chapter 8 Results

(these solutions will be discussed in Sections 8.2, 8.4 and 8.5).

A comparison between the various direct transfer solutions found is presented below. The results are compared by considering how the final mass evolves as either the departure date (at fixed duration) or the duration (at fixed departure date) varies.



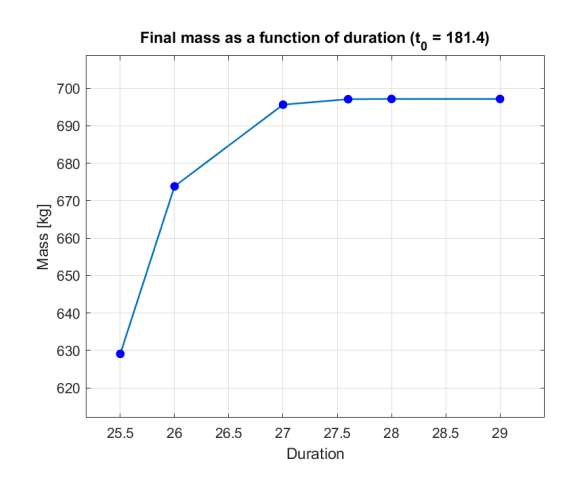


Figure 8.1: Direct transfers - final mass vs  $t_0$  (duration = 27)

Figure 8.2: Direct transfers - final mass vs duration ( $t_0 = 181.4$ )

As can be seen from these first two graphs, at a fixed duration there will be a value of  $t_0$  at which the final mass is maximized. At a fixed departure date, however, it is observed that the mass tends to increase with duration, until a value is reached beyond which no further gain in terms of final mass is achieved. This is due to the fact that, for the type of trajectory considered, increasing the duration beyond a certain threshold results in a coasting phase with the engines off, in which no further thrust is imparted to the spacecraft. Consequently, there is no further increase in final mass beyond that point.

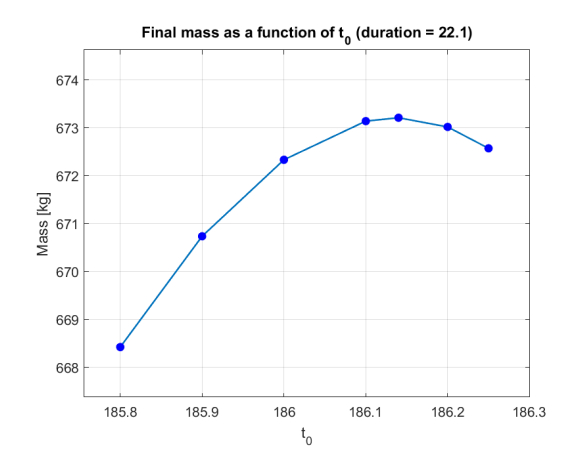
In particular, for the solutions of interest, at a fixed duration, a maximum in proximity of  $t_0$ =181.4 is reached. By fixing the starting time, it can be observed that the mass increases up to a duration of 27.6, beyond which no improvement is observed. Consequently, the final mass is maximized for:

- $t_0 = 181.4$
- duration=27.6

which corresponds to Solution 1.

These trends for fixed durations and  $t_0$  also recur in other cases. In particular, it is interesting to observe what happens for short durations and for starting times shifted by four years compared to Solution 1.

Chapter 8 Results



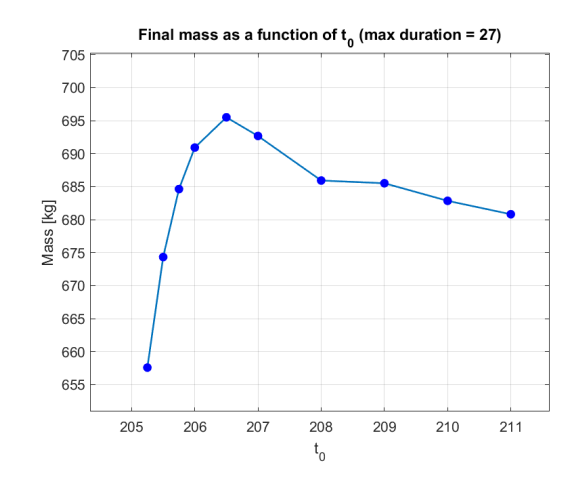
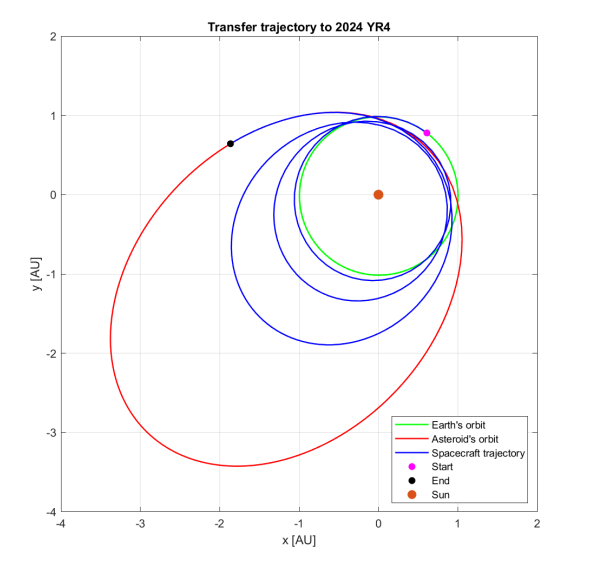


Figure 8.3: Direct transfers - final mass vs  $t_0$  (duration = 22.1)

Figure 8.4: Direct transfers - final mass vs  $t_0$  (max duration = 27)

From the graphs above, it is immediately observed that, as previously mentioned, for a fixed duration, a maximum is reached near a certain value of  $t_0$ . In particular, for orbital missions shifted by 4 years, the trend in final mass is very similar to the case shown in Figure 8.1. This occurs because, as already explained in Section 7.3, every 4 years the missions tend to repeat with very similar characteristics both in terms of trajectory traveled and launch window. For the case of shorter-duration solutions (duration equal to 22.1, or approximately 1285 days), it is observed that the final mass is maximized for a departure date value of 186.14, which corresponds to Solution 2.

## Trajectory followed by the spacecraft



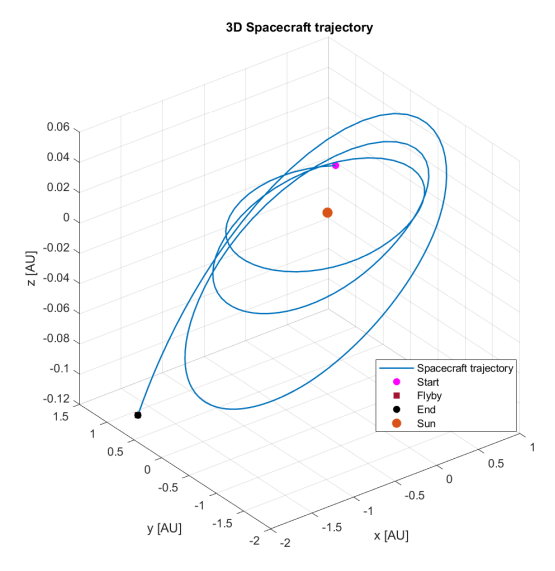


Figure 8.5: Solution 1 - Trajectory

Chapter 8 Results

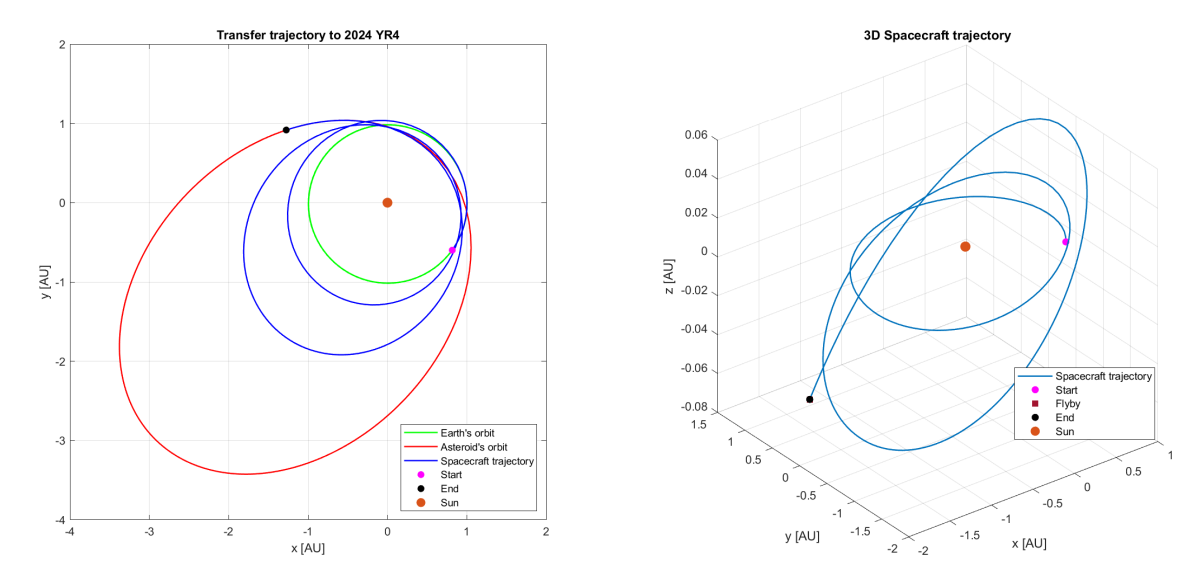


Figure 8.6: Solution 2 - Trajectory

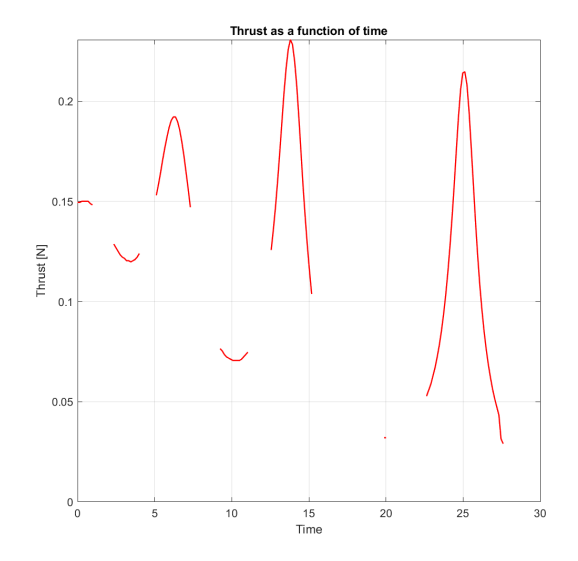
Figure 8.5 and 8.6 show the trajectories of the spacecraft and the orbits of the Earth and the asteroid 2024 YR4. Plotted distances are in astronomical units (1 AU =  $1.496 \cdot 10^8$  km).

The number of revolutions of the spacecraft around the Sun is slightly more than three and two, respectively. It is natural that shorter time intervals correspond to fewer revolutions and vice versa. Typically, the first revolution is approximately 1 year, the second roughly 1.5 years, and the possible third revolution roughly 2 years. As there is still a small fraction of the revolution left, the total mission times are barely less than 4.5 years for the case with duration equal to 27, and around 3.5 years for the case with duration equal to 22.1.

In the three-dimensional representation of the trajectory, the change in inclination of the space-craft's orbit required to reach that of the asteroid can be observed. These variations are intentionally accentuated in the image for better visualization. It should be noted that, since the orbit of 2024 YR4 is inclined by only about  $3.4^{\circ}$ , the variations along the z-axis are limited. To highlight this phenomenon, the range of values reported on the z-axis is much narrower than those reported along the x-axis and y-axis.

The same reasoning also applies to the trajectories reported in the other sections.

### Variation of thrust with time



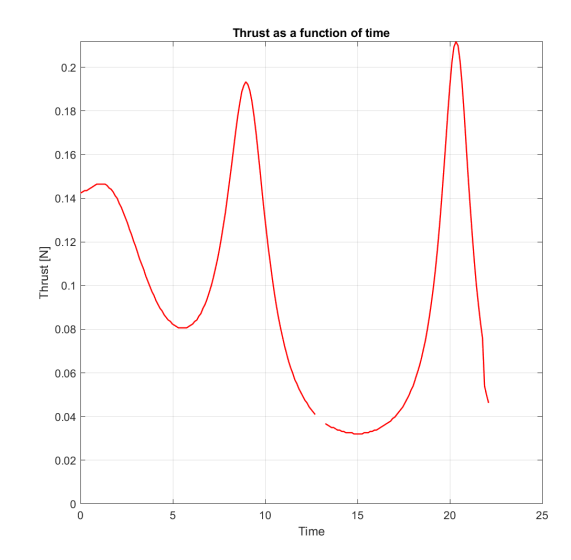


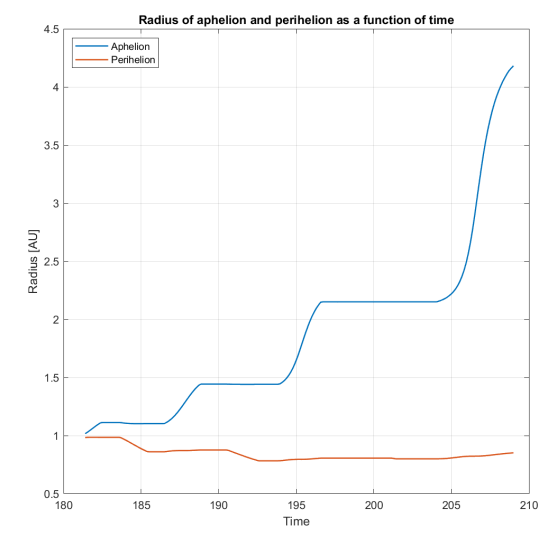
Figure 8.7: Solution 1 - Thrust

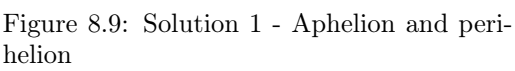
Figure 8.8: Solution 2 - Thrust

Graphs 8.7 and 8.8 show the thrust profile over time. It can be seen that for longer durations, there are periods in which the engines are off and do not generate thrust, while for shorter durations, since the final orbit must be reached in less time, the thrust profile is nearly continuous, and therefore there are almost no coasting phases with the engines off.

In both thrust profiles, the higher thrust peaks correspond to manoeuvres intended to increase the aphelion of the orbit, while the smaller peaks are associated with thrust phases aimed at reducing the perihelion. These thrust segments are timed to modify the orbit shape progressively, according to the mission requirements.

### Evolution of aphelion and perihelion as a function of time





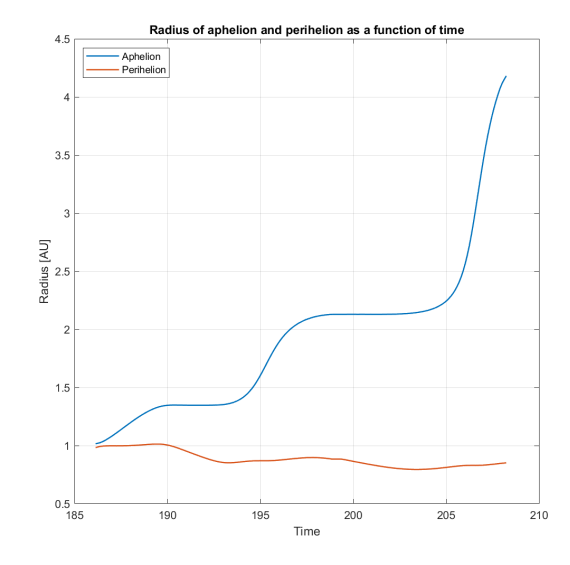


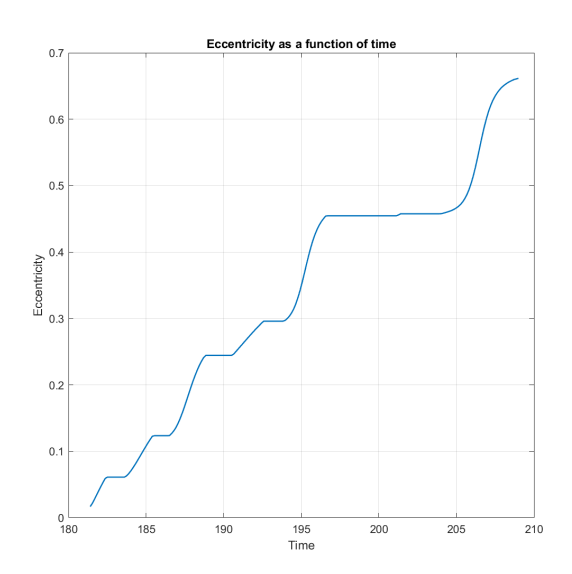
Figure 8.10: Solution 2 - Aphelion and perihelion

The above graphs show how the aphelion and perihelion radii vary with time. The spacecraft have to reach high levels of aphelion due to the high eccentricity of the orbit of 2024 YR4. On the other

hand, the perihelion must be reduced, since the asteroid's perihelion is lower than the Earth's. As previously outlined, the engines are fired at the appropriate times to regularly raise the aphelion and lower the perihelion, gradually shaping the spacecraft's trajectory into that of the target.

By comparing the two trends, it can be observed that in Solution 1 the changes in aphelion and perihelion are more distinctly marked than in Solution 2. This is consistent with the earlier discussion on the thrust profiles: for shorter durations, the engines remain active for a greater percentage of the mission time, resulting in more continuous modifications of the orbital parameters. In contrast, for longer durations, there are periods during which neither the aphelion nor the perihelion is significantly altered.

#### Evolution of eccentricity as a function of time



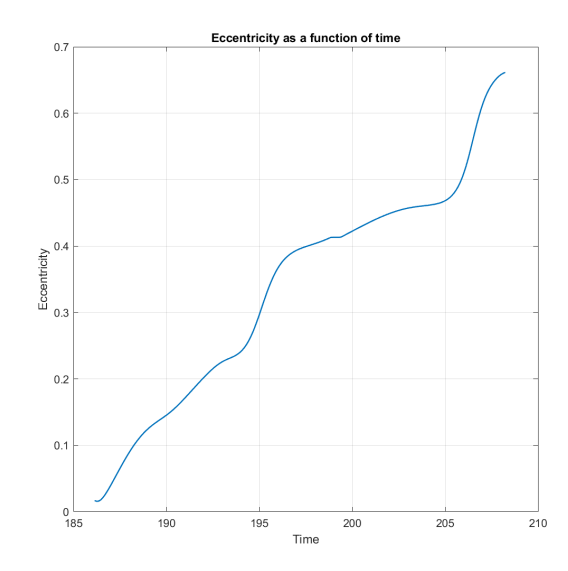


Figure 8.11: Solution 1 - Eccentricity

Figure 8.12: Solution 2 - Eccentricity

The comments regarding the aphelion and the perihelion radii can also be extended to the eccentricity trend, since these three parameters are correlated. Indeed, here too, it can be observed that the variation is much more marked for the longer-duration solution than for the shorter one. Obviously, since the asteroid's orbit is more elliptical than the Earth's, the eccentricity must increase. This growth is caused by both the increase in aphelion and the decrease in perihelion, two effects that lead to a more elliptical orbit.

# 8.2 Earth flyby transfer trajectories

Analysing the results reported in Section 7.2, it is observed that, after approximately one revolution (and therefore approximately a year after the start of the mission), the spacecraft's trajectory intersects Earth's orbit. It is therefore possible to exploit an Earth flyby to reduce the mission cost in terms of  $\Delta V$ , consequently reducing the propellant mass required for the transfer.

The two most interesting solutions involving Earth flybys are reported below.

Solution	Duration		$\mathbf{t_0}$		$ m t_{fb}$		$\mathbf{t_f}$	
	Normalized	Days	Normalized	Date	Normalized	Date	Normalized	Date
3	24	1395.18	185.17	21/06/2029	193.72	31/10/2030	209.17	16/04/2033
4	21	1220.78	186.93	01/10/2029	193.83	06/11/2030	207.93	03/02/2033

Table 8.3: Earth flyby transfers - duration and timeline comparison

Solution	$ m M_{fb}~[kg]$	$M_{\mathrm{f}}~[\mathrm{kg}]$	$\Delta V_1 \; [\mathrm{km/s}]$	$\Delta V_2 \ [\mathrm{km/s}]$	$\Delta V_{ m tot} \; [{ m km/s}]$
3	908.209	785.178	3.116	4.711	7.827
4	905.573	758.522	3.210	5.734	8.944

Table 8.4: Earth flyby transfers - mass and  $\Delta V$  comparison

Comparing the results above with the direct transfer results reported in Tables 8.1 and 8.2, the gains in terms of  $\Delta V$  and final mass are immediately noticeable. More specifically, using the Earth flyby allows for a saving of almost 100 kg of propellant mass, with transfers requiring approximately 4 km/s less in terms of  $\Delta V$ .

For Earth flyby transfers too, it is possible to compare the various solutions by varying the departure date for a fixed duration.

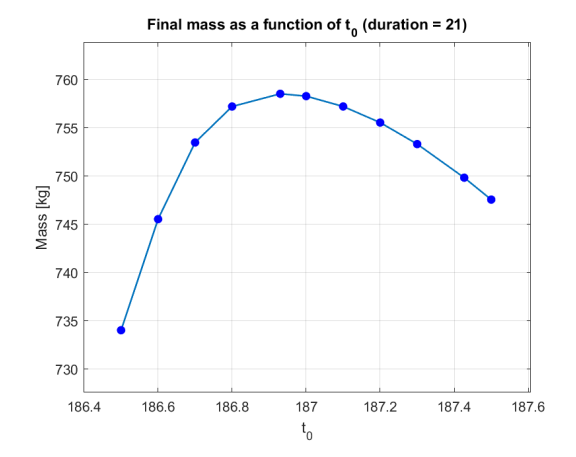


Figure 8.13: Earth flyby transfers - final mass vs  $t_0$  (duration = 21)

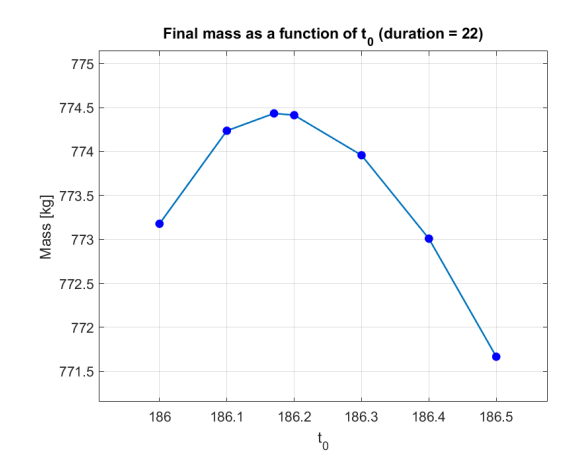
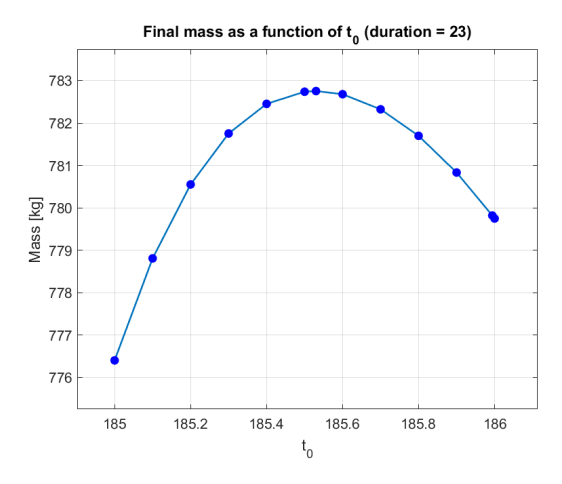


Figure 8.14: Earth flyby transfers - final mass vs  $t_0$  (duration = 22)

As with the direct solutions, there exists a departure date at which the value of  $m_f$  is maximized.

Comparing the range of  $t_0$  values present in this case with those for direct transfers, it can be seen that the Earth flyby solutions have narrower launch windows. In fact, increasing or decreasing the values of  $t_0$  reported above significantly reduces the final mass value.



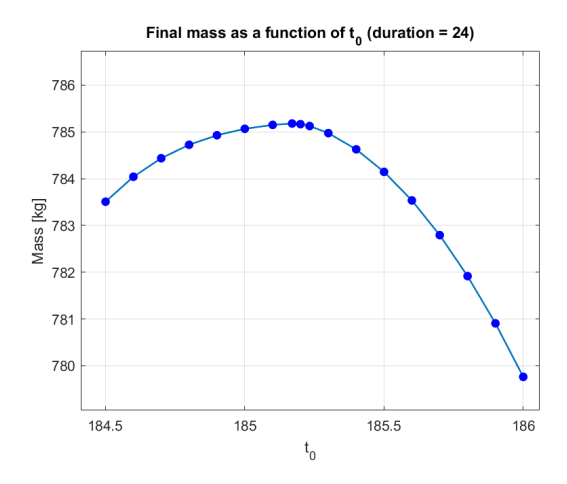


Figure 8.15: Earth flyby transfers - final mass vs  $t_0$  (duration = 23)

Figure 8.16: Earth flyby transfers - final mass vs  $t_0$  (duration = 24)

For longer durations, the same trend is observed, but shifted to higher  $m_f$  values. This occurs precisely because, as already mentioned when discussing direct transfers, increasing the mission duration results in a gain in terms of total mission cost.

# Trajectory followed by the spacecraft

The trajectories with Earth flyby are shown below, with the exact flyby point highlighted.

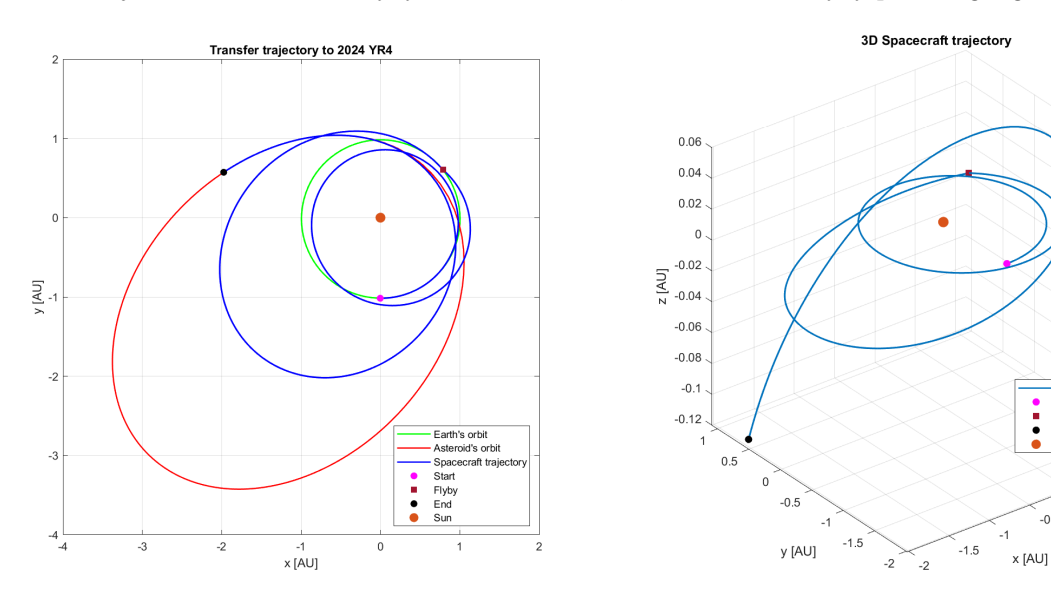


Figure 8.17: Solution 3 - Trajectory

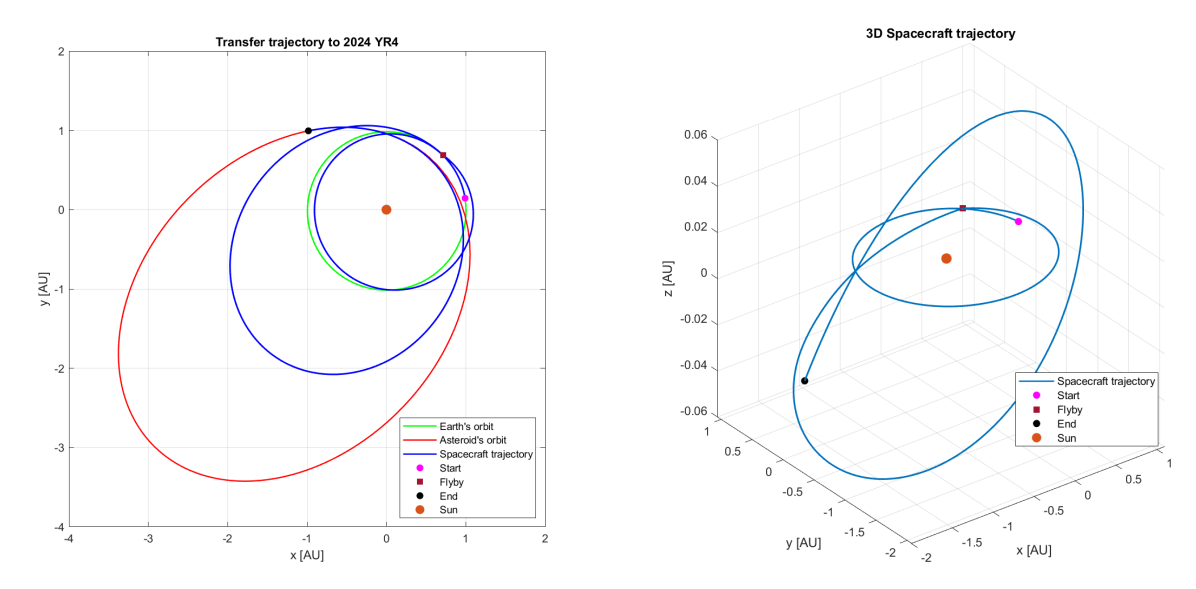


Figure 8.18: Solution 4 - Trajectory

Compared to direct solutions, it's immediately noticeable that the spacecraft completes fewer revolutions around the Sun. The flyby allows the mission duration to be shortened, albeit slightly. This is because, as will be analysed later, the flyby significantly raises the aphelion, reducing the thrust required by the engine. Consequently, since it's sufficient to push for a shorter time, the overall mission duration can be reduced.

There are, in fact, solutions with durations around 19–20, which correspond to transfers up to a year shorter than the direct ones. Naturally, these solutions have lower final mass values than those reported here, as they are associated with shorter transfer times.

### Variation of thrust with time

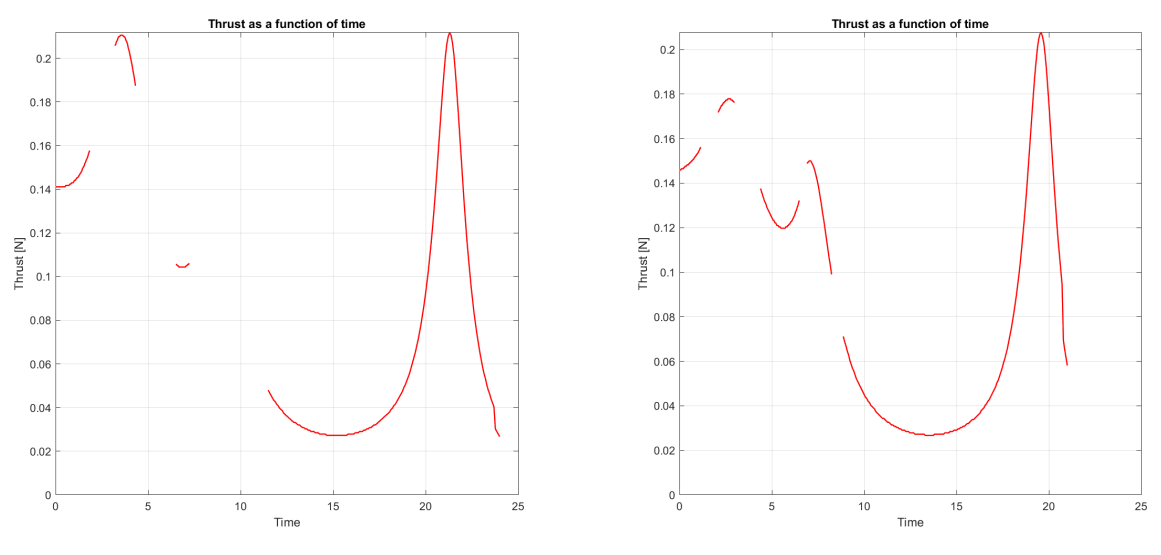
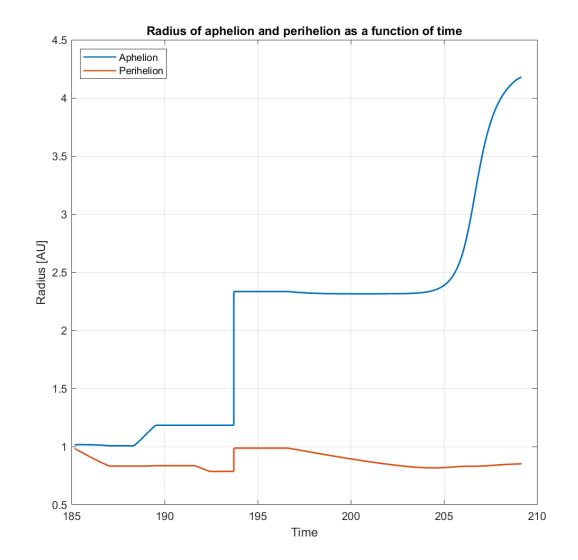


Figure 8.19: Solution 3 - Thrust

Figure 8.20: Solution 4 - Thrust

Graphs 8.19 e 8.20 show that the greatest thruster contribution occurs after the Earth flyby, which happens about a year into the mission. In both cases, in fact, a nearly continuous thrust phase is observed starting about a year and a half or two into the mission.

## Evolution of aphelion and perihelion as a function of time



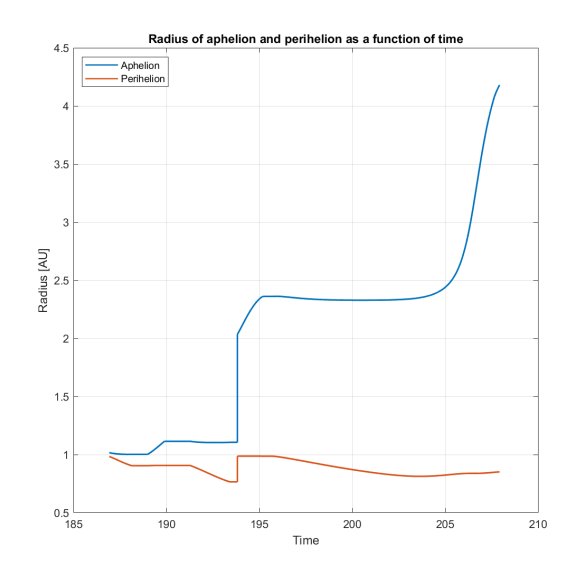
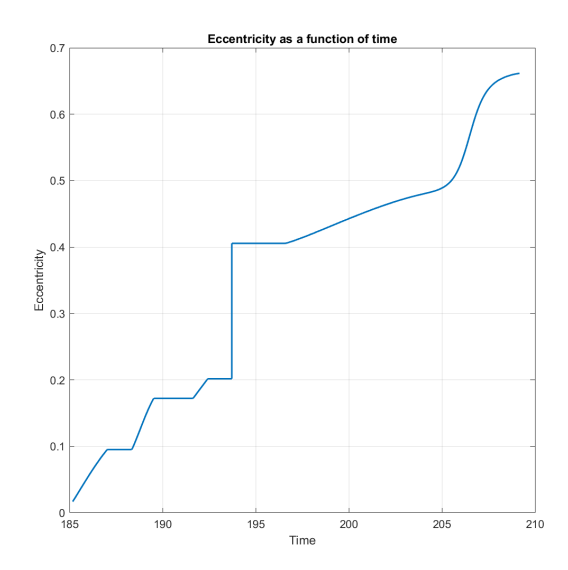


Figure 8.21: Solution 3 - Aphelion and perihelion

Figure 8.22: Solution 4 - Aphelion and perihelion

From the graphs above, it can be seen that, at  $t_0$ =193.72 for Solution 3 and at  $t_0$ =193.83 for Solution 4, i.e., at the moment the flyby occurs, a significant increase in the aphelion radius is recorded. This gain is accompanied by a slight increase in the perihelion, a negative aspect for the mission, since this quantity must be reduced overall. However, performing the flyby remains very advantageous, since the aphelion gain is far greater than the cost in terms of thrust required to bring the perihelion back to the desired level. The flyby, in fact, allows the aphelion to be raised by approximately 50% of the total required, thus enabling significant savings in terms of propellant.

# Evolution of eccentricity as a function of time



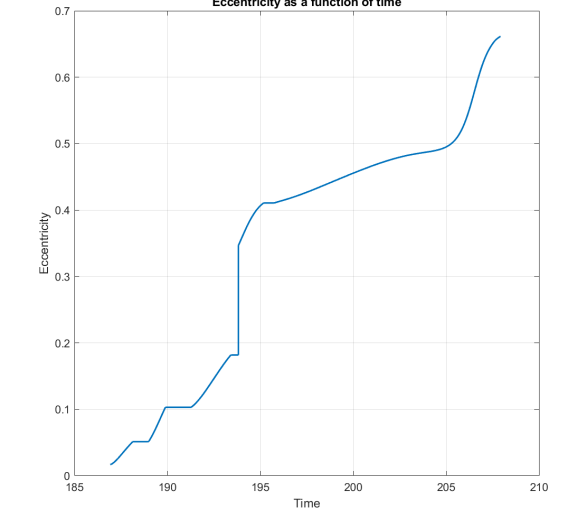


Figure 8.23: Solution 3 - Eccentricity

Figure 8.24: Solution 4 - Eccentricity

In addition to observing it visually in the graphs 8.21 and 8.22, it is also possible to note through the eccentricity trend how, at the moment of the flyby, the increase in the aphelion (which increases the eccentricity value) is larger than that of the perihelion (which reduces it). The fact that overall

the eccentricity increases confirms what was said in the previous paragraph: the gain in terms of aphelion radius is greater than the cost of lowering the perihelion after the flyby.

## 8.3 Later direct transfer solutions

As highlighted in Section 7.3, the same mission can be repeated every four years while maintaining very similar characteristics in terms of trajectory and duration. This section presents two solutions similar to Solution 1, postponed by four and eight years respectively, with departure dates in 2032 and 2036.

Solution	Duration		$\mathbf{t}_0$	1	$\mathbf{t_f}$		
Solution	Normalized	Days	Normalized	Date	Normalized	Date	
5	27	1569.58	206.5	12/11/2032	233.5	28/02/2037	
6	27	1569.58	231.6	10/11/2036	258.6	27/02/2041	

Table 8.5: Later direct transfers - duration and timeline comparison

Solution	$M_{\mathrm{f}}~[\mathrm{kg}]$	$\Delta V [km/s]$
5	695.501	11.751
6	695.329	11.759

Table 8.6: Later direct transfers - mass and  $\Delta V$  comparison

From the data reported in the two tables, the similarity between these two solutions and the solution with duration equal to 27.6 starting in 2028 is immediately noticeable. In fact, even when solutions with slightly shorter durations are considered, the results for final mass and required  $\Delta V$  are virtually identical.

The observations regarding the spacecraft trajectory, the evolution of the thrust, and the variations of aphelion, perihelion and eccentricity over time are the same as those discussed in Section 8.1.

#### Trajectory followed by the spacecraft

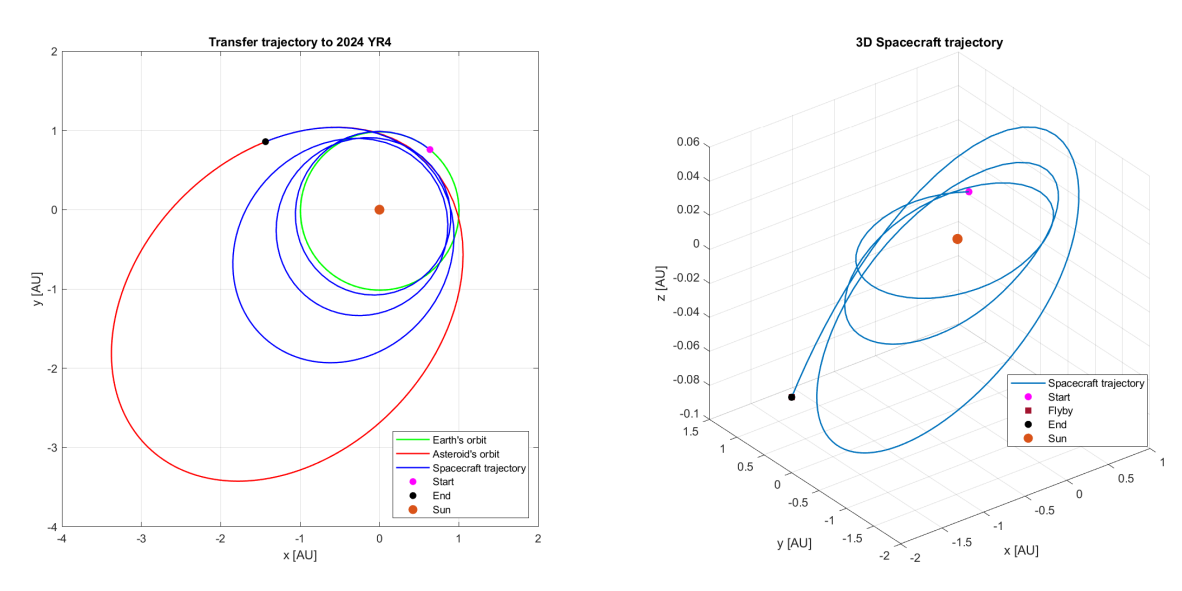


Figure 8.25: Solution 5 - Trajectory

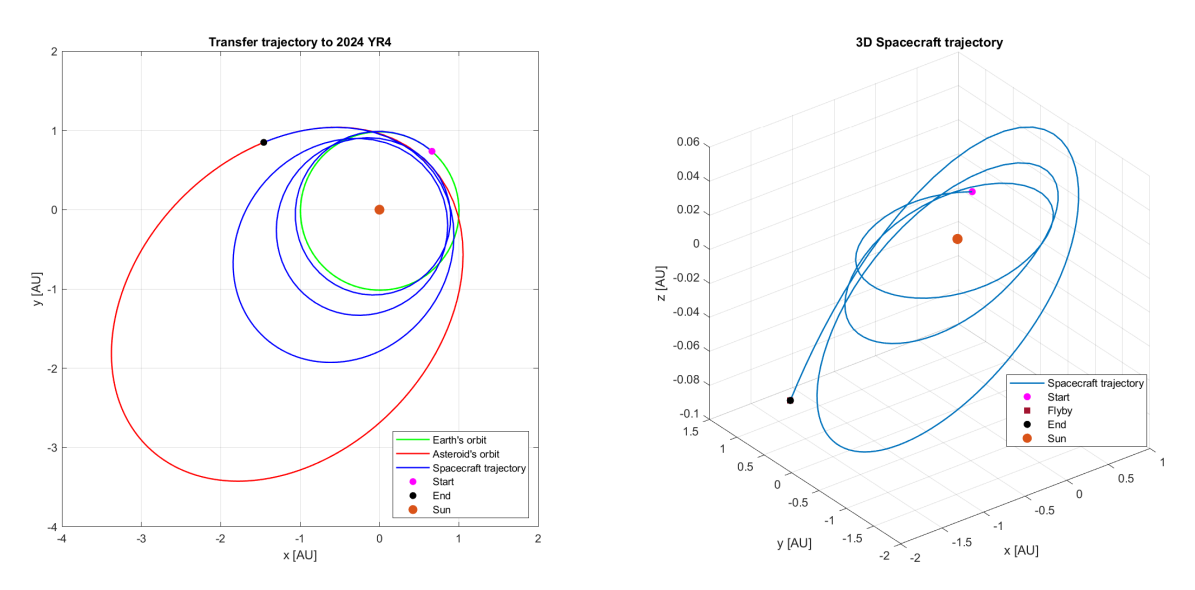


Figure 8.26: Solution 6 - Trajectory

# Variation of thrust with time

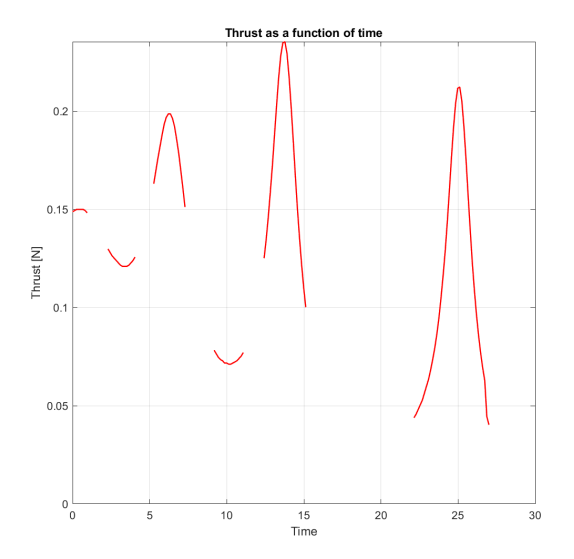


Figure 8.27: Solution 5 - Thrust

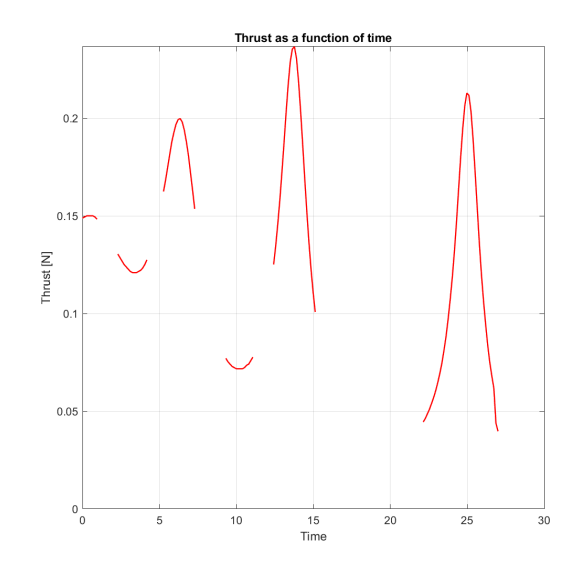
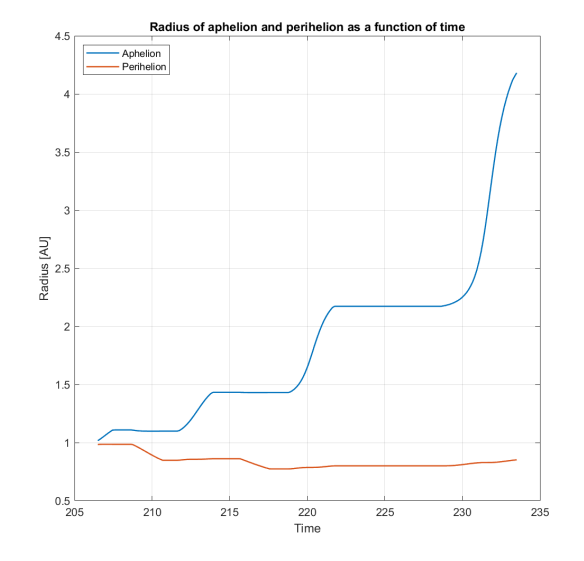


Figure 8.28: Solution 6 - Thrust

# Evolution of aphelion and perihelion as a function of time



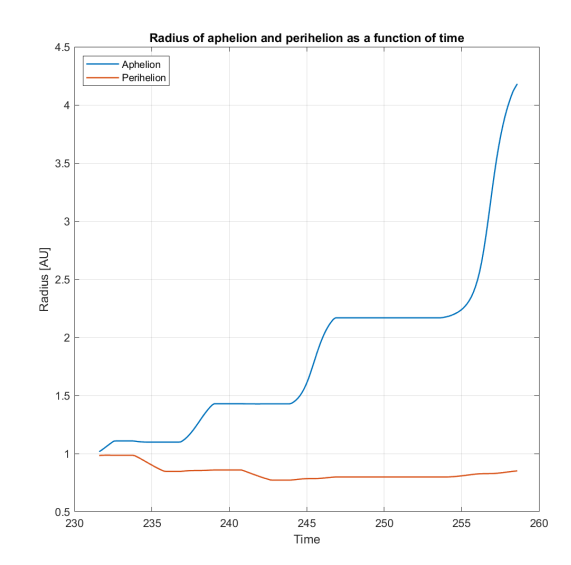
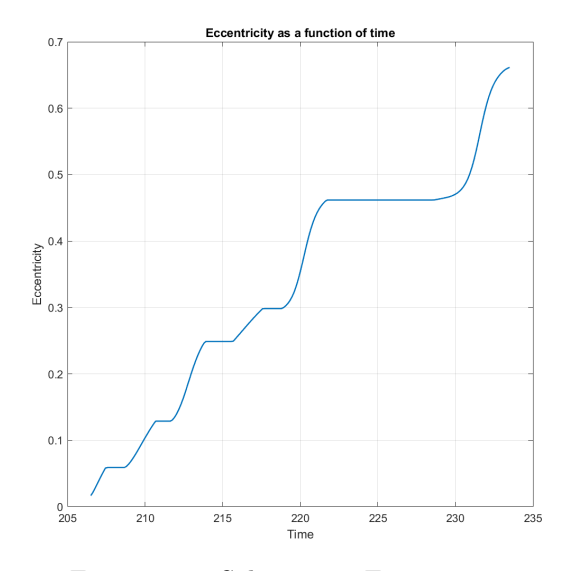
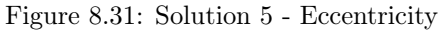


Figure 8.29: Solution 5 - Aphelion and perihelion

Figure 8.30: Solution 6 - Aphelion and perihelion

# Evolution of eccentricity as a function of time





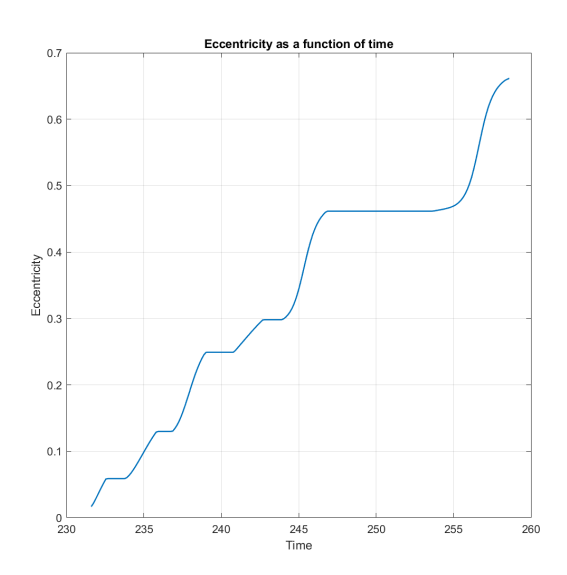


Figure 8.32: Solution 6 - Eccentricity

# 8.4 Later Earth flyby transfer solutions

As with direct transfers, a similar reasoning holds for Earth flyby missions planned further ahead in time, with launch windows that will be narrower in this case.

Solutions 7 and 8 are reported here, which correspond to Solutions 3 and 4 moved forward in time by four years.

Solution	Duration		$\mathbf{t_0}$		${ m t_{fb}}$		$\mathbf{t_f}$	
	Normalized	Days	Normalized	Date	Normalized	Date	Normalized	Date
7	24	1395.18	210.31	21/06/2033	218.86	31/10/2034	234.31	17/04/2037
8	21	1220.78	212.05	30/09/2033	218.96	06/11/2034	233.05	02/02/2037

Table 8.7: Later Earth flyby transfers - duration and timeline comparison

Solution	$ m M_{fb}~[kg]$	$M_{\mathrm{f}}~[\mathrm{kg}]$	$\Delta V_1 \; [\mathrm{km/s}]$	$\Delta V_2 \; [\mathrm{km/s}]$	$\Delta  m V_{tot} \ [km/s]$
7	908.569	784.395	3.103	4.756	7.859
8	906.130	758.321	3.190	5.763	8.953

Table 8.8: Later Earth flyby transfers - mass and  $\Delta V$  comparison

Here too, the results reported in the tables immediately show the similarity with the solutions reported in Section 8.2, both in terms of masses and the required  $\Delta V$ .

The observations regarding the spacecraft trajectory, the evolution of the thrust, and the variations of aphelion, perihelion and eccentricity over time are the same as those discussed in Section 8.2.

# Trajectory followed by the spacecraft

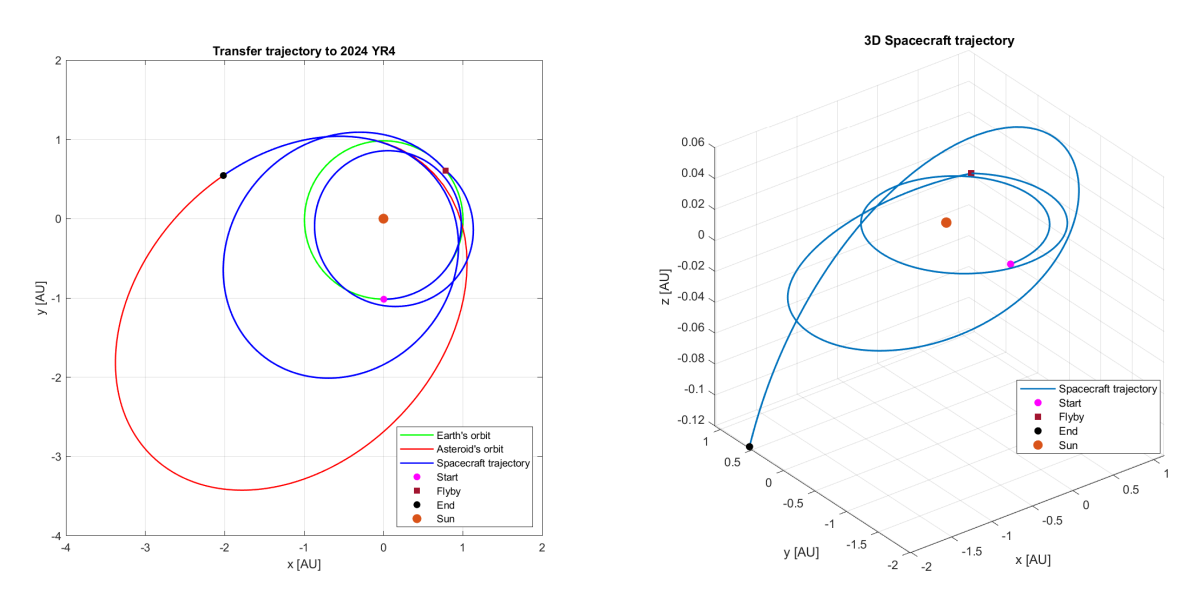


Figure 8.33: Solution 7 - Trajectory

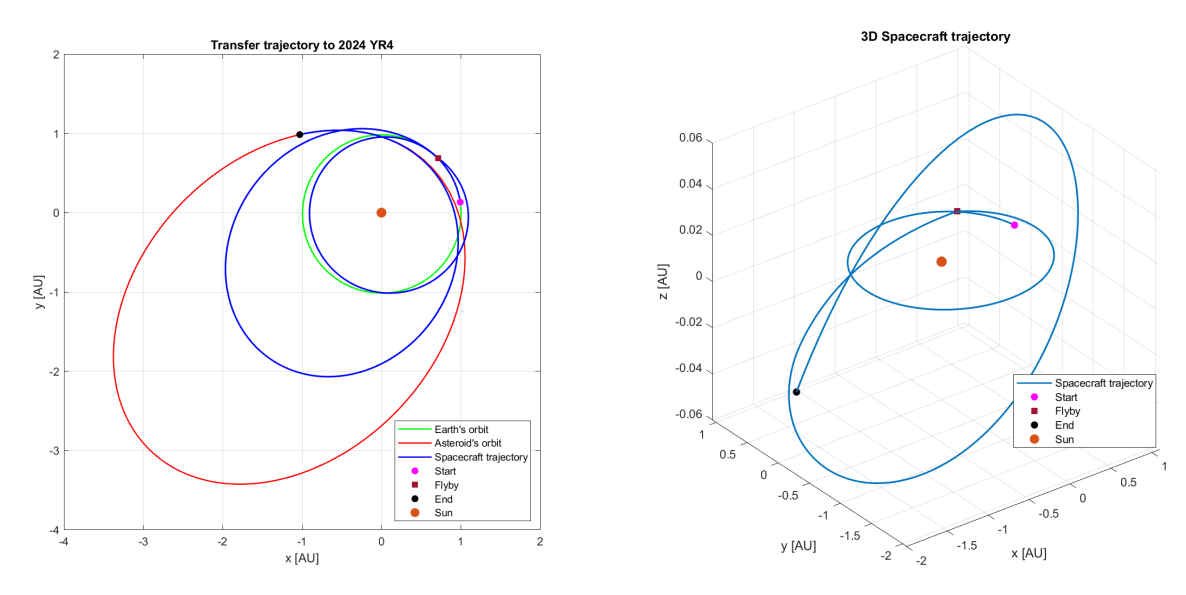


Figure 8.34: Solution 8 - Trajectory

# Variation of thrust with time

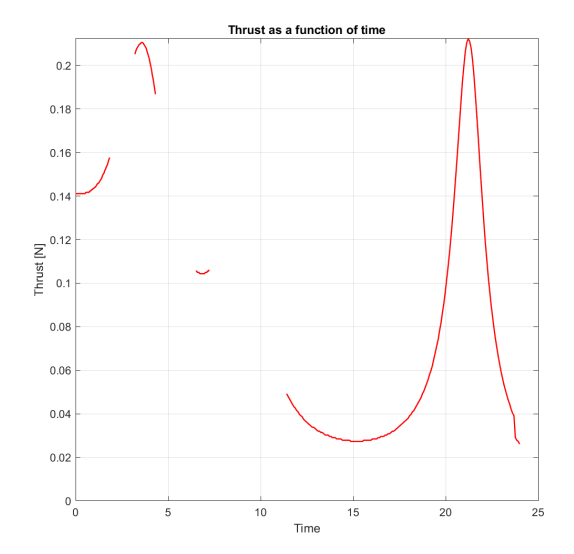


Figure 8.35: Solution 7 - Thrust

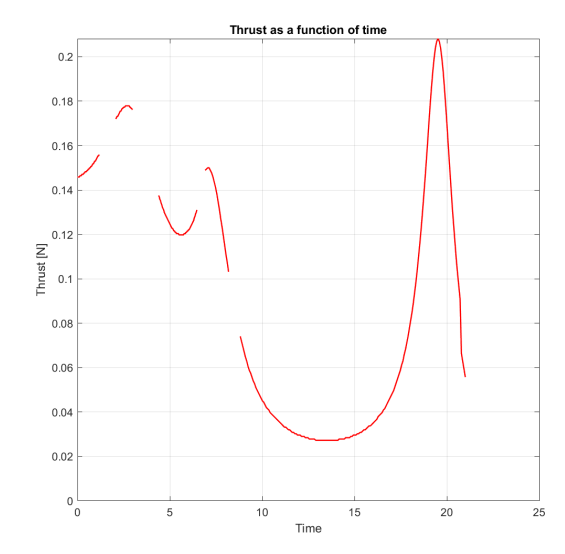
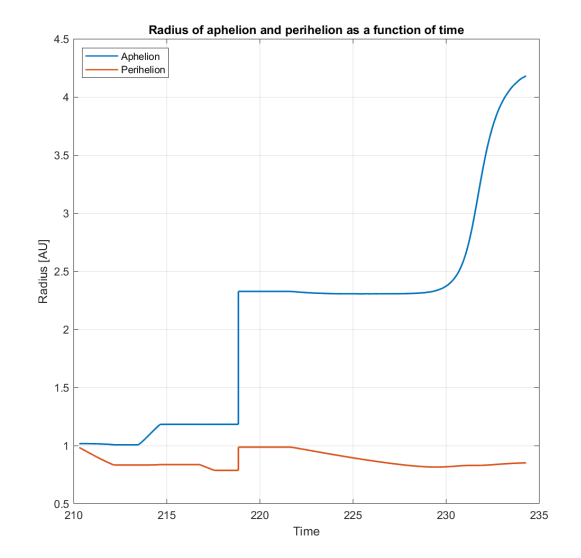


Figure 8.36: Solution 8 - Thrust

# Evolution of aphelion and perihelion as a function of time



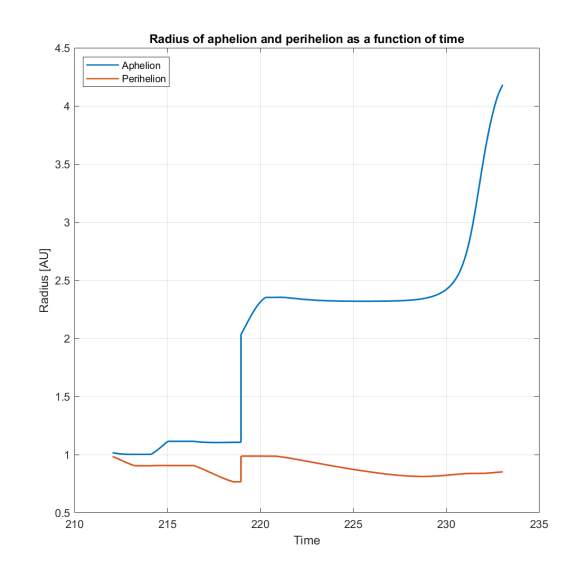
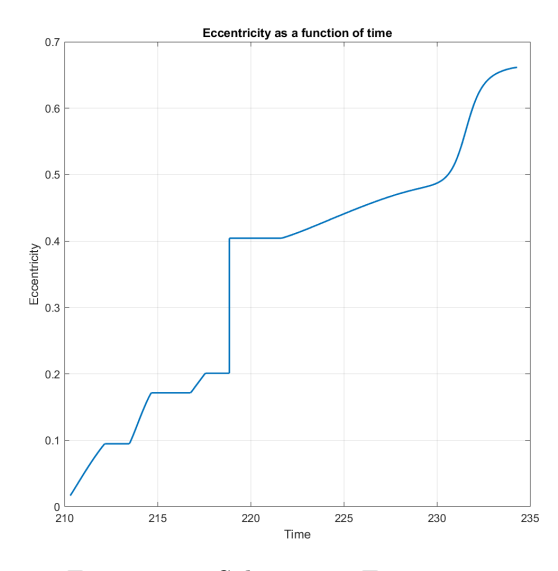
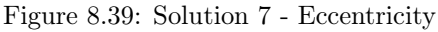


Figure 8.37: Solution 7 - Aphelion and perihelion

Figure 8.38: Solution 8 - Aphelion and perihelion

# Evolution of eccentricity as a function of time





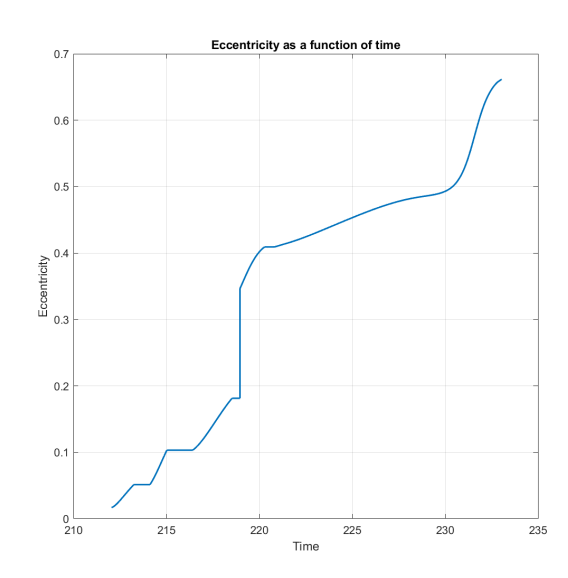


Figure 8.40: Solution 8 - Eccentricity

# 8.5 Trajectory options before the expected impact date

It is interesting to explore solutions with arrival dates before December 22, 2032, the day on which asteroid 2024 YR4 is expected to have a probability of 4.3% of impacting the Moon. The solutions reported in this section are Earth flyby transfers with an arrival date around 2031, approximately one year before the potential collision with the natural satellite. Below are the main data for two solutions with not too long durations and final masses almost close to those obtained in Sections 8.2 and 8.4.

Solution	Duration		$\mathbf{t_0}$		${ m t_{fb}}$		$\mathbf{t_f}$	
	Normalized	Days	Normalized	Date	Normalized	Date	Normalized	Date
9	27	1569.58	171.67	28/04/2027	180.81	10/10/2028	198.67	15/08/2031
10	24	1395.18	171.56	22/04/2027	180.79	09/10/2028	195.56	15/02/2031

Table 8.9: Earth flyby transfers before December 22, 2032 - duration and timeline comparison

Solution	$ m M_{fb}~[kg]$	$M_{\mathrm{f}}~[\mathrm{kg}]$	$\Delta V_1 \; [\mathrm{km/s}]$	$\Delta V_2 \; [\mathrm{km/s}]$	$\Delta V_{tot} \; [km/s]$	
9	846.462	773.428	5.394	2.920	8.314	
10	821.050	751.962	6.380	2.845	9.225	

Table 8.10: Earth flyby transfers before December 22, 2032 - mass and  $\Delta V$  comparison

It is immediately evident that, compared to the Earth flyby solutions discussed previously, the final masses are lower due to slightly higher costs in terms of  $\Delta V$ . However, as expected, by increasing the mission duration even beyond the value 30, which corresponds to almost five years of transfer time, final masses very similar to those of Solutions 3, 4 and 7 can be obtained. Consequently, to reach values of  $m_f$  around 785 kg, it is necessary to plan missions extending up to almost two years beyond those discussed in the previous sections.

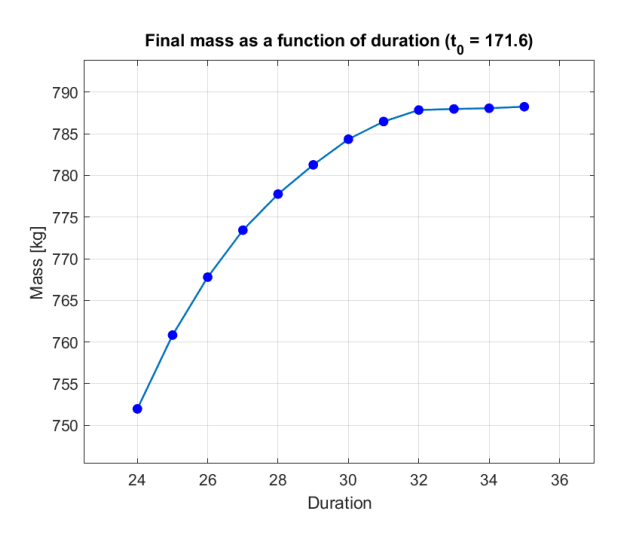


Figure 8.41: Earth flyby transfer - final mass vs duration ( $t_0$ =171.6)

From the graph it can be observed that, for durations exceeding 32 (and therefore exceeding 5 years), the final mass seems to reach a limit value around 788 kg beyond which it does not increase further. This occurs for the same reasoning as for direct transfers: after a certain amount of time sufficient to reach the required aphelion and perihelion radii, thrust is no longer required from the engine. This is followed by a coasting phase with the engines off, during which no fuel is consumed, without attempting to redistribute the thrust more efficiently than in previous cases, thus keeping the final mass within its limit.

# Trajectory followed by the spacecraft

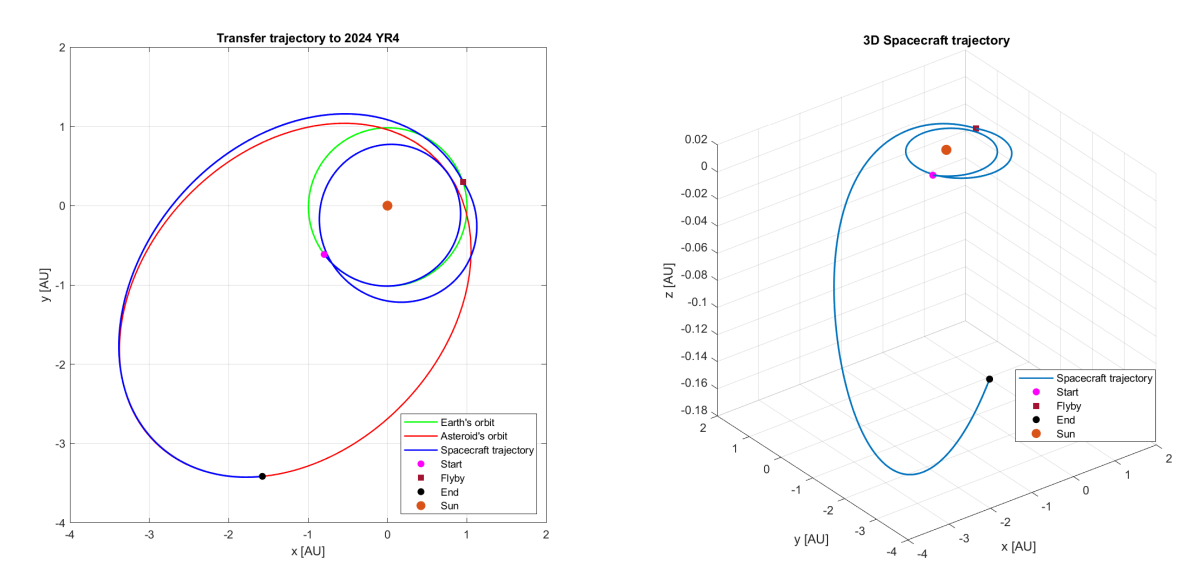


Figure 8.42: Solution 9 - Trajectory

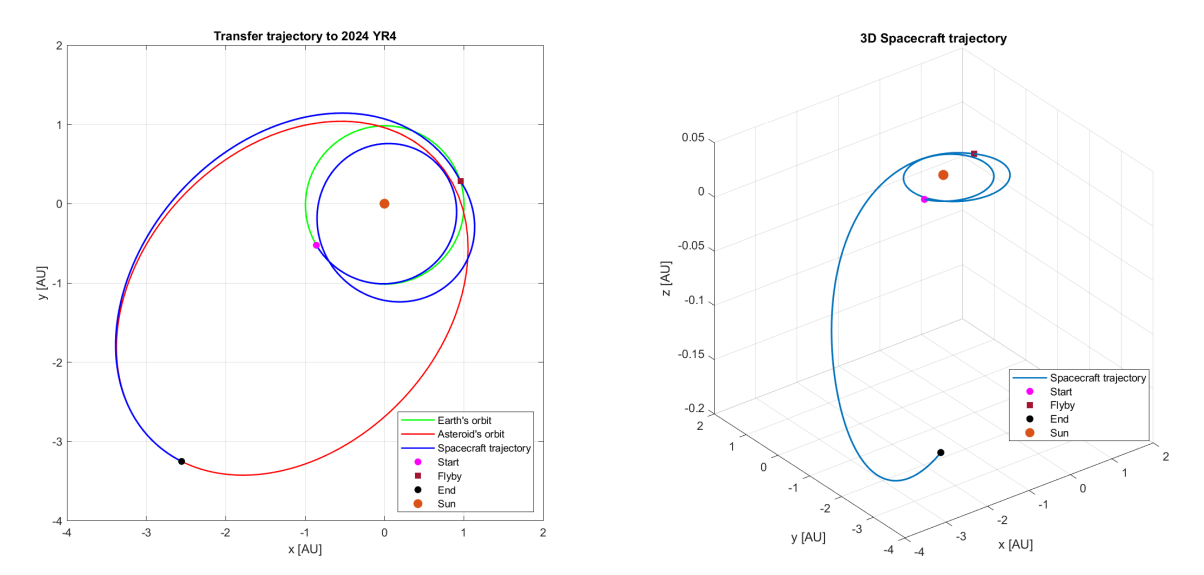
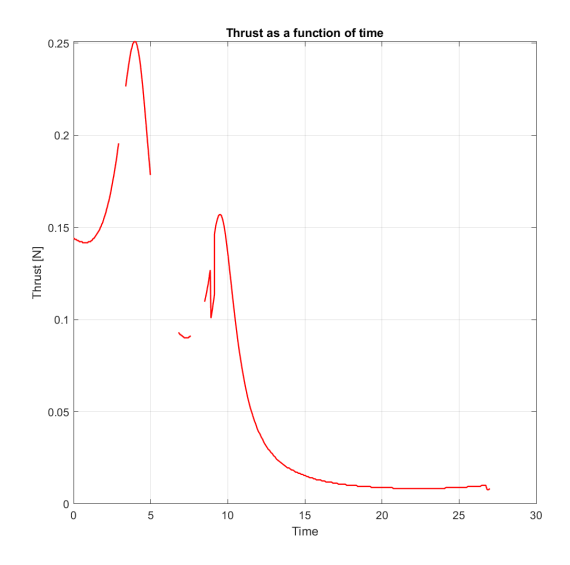


Figure 8.43: Solution 10 - Trajectory

It is immediately apparent that, compared to other flyby solutions, the arrival point is no longer located at perihelion but at aphelion of the 2024 YR4 orbit. The spacecraft completes two revolutions around the Sun. The first lasts about a year, and the second, half of which occurs after the flyby, takes up the remainder of the mission, approximately three years.

In addition to the arrival dates reported in Table 8.9, the figures also show that the asteroid is reached before it crosses the Earth's orbit and, consequently, also that of the Moon. Specifically, analysing the various output files obtained from the optimization code, it is observed that the potential collision with the asteroid would occur at the second trajectory crossing between Earth and 2024 YR4. The solutions presented guarantee arrival before this event and, in general, before both orbital crossings.

### Variation of thrust with time



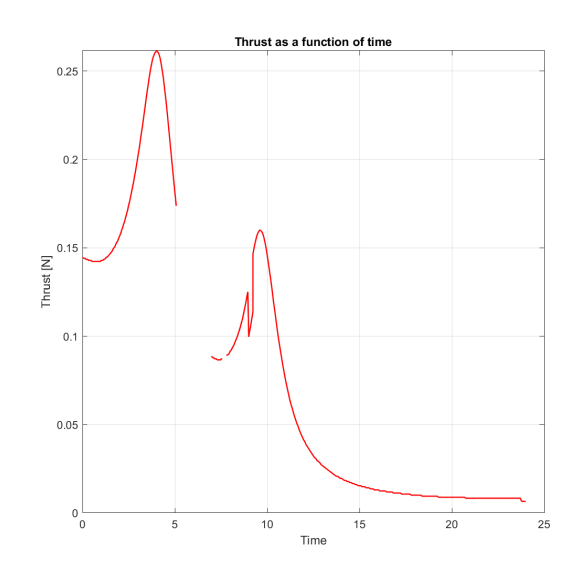
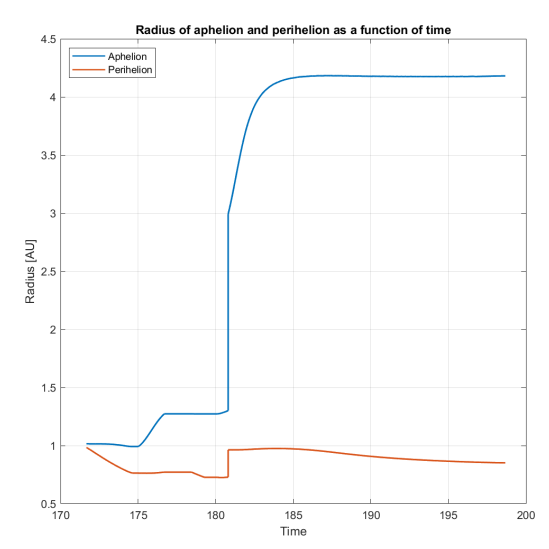


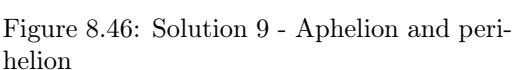
Figure 8.44: Solution 9 - Thrust

Figure 8.45: Solution 10 - Thrust

Thrust profile over time appears to be more irregular than in previous cases. It is also noted that, after about 2.5 years (i.e., after a mission duration equal to 15), the thrust is used only to lower the perihelion. In fact, the aphelion is raised by the thrust only twice, near the two peaks observed in the graphs above.

# Evolution of aphelion and perihelion as a function of time





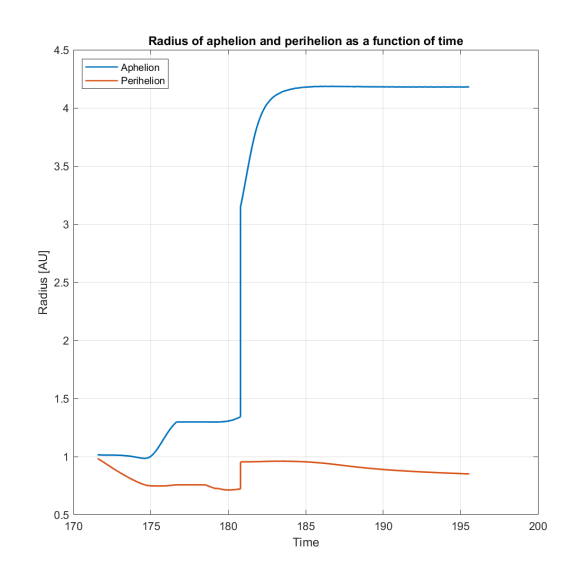
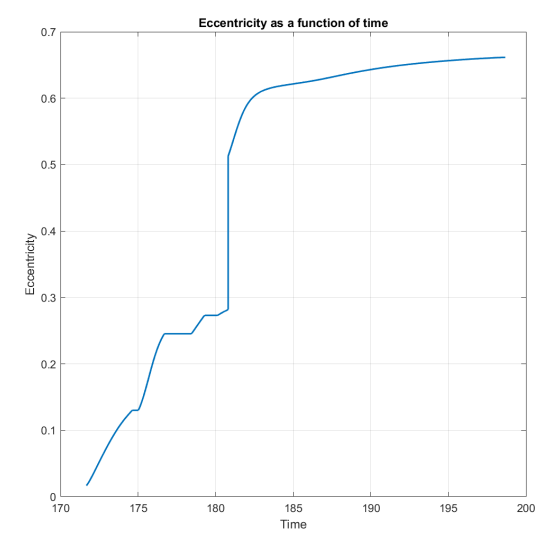


Figure 8.47: Solution 10 - Aphelion and perihelion

The two graphs show that, close to the flyby, approximately one year after the start of the mission, there is a significant rise in aphelion and a modest increase in perihelion, which will subsequently be lowered again by thrust. In this case, too, the flyby achieves an aphelion increase of approximately 50% of the total required, thus significantly reducing the mission costs. The discussion regarding the perihelion increase and the resulting cost required to lower it is the same as in Section 8.2: the aphelion gain is far greater than the cost in terms of thrust required to bring the perihelion back to the desired level.

Compared to previous flyby cases, where the aphelion radius was increased with thrust up to that of the asteroid towards the end of the mission, in this case this parameter is raised immediately after the flyby. The spacecraft's trajectory will then be adjusted without further affecting the aphelion but by gradually decreasing the perihelion radius.

# Evolution of eccentricity as a function of time



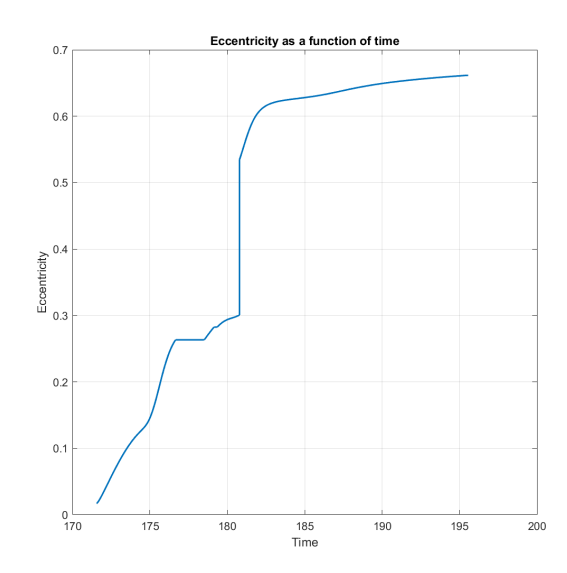


Figure 8.48: Solution 9 - Eccentricity

Figure 8.49: Solution 10 - Eccentricity

In this case, too, the eccentricity shows an upward trend. It can be seen how it rises sharply near the flyby due to the increase in aphelion (which here also prevails over that of perihelion) and then continues to grow at a reduced rate as the perihelion gradually decreases.

It can be concluded that, based on the duration times and final mass values, this type of solutions, although not the most performing compared to those presented in the other sections, still allow reaching the asteroid 2024 YR4 while respecting the arrival constraint before December 22, 2032, with final mass values that remain acceptable.

# Chapter 9

# Conclusions

The work presented in this thesis concerns the optimization and analysis of space trajectories toward the celestial body 2024 YR4, a Near-Earth asteroid that currently has a 4.3% probability of impacting the Moon.

Trajectory search was performed using indirect optimization methods based on optimal control theory. Specifically, the study initially focused on finding direct trajectories, meaning transfers without exploiting the gravitational fields of planets or other asteroids. Following observations of direct solutions, given that the spacecraft's initial trajectory does not deviate significantly from Earth's orbit, the focus shifted to finding solutions that included a flyby of the planet with the aim of saving propellant mass. Of the many trajectories identified, the ten most interesting solutions were included in this thesis and are summarized in the following table.

Direct transfer solutions									
Solution	Departure date	Flyby date	Arrival date	Duration [years]	$m_f$ [kg]	$\Delta V  [\mathrm{km/s}]$			
1	14/11/2028	N/A	06/04/2033	4.4	697.100	11.677			
2	16/08/2029	N/A	21/02/2033	3.5	673.212	12.805			
5	12/11/2032	N/A	28/02/2037	4.3	695.501	11.751			
6	10/11/2036	N/A	27/02/2041	4.3	695.329	11.759			
	Earth flyby transfer solutions								
Solution	Departure date	Flyby date	Arrival date	Duration [years]	$m_f$ [kg]	$\Delta V  [\mathrm{km/s}]$			
3	26/09/2029	31/10/2030	16/04/2033	3.8	785.178	7.827			
4	01/10/2029	06/11/2030	03/02/2033	3.3	758.522	8.944			
7	21/06/2033	31/10/2034	17/02/2037	3.8	784.395	7.859			
8	30/09/2033	06/11/2034	02/02/2037	3.3	758.321	8.953			
9	28/04/2027	10/10/2028	15/08/2031	4.3	773.428	8.314			
10	22/04/2027	09/10/2028	15/02/2031	3.8	751.962	9.225			

N/A = Not applicable (value not present for this solution)

Table 9.1: Transfer solutions

The results show that trajectories that exploit Earth's gravitational field are those that allow for the lowest propellant consumption. Furthermore, these solutions are characterized by a shorter average mission duration, since much of the increase in the aphelion radius, which would require multiple thrust arcs distributed over time, occurs during the flyby of the planet in a single manoeuvre.

Particular attention should also be paid to Solutions 9 and 10, i.e., those trajectories with an arrival date prior to the potential impact with the Moon, scheduled for December 22, 2032. On average, these solutions have slightly lower final mass values, but still acceptable, thanks in part to the extension of the mission duration compared to Solutions 3 and 4.

Chapter 9 Conclusions

It should be noted that the solutions found using the optimization code depend heavily on the initial trial values, and therefore, even by slightly varying some initial parameters, new solutions may be found. The difficulty in finding these trajectories is also due to the fact that the target asteroid's orbit is highly eccentric, making it more difficult for the code to converge.

A possible future development involves the search for new solutions that introduce new features or improvements over those found so far, such as missions scheduled in different launch windows, missions with additional flybys to further reduce propellant mass consumption and missions with shorter transfer durations, which could, however, result in lower final masses.

# Bibliography

- [1] Aerospace Notes. Ion Propulsion. URL: https://aerospacenotes.com/ion-propulsion/.
- [2] European Space Agency. Close Approach Fact Sheet for Asteroid 2024 YR4. Tech. rep. 2024. URL: https://neo.ssa.esa.int/.
- [3] Brent William Barbee. Mission planning for the mitigation of hazardous Near Earth Objects [electronic resource]. 2010.
- [4] Roger R. Bate, Donald D. Mueller, and Jerry E. White. Fundamentals of Astrodynamics. Dover Publications, 1971.
- [5] Manuela Battipede. "Meccanica del Volo Spaziale". Slide del corso, Politecnico di torino. 2025.
- [6] Lorenzo Casalino. "Equazioni in coordinate sferiche". Appunti concessi dal professore.
- [7] Lorenzo Casalino. "Ottimizzazione Indiretta di Traiettorie Spaziali". Appunti concessi dal professore.
- [8] Lorenzo Casalino. "Space propulsion". Slide del corso, Politecnico di torino. 2025.
- [9] Wikipedia contributors. 2024 YR4. URL: https://it.wikipedia.org/wiki/2024\_YR4.
- [10] Wikipedia contributors. Asteroid. URL: https://en.wikipedia.org/wiki/Asteroid.
- [11] Wikipedia contributors. Asteroid impact avoidance. URL: https://en.wikipedia.org/wiki/Asteroid\_impact\_avoidance.
- [12] Wikipedia contributors. Asteroid impact prediction. URL: https://en.wikipedia.org/wiki/Asteroid\_impact\_prediction.
- [13] Wikipedia contributors. Asteroid Spectral Types. URL: https://en.wikipedia.org/wiki/Palermo\_scale.
- [14] Wikipedia contributors. *Palermo Scale*. URL: https://en.wikipedia.org/wiki/Palermo\_scale.
- [15] Wikipedia contributors. Torino Scale. URL: https://en.wikipedia.org/wiki/Torino\_scale.
- [16] Wikipedia contributors. Variable Specific Impulse Magnetoplasma Rocket. URL: https://en.wikipedia.org/wiki/Variable\_Specific\_Impulse\_Magnetoplasma\_Rocket.
- [17] Tiankun Huang et al. Study on propellant utilization in pulsed plasma thrusters. 2021.
- [18] NASA, Jet Propulsion Laboratory. Asteroid 2024 YR4. URL: https://science.nasa.gov/solar-system/asteroids/2024-yr4/.
- [19] NASA, Jet Propulsion Laboratory. Asteroids. URL: https://science.nasa.gov/solar-system/asteroids/.
- [20] Jean-Baptiste Lanvin. Distance, Elevation and Azimuth Calculation. 2015. URL: https://sourceforge.isae.fr/projects/building-blocks-for-a-leo-ground-station/wiki/Distance\_Elevation\_and\_Azimuth\_Calculation/5.
- [21] Dan Lev. Investigation of Efficiency in Applied Field MagnetoPlasmaDynamic Thrusters. 2012.
- [22] S. Mazouffre. Electric propulsion for satellites and spacecraft: Established technologies and novel approaches. 2016.

Chapter 9 Bibliography

[23] NASA/JPL - Center for Near-Earth Object Studies. NEO Groups. NASA / Jet Propulsion Laboratory. URL: https://cneos.jpl.nasa.gov/about/neo\_groups.html.

- [24] Kyle Niemeyer. Introduction to Orbital Mechanics: Conic Sections. URL: https://kyleniemeyer.github.io/space-systems-notes/orbital-mechanics/conic-sections.html.
- [25] Princeton Plasma Physics Laboratory. What is a Hall thruster? URL: https://htx.pppl.gov/thrusters.html.
- [26] ScienceFacts. Kepler's Laws: Statements, Equation, and Application. URL: https://www.sciencefacts.net/keplers-laws.html.
- [27] Teledyne Technologies. Asteroid Primer. Mar. 2024. URL: https://www.teledyne.com/digital-imaging-space-science-monthly/asteroid-primer.
- [28] A Liquid Universe. General Hohmann Transfer. URL: https://aliquiduniverse.com/general-hohmann-transfer/.
- [29] Bryan Weber. Interplanetary trajectories and maneuvers. URL: https://orbital-mechanics.space/interplanetary-maneuvers/introduction.html.
- [30] Katherine Yoshiwara. Intermediate Algebra: Conic Sections: Ellipses. URL: https://yoshiwarabooks.org/int-algebra/Ellipses.html.